INVESTIGATION OF SMALL D. C. ELECTROMAGNETIC PUMPS

ROBERT L. EDIIN
AND
JAY W. LAMB

[redacted]

INVESTIGATION OF SMALL D.C. ELECTROMAGNETIC PUMPS

by

Robert L. Ediin
Lieutenant Commander, United States Navy
B. S., Webb Institute of Naval Architecture, 1954

and

Jay W. Lamb
Lieutenant, United States Navy
B.S., Stanford University, 1960

Submitted in partial fulfillment
for the degree of

MASTER OF SCIENCE IN ELECTRICAL ENGINEERING

from the

UNITED STATES NAVAL POSTGRADUATE SCHOOL
May 1966

ABSTRACT

A small, direct current electromagnetic conduction pump was designed according to the equivalent circuit theory of A. H. Barnes. Design was aided by data from a prototype also constructed by the authors. Distinguishing features of the pump are its small size, the use of non-conducting pump walls, and the use of mercury as the working fluid. Performance was compared with theory. Deviations were attributed to electrode contact resistance and to the interaction between magnetic leakage flux and fringe current. Contact resistance to mercury of rhodium and nickel electrodes was determined with the aid of a jig designed for the purpose. A magnet design using flux plotting techniques is presented. Distinguishing feature of the magnet is its cylindrically shaped yoke.

TABLE OF CONTENTS

		Page
1.	Introduction	9
	Background	9
	Electromagnetic Pumps	9
2.	Theory	12
	Mathematical Derivation of Model	12
	Practical Application of Model	15
3.	Prototype Pump	17
	Construction of Pump and System #1	17
	Experimental Results	21
	Discussion and Conclusions	30
4.	Second Pump	32
	Construction of Pump and System #2	32
	Static Head Determinations	38
	Hydraulic Losses	38
	Flow Rate Determinations	41
	Efficiency Determinations	41
	Discussion and Conclusions	45
5.	Summary	48
	Conclusions	48
	Recommendations	48
	Acknowledgements	50
	Bibliography	51
	Appendix I - Pump Design	54
	Appendix II - Magnet Design	65
	Appendix III - Pump Test Loop Design	82
	Appendix IV - Contact Resistance	92

LIST OF ILLUSTRATIONS

Figure		Page
1.	Conduction Pump Schematic	10
2.	Differential Fluid Particle	12
3.	Pump Equivalent Circuit	13
4.	Theoretical Current Distribution	16
5.	First System	18
6.	D.C. Magnetization Curve of Magnet Number One	19
7.	Schematic Drawing of Pump Number One	20
8.	Schematic of System Number One	22
9.	Static Head vs. Electrode Current	23
10.	Flow Rate vs. Head at I = 10.8 Amps.	25
11.	Flow Rate vs. Head at I = 19.7 Amps.	26
12.	Flow Rate vs. Head at I = 30.4 Amps.	27
13.	Hydraulic Losses of System Number One	28
14.	Pump Efficiency vs. Electrode Current	29
3a.	Revised Pump Equivalent Circuit	31
15.	Second Pump	33
16.	D.C. Magnetization Curve of Magnet Number Two	34
17a.	Second System	36
17b.	Exploded View of Magnet and Pump Number Two	37
18.	Static Head vs. Electrode Current	39
19.	Hydraulic Losses of System Number Two	40
20.	Flow Rate vs. Head at I = 10.4 Amps.	42
21.	Flow Rate vs. Head at I = 19.7 Amps.	43
22.	Flow Rate vs. Head at I = 30.4 Amps.	44

Figure		Page
23.	Pump Efficiency vs. Electrode Current	46
24.	Magnetic Flux Density Profile	58
25.	Magnetic Flux Density and Current Function Contours	59
26.	Pump Equivalent Circuit	60
27.	Pump Elevation and Plan Views	63
28.	Transition Piece Jig	64
29.	Flux Plot Nomenclature	69
30.	Final Pole Piece Flux Plot	72
31.	Profile of Magnet Frame and Poles	78
32.	Section Through Center of Magnet	79
33.	Coil Bobbin	80
34.	Coil Bobbin Support	81
35.	Pump Table Layout	86
36.	Bottom Head of Lower Reservoir	87
37.	Cylinder Portion of Lower Reservoir	88
38.	Top Head of Lower Reservoir	89
39.	Upper Reservoir	90
40.	Upper Reservoir Support Plate	91
41.	Contact Resistance Jig	101
42.	Contact Resistance Jig Profile	102
43.	Contact Resistance Jig Details (1)	103
44.	Contact Resistance Jig Details (2)	104

LIST OF SYMBOLS

B	Flux density (gauss)
I	Current (amperes)
P	Pressure (kg/cm^2)
E_c	Back EMF (volts)
R_w	Resistance of pump wall (ohms)
R_b	Resistance to ineffective current (ohms)
R_e	Resistance to effective current (ohms)
I_w	Wall current (amperes)
I_b	Ineffective current (amperes)
I_e	Effective current (amperes)
V_t	Electrode potential difference (volts)
W_t	Power input to pump (watts)
η_e	Pump efficiency (%)
η	Combined efficiency of pump and magnet (%)
R_m	Magnet coil resistance (ohms)
l_e	Pump channel width in direction of electric field (centimeters)
l_h	Electrode length in direction of mercury flow (centimeters)
l_m	Pump channel thickness in direction of magnetic field (centimeters)
Q	Mercury flow rate (cm^3/sec)
P_s	Pressure under static conditions (i.e., $Q = 0$), (kg/cm^2)
R_{tot}	Total mercury resistance (ohms)
R_c	Contact resistance both electrodes to mercury (ohms)
v	Mercury velocity (cm/sec)
H_s	Static head (cm)

1. INTRODUCTION

BACKGROUND

With the advent of the nuclear age and specifically nuclear power for propulsion, scientists and engineers have again been delving into the realm of electromagnetic pumping. Because an electromagnetic pump has no moving parts and hence may be completely maintenance free, such a pump could be permanently installed in a sealed reactor heat exchanger loop and one major contamination problem would be solved. Unfortunately there are many problems with these pumps which have not yet been solved and much work is being done both in industry and educational institutions in this field.

ELECTROMAGNETIC PUMPS

There are two broad classifications of electromagnetic pumps:

(1) Induction pumps, which will only be mentioned here, and

(2) Conduction pumps which will be covered in detail beginning in the next section.

The basis of an electromagnetic pump (EMP) is the simple statement $\bar{F} = \bar{I}l \times \bar{B}$. That is, if an electric current flows orthogonally to a magnetic field, a force will result in the direction mutually perpendicular to both the field and the current.

Therefore if, as in the case of a conduction pump, (Figure 1) current flows across some conducting fluid (such as a liquid metal or some ionized solution) in the presence of an orthogonal magnetic field, a force will result and the fluid will move -- hence a pump. Similarly one could move a conducting fluid (by some external means) orthogonally to a field and voltage would result -- hence a generator.

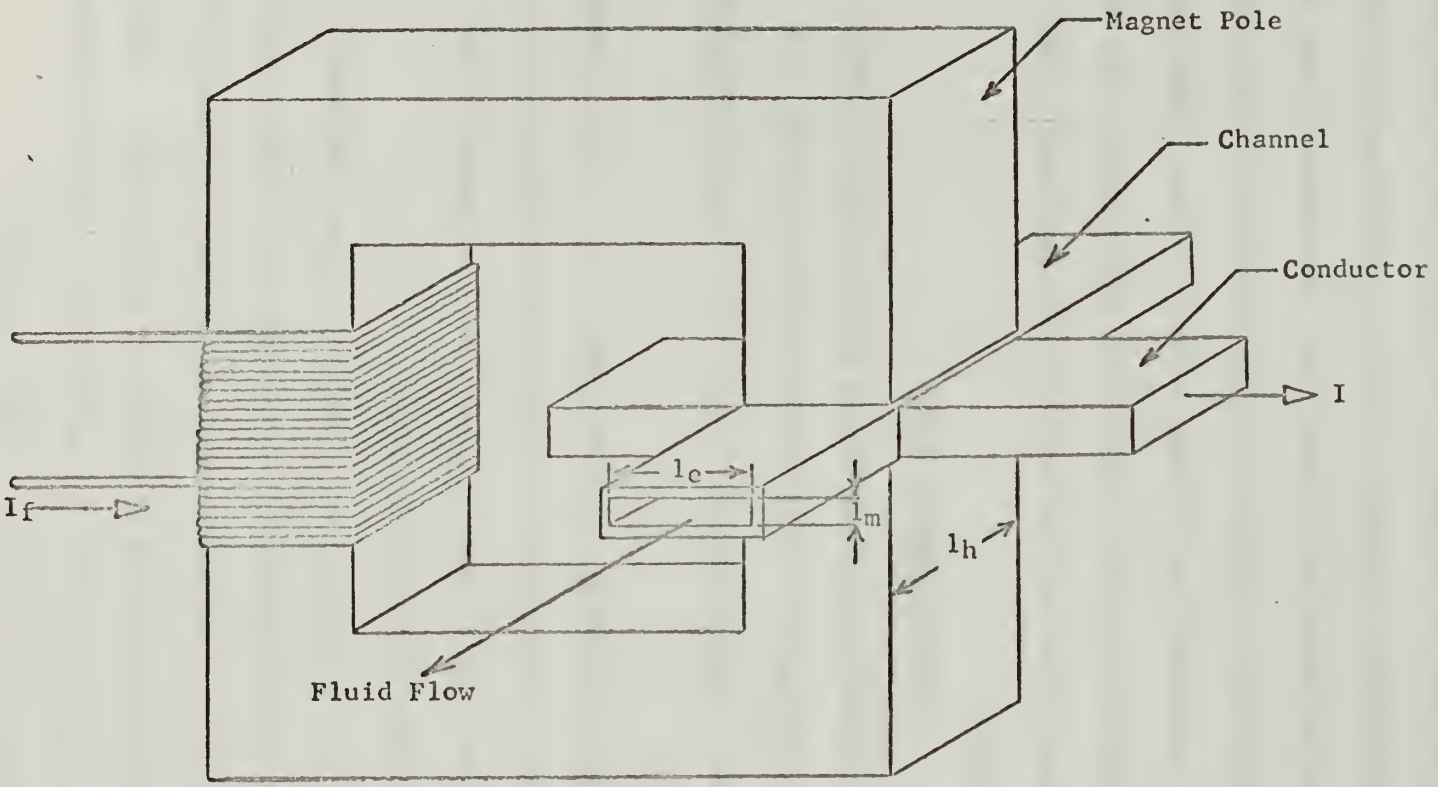

FIGURE 1
CONDUCTION PUMP SCHEMATIC

In an induction pump the current is induced in the conducting fluid by a changing magnetic flux in such a way as to have a current component perpendicular to, and in phase with, the flux. This combination again causes a force in the fluid resulting in a pumping action. A thorough coverage of these pumps may be found in [11], which reference also has a fine bibliography of specific articles covering many pumps of this class.

2. THEORY

MATHEMATICAL DERIVATION OF MODEL

To enable a better understanding of the pump we will consider the differential force exerted on a differential fluid particle by an incremental current flowing through it (Figure 2) and develop the theory advocated by Barnes [3].

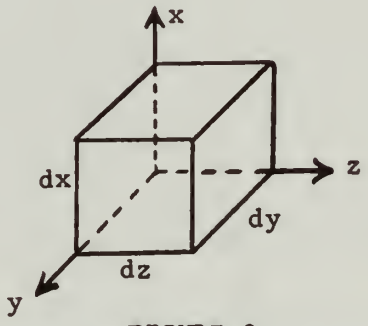

FIGURE 2
DIFFERENTIAL FLUID PARTICLE

Since

$$\bar{F} = \bar{I}l \times \bar{B} \tag{1}$$

$$d\bar{F} = \overline{dI}l \times \bar{B}$$

$$dF_z = J_y B_x \, dx \, dy \, dz \tag{2}$$

where fluid flow is constrained to the z direction, magnetic flux density (B) is constrained in the x direction and current density (J) is constrained to the y direction. Further, end effects, fringing, and turbulence are neglected. Because pressure (P) is force per unit area, the pressure from equation (2) is

$$\frac{dF_x}{dA} = \frac{dF_x}{dx \, dy} = J_y B_x \, dz = dP \tag{3}$$

or the pressure gradient is

(4) $$\frac{dP}{dz} = J_y B_x$$

Therefore

(5) $$\Delta P = \int_0^{l_h} J_y B_x \, d_z = J_y B_x l_h$$

and since

(6) $$I_e = J_y l_h l_m$$

then

(7) $$\Delta P = \frac{I_e B_y}{l_m}$$

The equivalent circuit of the pump is as found in Figure 3.

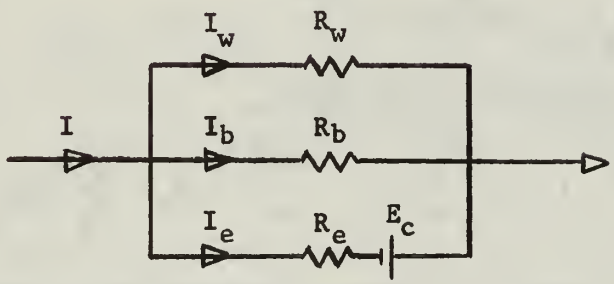

FIGURE 3
PUMP EQUIVALENT CIRCUIT

and therefore

(8) $$I = I_w + I_b + I_e$$

where I_w is the current in the wall, I_b is the current through the weak fields at both the pump exit and entrance, and I_e is the current through the fluid in the strong field between the magnet pole faces.

As,

(9) $$I_w R_w = I_e R_e + E_c$$

and

(10) $$I_b R_b = I_e R_e + E_c$$

then solving equations (8), (9), and (10) simultaneously

$$(11) \qquad I = I_e R_e \left(\frac{R_w + R_b}{R_w R_b} \right) + I_e + E_c \left(\frac{R_w + R_b}{R_w R_b} \right)$$

But,

$$(12) \qquad E_c = B\, l_h\, v \cdot 10^{-8} \quad \text{volts}$$

where v is the velocity of the fluid, and

$$(13) \qquad v = \frac{Q}{l_h\, l_m} \quad \frac{\text{cm}}{\text{sec}}$$

where Q is the flow through the channel, therefore

$$(14) \qquad E_c = \frac{B l_h\, v}{10^8 l_h\, l_m} = \frac{BQ}{10^8 l_m} \quad \text{volts}$$

but from equation (7), substituting for I_c,

$$(15) \qquad Q = \frac{10^8 l_m}{B} \left[I \left(\frac{R_w R_b}{R_w + R_b} \right) - \frac{10 P l_m}{B} \left(R_e + \frac{R_w R_b}{R_w + R_b} \right) \right] \quad \frac{\text{cm}^3}{\text{sec}}$$

from which we readily have relationships between design parameters namely, flow versus current, magnetic field intensity, and pump geometry. To develop static pressures, Q = 0 and therefore

$$(16) \qquad P_s = \frac{BI}{10 l_m} \left[\frac{R_w R_b}{R_w R_b + R_e (R_w + R_b)} \right] \quad \frac{\text{dynes}}{\text{cm}^2}$$

From equations (15) and (16) it can be seen that static pressure and flow rate both vary in a linear manner with the design parameters.

In order to determine pump efficiency, the potential difference between the electrodes is

$$(17) \qquad V_t = E_e + I_e R_e = \frac{BQ}{10^8 l_m} + \frac{10 P l_m R_e}{B} \quad \text{volts}$$

and the power input is therefore

(18) $$W_t = V_t I = I\left[\frac{BQ}{10^8 l_m} + \frac{10Pl_m R_e}{B}\right] \quad \text{watts}$$

giving an efficiency of

(19) $$\eta_p = \frac{10^{-7}\,PQ}{I\left[\frac{BQ}{10^8 l_m} + \frac{10Pl_m R_e}{B}\right]}$$

(20) $$\eta_p = \frac{10Pl_m}{BI}\left[\frac{IR_eR_b - \frac{10Pl_m}{B}(R_wR_b + R_eR_b + R_eR_w)}{IR_wR_b - \frac{10Pl_m}{B}(R_wR_b)}\right]$$

And, also considering the energy required to maintain the magnetic field,

(21) $$\eta_T = \frac{10Pl_m}{BI}\left[\frac{IR_wR_b - \frac{10Pl_m}{B}(R_wR_b + R_eR_b + R_eR_w)}{IR_wR_b - \frac{10Pl_m}{B}(R_wR_b) + \frac{I_m^2 R_m}{I}(R_w + R_b)}\right]$$

where R_m is the coil resistance and I_m is the coil current. It should be noted that this efficiency neglects hydraulic losses in both the pump and system which will, of course, have to be taken into account in a practical analysis.

PRACTICAL APPLICATION OF MODEL

With the theory here developed it is possible to predict the action of a pump whose physical configuration is known. Assume, therefore, the pump channel is made of a non-conducting plastic, and therefore:

(16) $$P_s = \frac{BI}{101_m}\left[\frac{R_b}{R_b + R_e\left(1 + \frac{R_b}{R_w}\right)}\right]$$

becomes

(16a) $$P_s = \frac{BI}{101_m}\,\frac{R_b}{R_b + R_e}$$

and

$$(15) \qquad Q = \frac{10^8 l_m}{B}\left[I \frac{R_w R_b}{R_w + R_b} - \frac{10 P l_m}{B}\left(R_e + \frac{R_w R_b}{R_w + R_b} \right) \right]$$

becomes

$$(15a) \qquad Q = \frac{10^8 l_m}{B}\left[I R_b - \frac{10 P l_m}{B} (R_e + R_b) \right]$$

Also, plotting current for a 1:1 ratio pump with square pole pieces, Figure (4) shows that approximately 68% of the current flows directly between the electrodes [25] and thereby corresponds to I_e. From this, quality factor $= \frac{I_e}{I} = \frac{R_b}{R_b + R_e} = 68\%$.

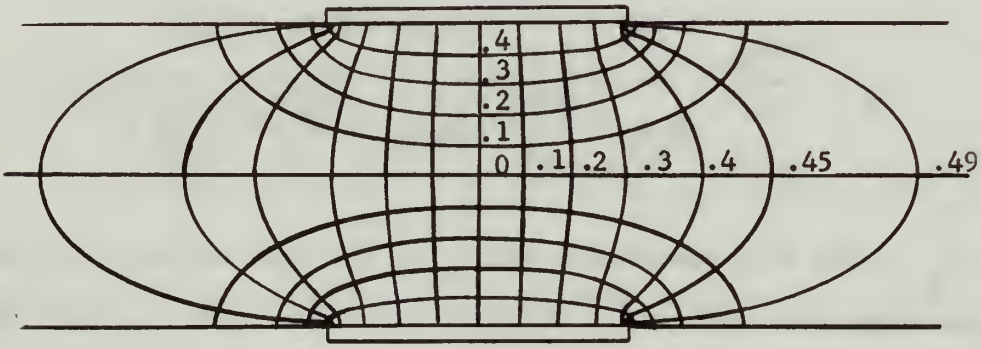

FIGURE 4
THEORETICAL CURRENT DISTRIBUTION

Therefore, using this and a theoretical flux plot to determine R_e and R_b, equations (15a), (16a), and (19) predict static head, flow rate and pump efficiency for any combination of current and flux.

3. PROTOTYPE PUMP

CONSTRUCTION OF PUMP AND SYSTEM #1

INTRODUCTION

The first pump the authors constructed was designed purely as a prototype model. The guiding idea was one of building a workable small pump rather than one of optimization. For this reason little is included on design data; rather, emphasis is placed on experimental results. Appendices I, II, and III contain detailed design data for the author's second pump and system and would be much more beneficial to the reader than similar information on this first pump. Figure 5 is a photograph of the first system.

The authors considered three conducting fluids as possibilities for use in this pump; mercury, sodium-potassium eutectic, and a metallic salt solution. The latter was discarded because of inherent problems with electrolysis in the solution and low maximum output pressures possible. Of the two remaining possibilities, mercury was chosen because the projected plans for this pump included its use in laboratory demonstrations and as such, mercury was an easier fluid to handle. It should be noted that the NAK solution should work very well in this pump even though it was not the designed working fluid.

SYSTEM DESCRIPTION

The magnet body and pole pieces were made of low carbon (10-20) steel which had magnetic characteristics as shown by the magnetization curve of Figure 6. Centered about the pole pieces and as close to the air gap as possible were four coils, each with 800 turns of 12 gauge copper wire. The pump body as shown in schematic in Figure 7 was

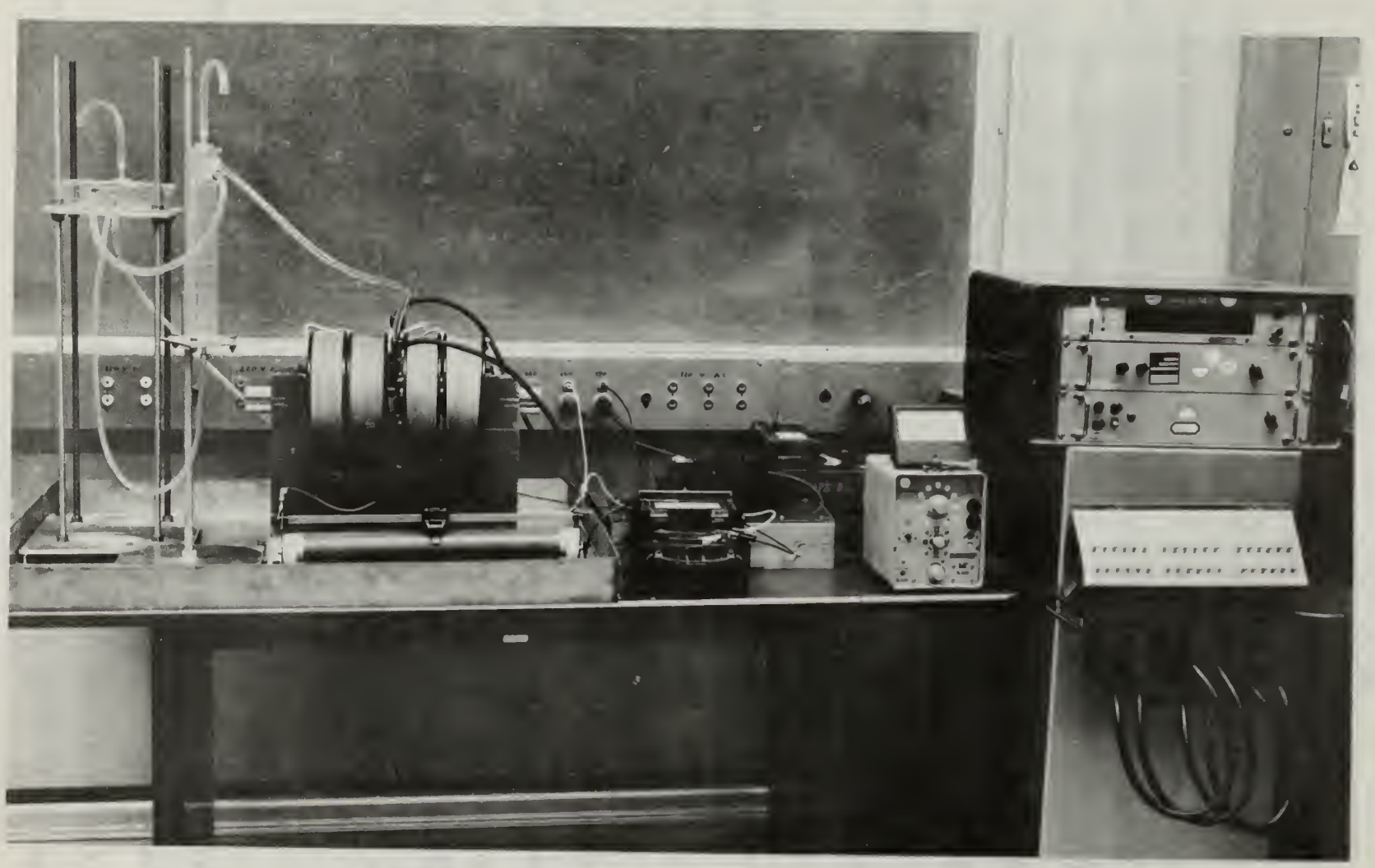

FIGURE 5
FIRST SYSTEM

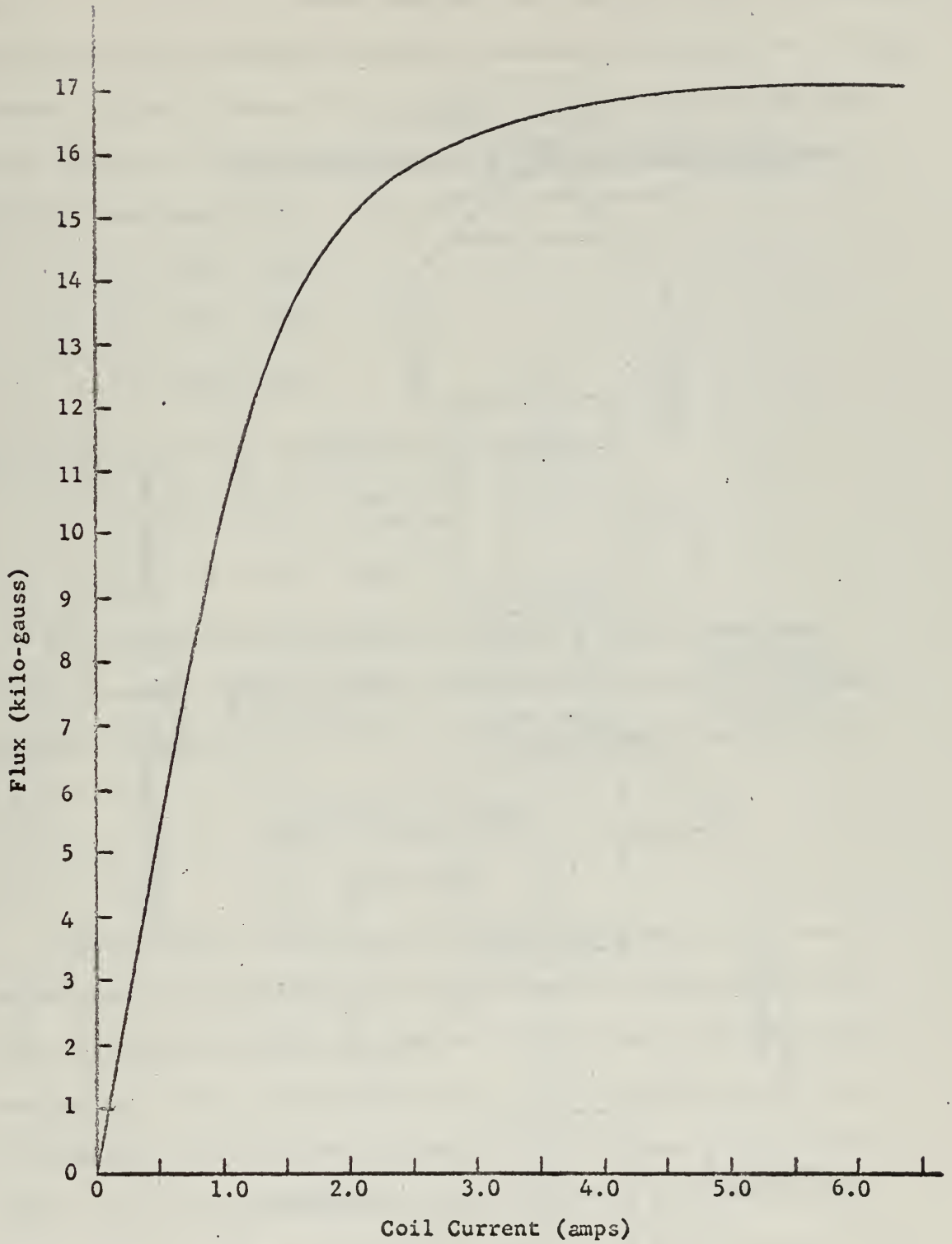

FIGURE 6
D.C. MAGNETIZATION CURVE OF MAGNET NUMBER ONE

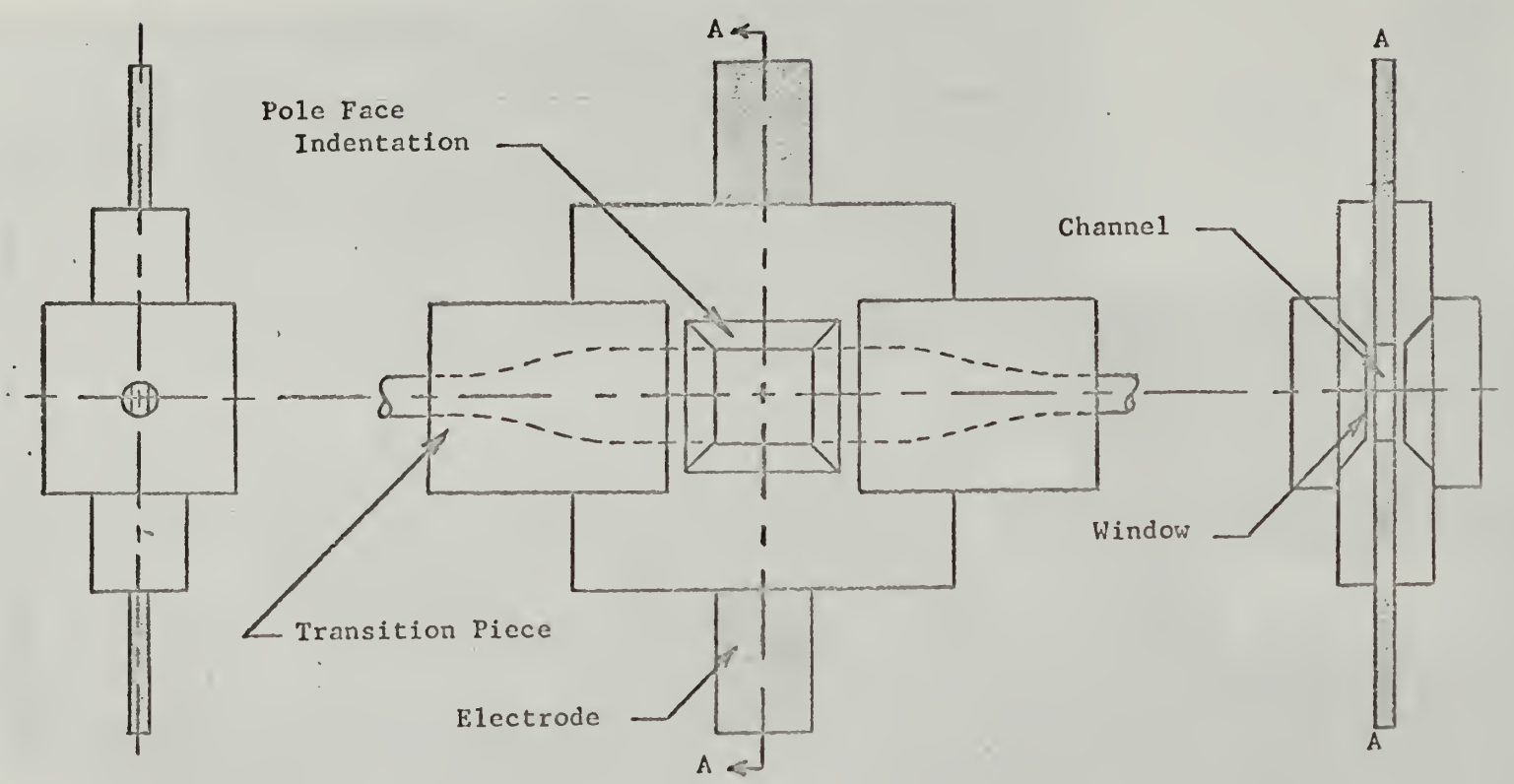

FIGURE 7
SCHEMATIC DRAWING OF PUMP NUMBER ONE

constructed of acrylic plastic and bonded with ethylene di-chloride to perform as one integral piece. Imbedded into the body during construction were two polished tungsten electrodes. Mercury was pumped from a fixed storage reservoir through 1/4 inch Tygon tubing to the pump and then again through 1/4 inch Tygon tubing to a movable receptive reservoir. Critical measurements are:

$$l_e = 1.00 \text{ inch}$$

$$l_h = 1.00 \text{ inch}$$

$$l_m = 0.060 \text{ inch}$$

and, using the theory as suggested in Section 2:

$$R_e = 6.51 \times 10^{-4} \text{ ohm}$$

$$R_b = 1.37 \times 10^{-3} \text{ ohm}$$

Flow and velocity recordings were made by measuring volume of mercury pumped to the receptable reservoir per unit time. All other data were collected as implied by the system schematic of Figure 8.

EXPERIMENTAL RESULTS

STATIC HEAD

Figure 9 shows the theoretically predicted static heads superimposed upon the experimentally obtained heads. Examination shows that the authors actually obtained much higher heads than predicted, especially at high electrode currents. This discrepancy is due to the commonly made approximation that fringe effects of flux are negligible. In the case of square tapered pole tips such as were used here, at a 2 cm distance vertically from the pole in the plane of the tip, there was over 4000 gauss leakage. Leakage such as this inter-

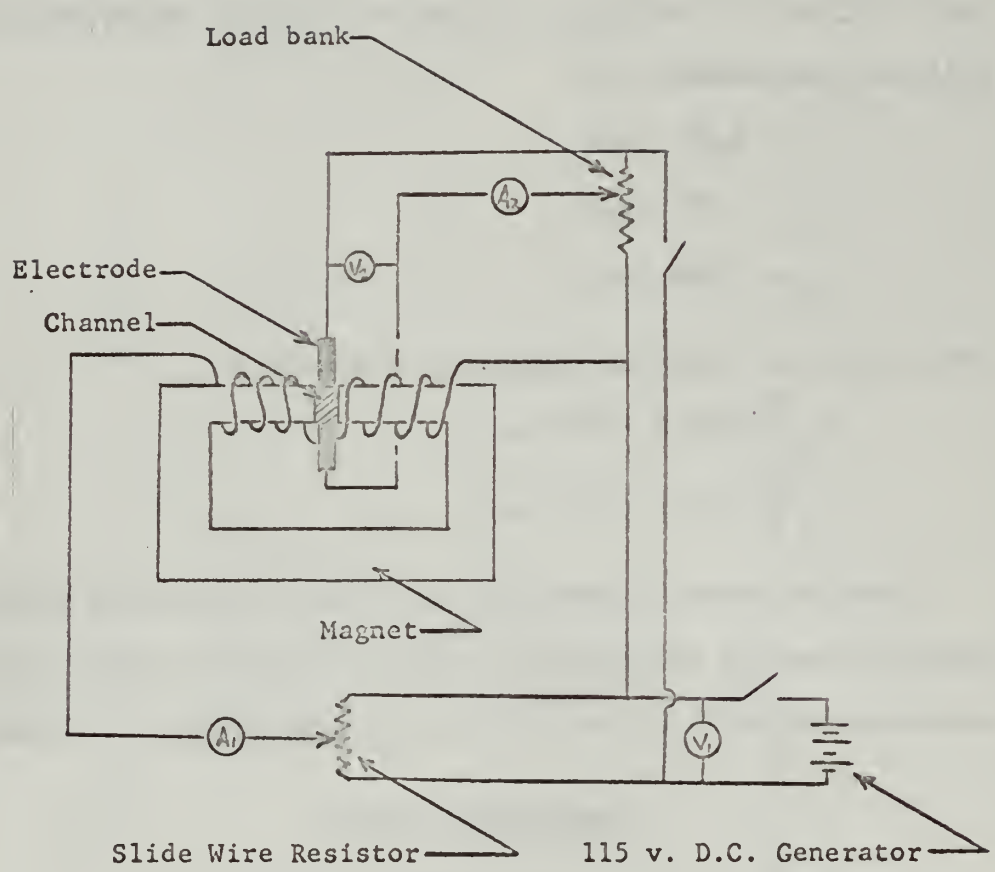

FIGURE 8
SCHEMATIC OF SYSTEM NUMBER ONE

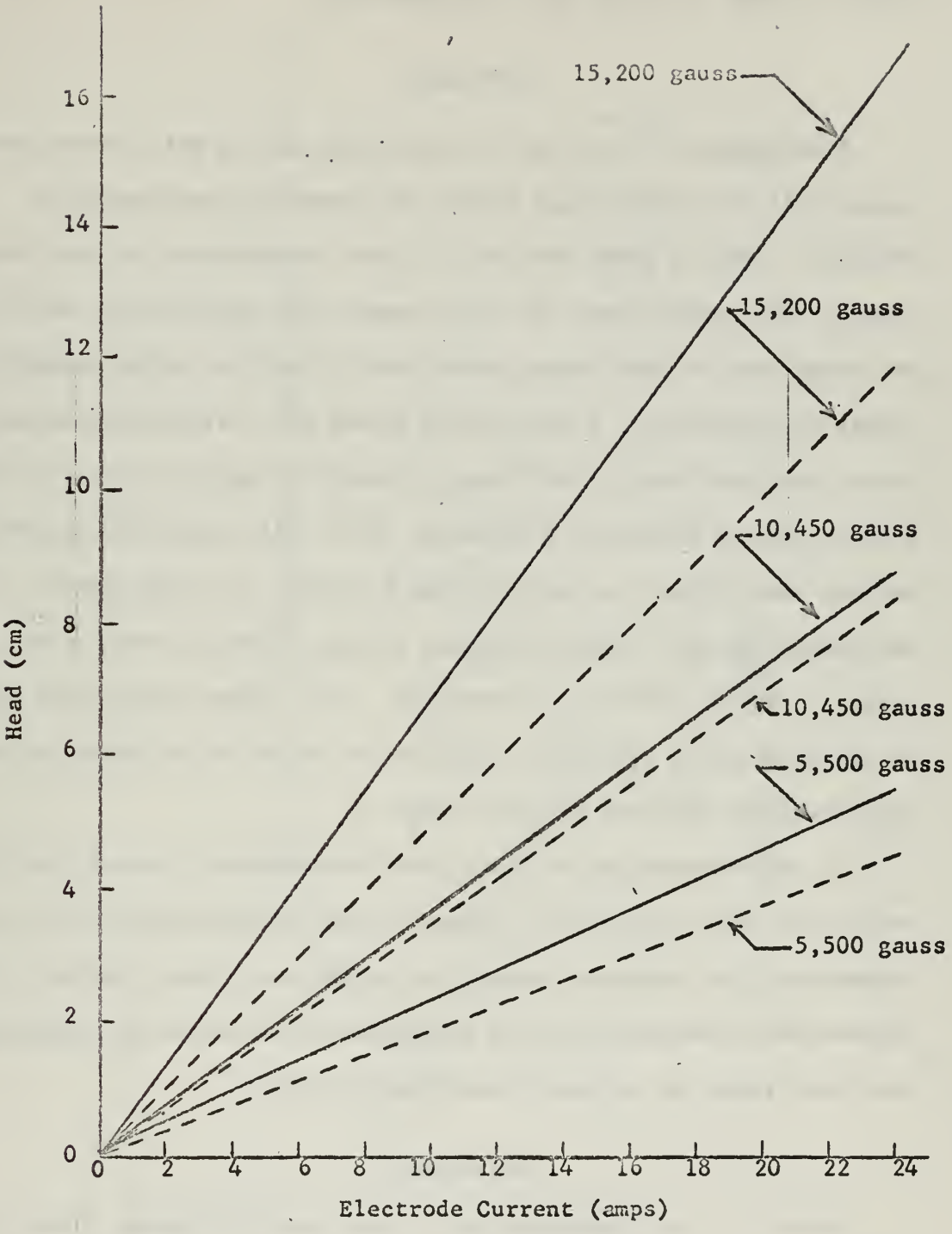

FIGURE 9
STATIC HEAD VS. ELECTRODE CURRENT

acting with the current pattern shown in Figure 4, enabled significantly greater values of static head than expected.

FLOW RATE

From Figures 10, 11, and 12 comparisons may be made between some theoretical flow versus head values and those data experimentally obtained. Data is shown for both 1/4 inch diameter and 3/8 inch diameter tubing. The authors used 1/4 inch diameter tubing initially until it was found that at flow rates greater than 15 cm^3/sec arcing occurred across the electrode. Investigation showed that cavitation was resulting due to the inability of the tubing to supply enough mercury to the pump without causing excessive turbulence. When this cavitation occurred, mercury vapor formed in the voids and a mercury arc would ensue. After the larger diameter tubing was used, arcing no longer occurred and flow rates of over 20 cm^3/sec were obtained. This larger tubing also served to markedly reduce hydraulic losses of the system as is shown by the experimentally obtained data of Figure 13.

As was observed in the static head measurements, actual flow rates were above those predicted by theory. When the experimental data were compensated for hydraulic losses, the slopes again were similar to the theoretical curve and again the differences were caused by neglecting the flux fringe and current fringe interactions.

EFFICIENCY

Figure 14 is a representation of the pump efficiency. Comparisons between theoretical and actual efficiencies are excellent if actual data is merely replaced in formula (19) for theoretical data. Conversely, correlation is very poor if actual efficiency is calculated by dividing

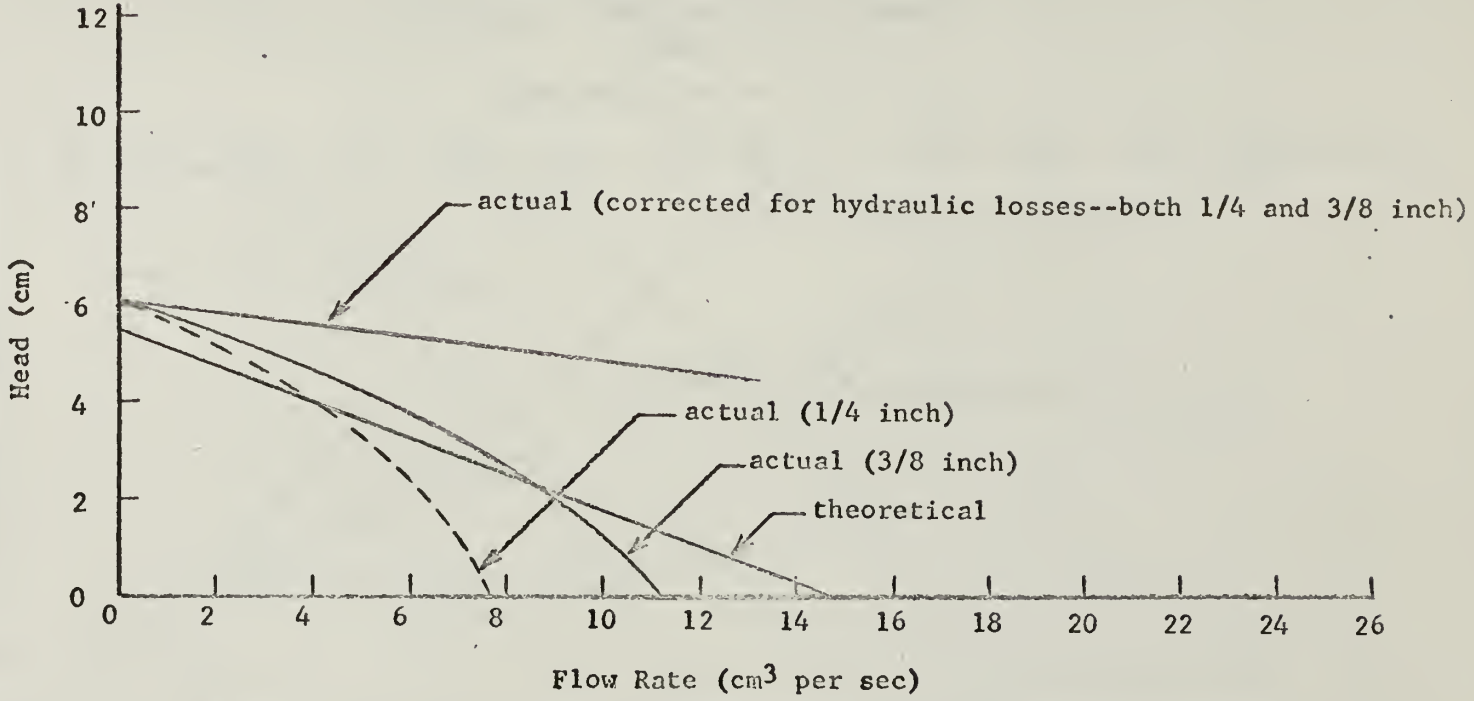

FIGURE 10
FLOW RATE VS. HEAD AT I = 10.8 AMPS.

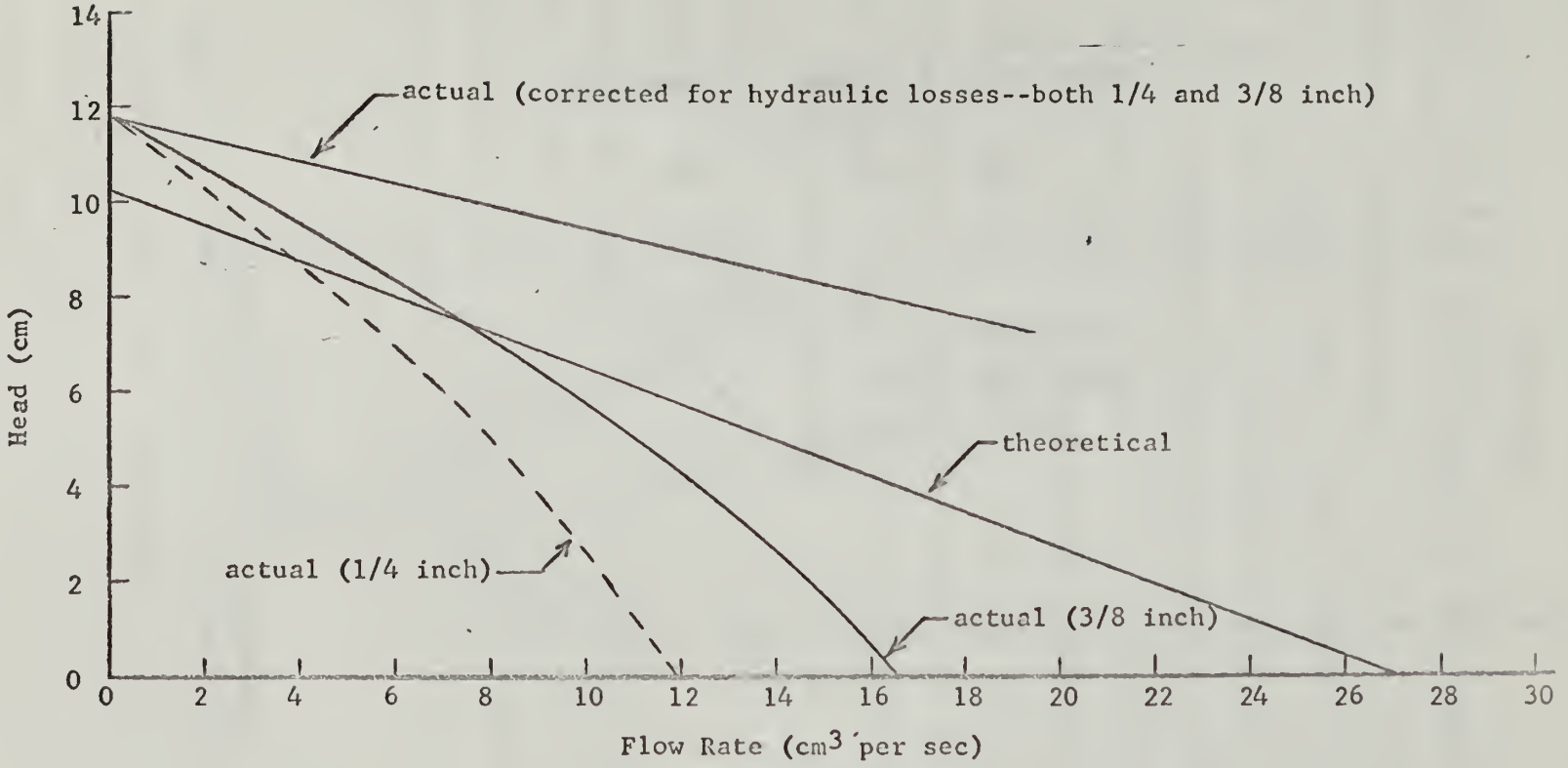

FIGURE 11
FLOW RATE VS. HEAD AT I = 19.7 AMPS.

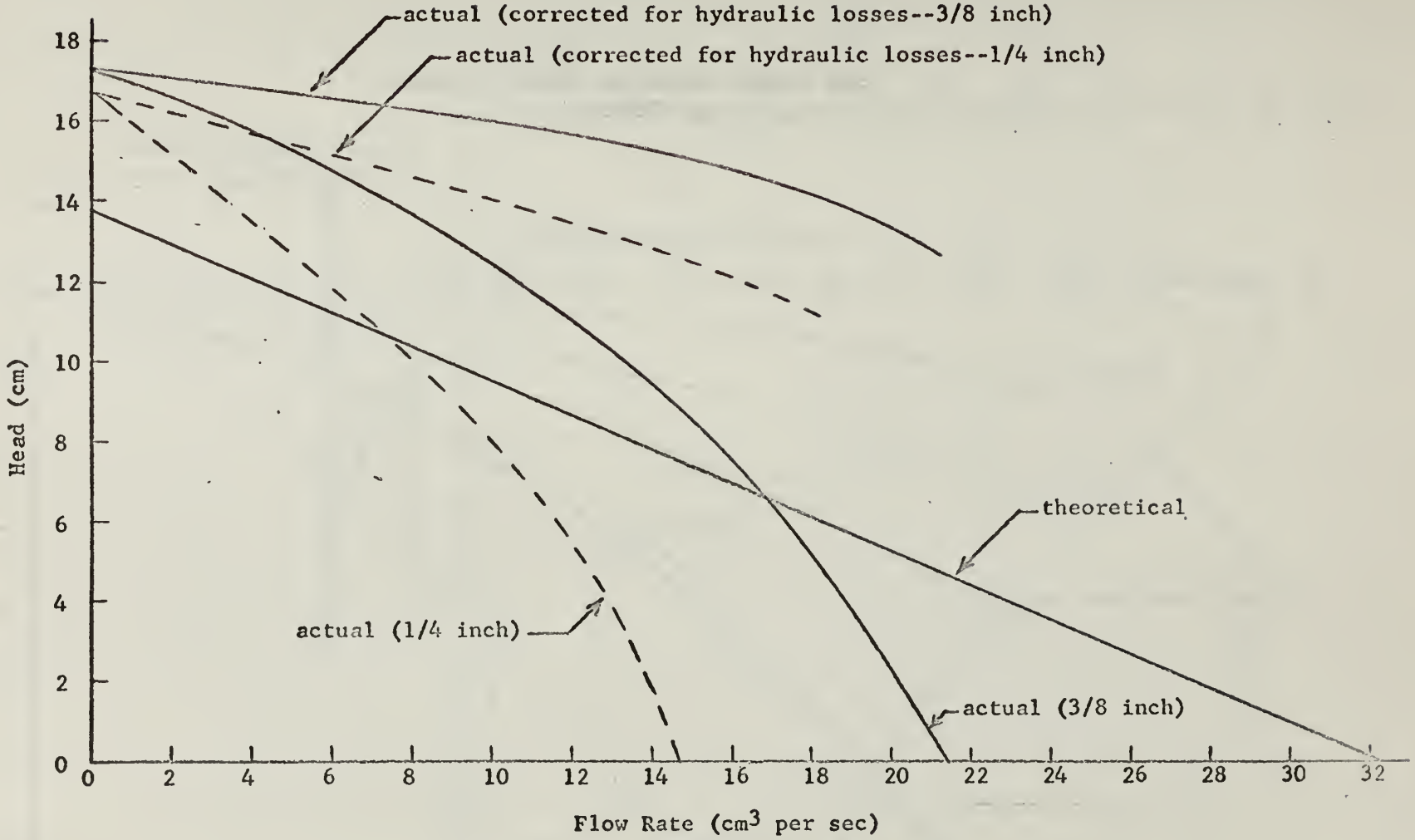

FIGURE 12
FLOW RATE VS. HEAD AT I = 30.4 AMPS.

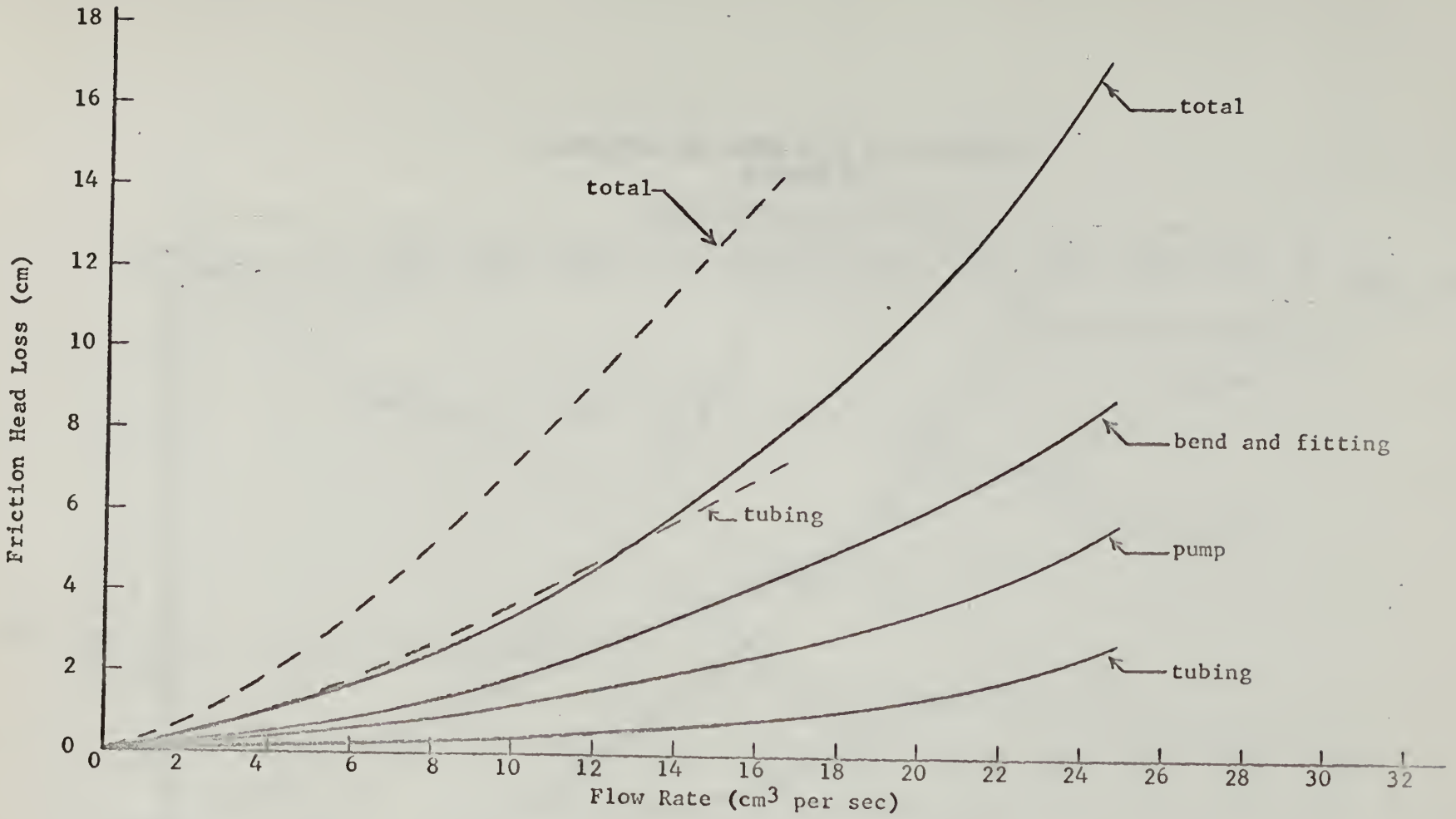

Legend:

- - - - 1/4 inch tubing
——— 3/8 inch tubing

FIGURE 13
HYDRAULIC LOSSES OF SYSTEM NUMBER ONE

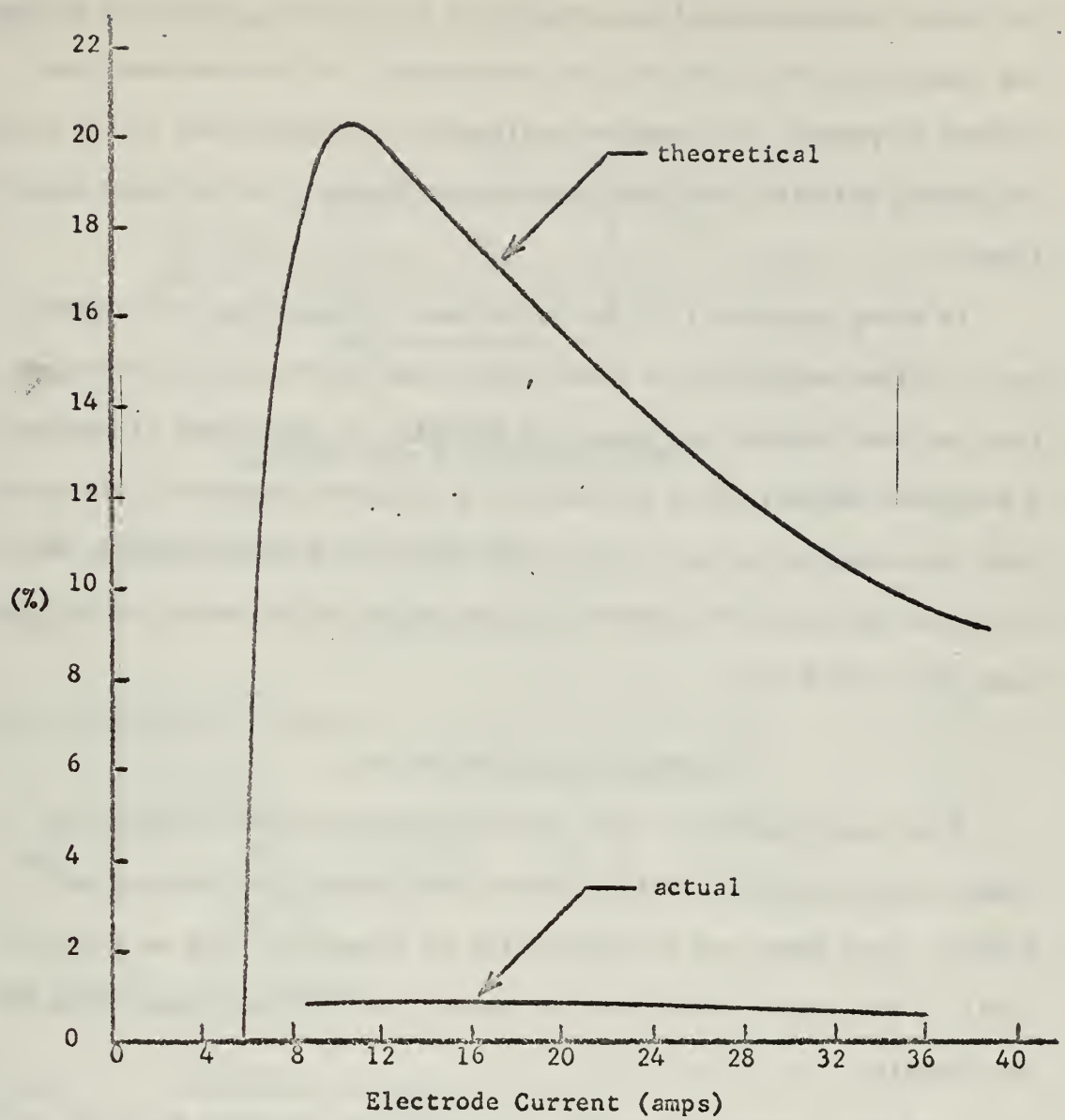

FIGURE 14
PUMP EFFICIENCY VS. ELECTRODE CURRENT

output power by power in. The major cause of this discrepancy is that the theory presented neglects completely any contact resistance between the conducting fluid and the pump electrodes. In the instance when mercury is pumped, this contact resistance is a major part of the circuit resistance and with many other conducting fluids it is at least significant.

In using equation (19) for efficiency calculations, the authors are in effect neglecting as power input that power used by the magnet. This was done because any magnet of any size or efficiency (including a permanent magnet) which delivered the necessary magnetic field could have been used and as such this power input would be arbitrary. Had this been included both theoretical and actual efficiencies would have been less than 0.1%.

DISCUSSION AND CONCLUSIONS

From the preceding it has been verified that small conduction pumps using relatively small currents can feasibly be constructed. Further, such pumps may be constructed of plastic as long as the heat level of the pumped fluid does not exceed the critical temperature of the plastic.

The tests performed upon the authors' pump indicate that (at least for small pumps) the existing theory does not adequately describe the predicted performance of the static head, flow rate or efficiency of this pump.

Static head and flow rate should be better described if flux fringe interaction with current fringing is included.

Theoretical efficiency would more accurately describe the system if contact resistance were included in the circuit diagram of the pump

and was therefore properly included in the development of the theory. Were this resistance included, Figure 3 would become

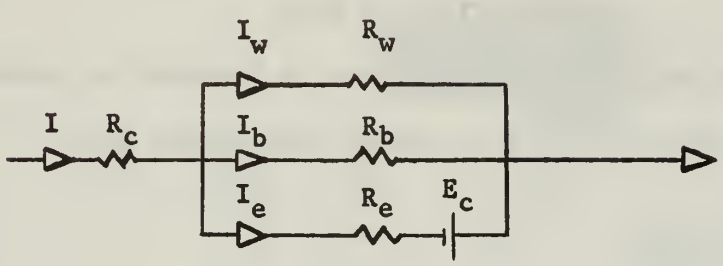

FIGURE 3A
REVISED PUMP EQUIVALENT CIRCUIT

and therefore equation (17) becomes

(17a) $$V_t = E_c + I_e R_e + IR_c$$

and equation (19) becomes

(19a) $$\eta_p = \frac{10^{-7} PQ}{I\left[\frac{BQ}{10^8 l_m} + \frac{10Pl_m R_e}{B} + IR_c\right]}$$

and equation (21) becomes

(21a) $$\eta_p = \frac{10^{-7} PQ}{I\left[\frac{BQ}{10^8 l_m} + \frac{10Pl_m R_e}{B}\right] + I_m^2 R_m}$$

Inasmuch as the contact resistance is quite large relative to other resistances in the pump, it seems advisable that some attempt be made to minimize it. To the authors' knowledge there is very little written in the field to this end.

4. SECOND PUMP

CONSTRUCTION OF PUMP AND SYSTEM #2

CONSTRUCTION OF PUMP

Pump #2, Figure 15, was constructed as designed in Appendix I with no significant deviations. The critical dimensions were:

l_e = 1.000 inch

l_m = 0.060 inch

l_h = 1.000 inch

Channel window thickness = 0.025 inch

Transition inlet diameter = 0.50 inch

CONSTRUCTION OF MAGNET

Attention is directed to Appendix II for all details on magnet design. The magnet performed within 8% of design specifications for flux density per amp turn which is considered good by the authors. The experimentally determined magnetization curve is found in Figure 16.

There were two major deviations from designed parameters due to construction. The first was that, because of the tendency of the copper wire to settle, it was found possible to apply extra turns of wire per coil. As such, actually 3200 turns were applied to each coil. This had the beneficial effect of giving the pump an added reserve of available flux density should it be desired. It was because of these extra turns that the magnetization curve reached the design point of 15,000 gauss before designed current had been applied to the coils.

The second deviation from design concerned coil temperature. Because of the necessity in magnet design to adequately design for hot spots

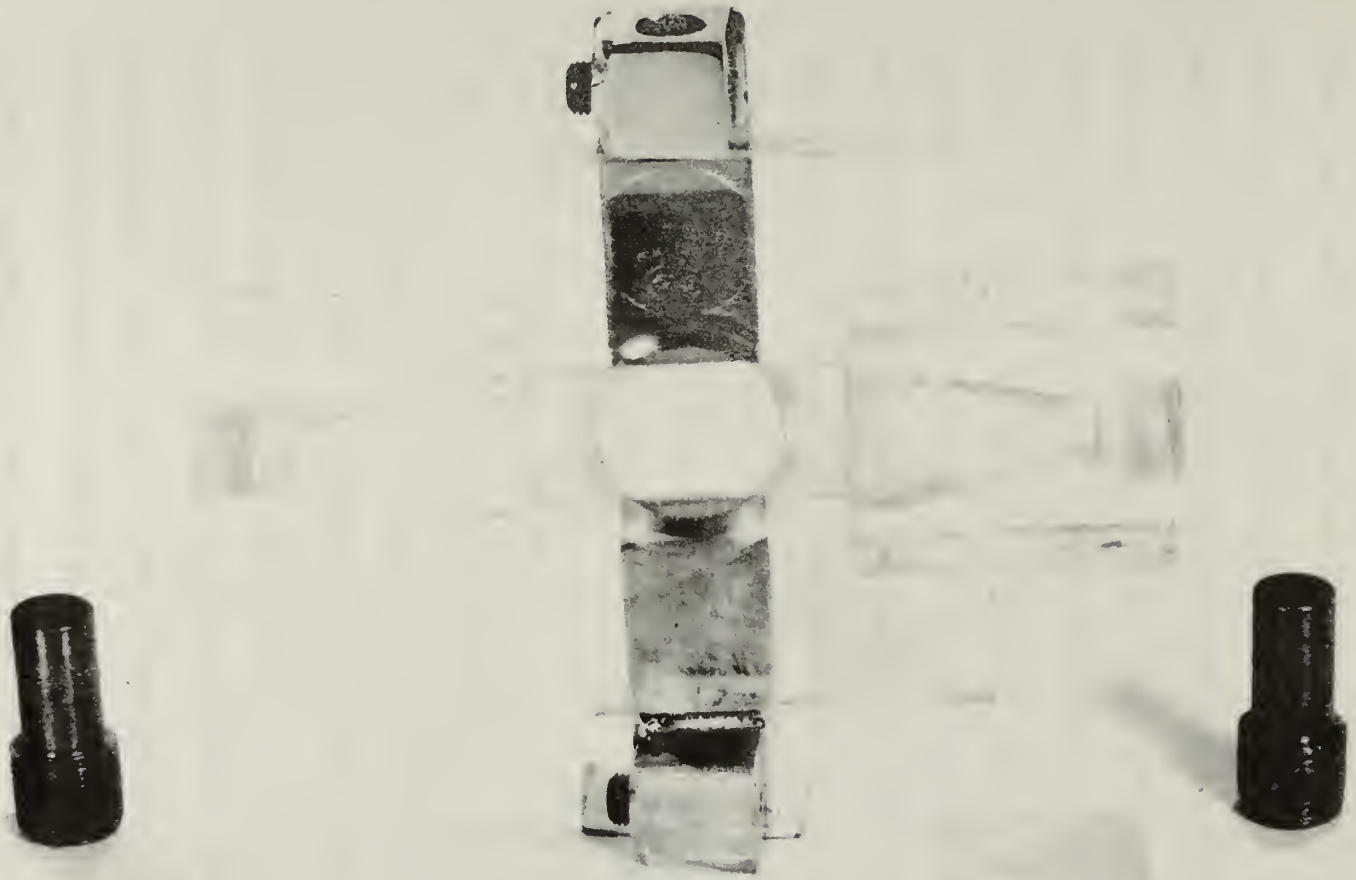

FIGURE 15
SECOND PUMP

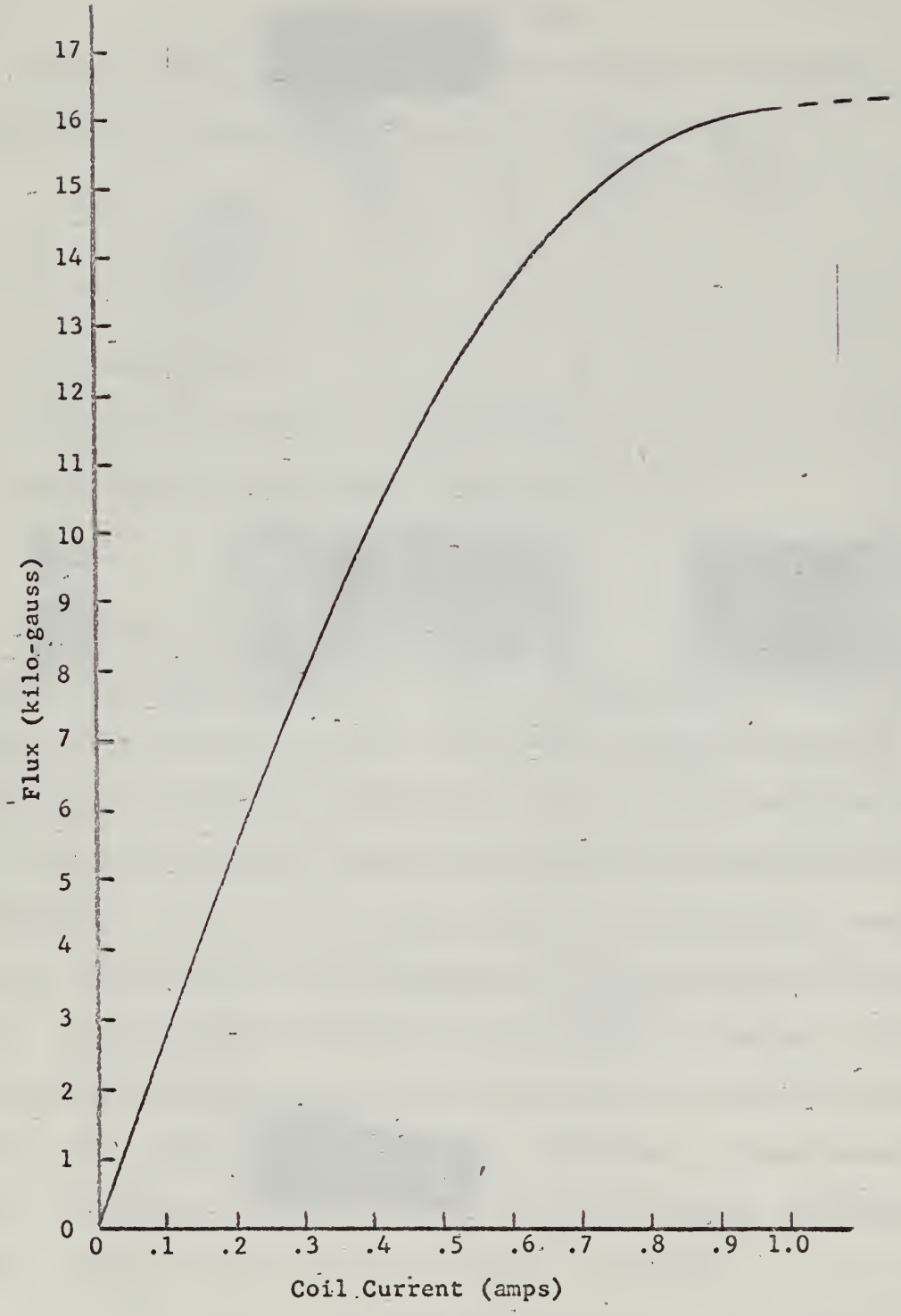

FIGURE 16
D.C. MAGNETIZATION CURVE OF MAGNET NUMBER TWO

within the coil, the authors took pains to allow for heating effects. In actuality it appears the design was very conservative in this respect as virtually no temperature rise was noted on the exterior of the coils after operation at rated current for over one hour. The reasons for this fact are twofold: (a) The coils were carefully constructed by epoxying each layer of wire as it was applied to the coil thus eliminating all air gaps within the coils and providing excellent heat transfer characteristics within the coils themselves, and (b) the authors did not include the magnet yoke as a heat sink for the coils when designing, whereas in actuality because of their very close proximity to the coils and the excellent heat conducting material (copper) separating the coils from the yoke, it was an excellent heat sink and added many square inches of heat transfer surface to the coils.

Neither of these deviations from design impair the magnet or pump operation. On the contrary, they both tend to add versatility to system operation.

CONSTRUCTION OF TEST LOOP

From Section 3 it was observed that increasing the tubing size of the test loop tended to increase the ability of the pump to approach theoretical performance. It also enabled the pump to function at lower loads than were obtainable with smaller diameter tubing. As such the system design of Appendix III incorporated tubing 1/2 inch in diameter. The practical effects of this are described hereafter. There were no major deviations in the construction of the auxiliary parts of the pump system from design. Figure 17A is a photograph of the entire apparatus of this second pump system and Figure 17B is an exploded view of the magnet and pump.

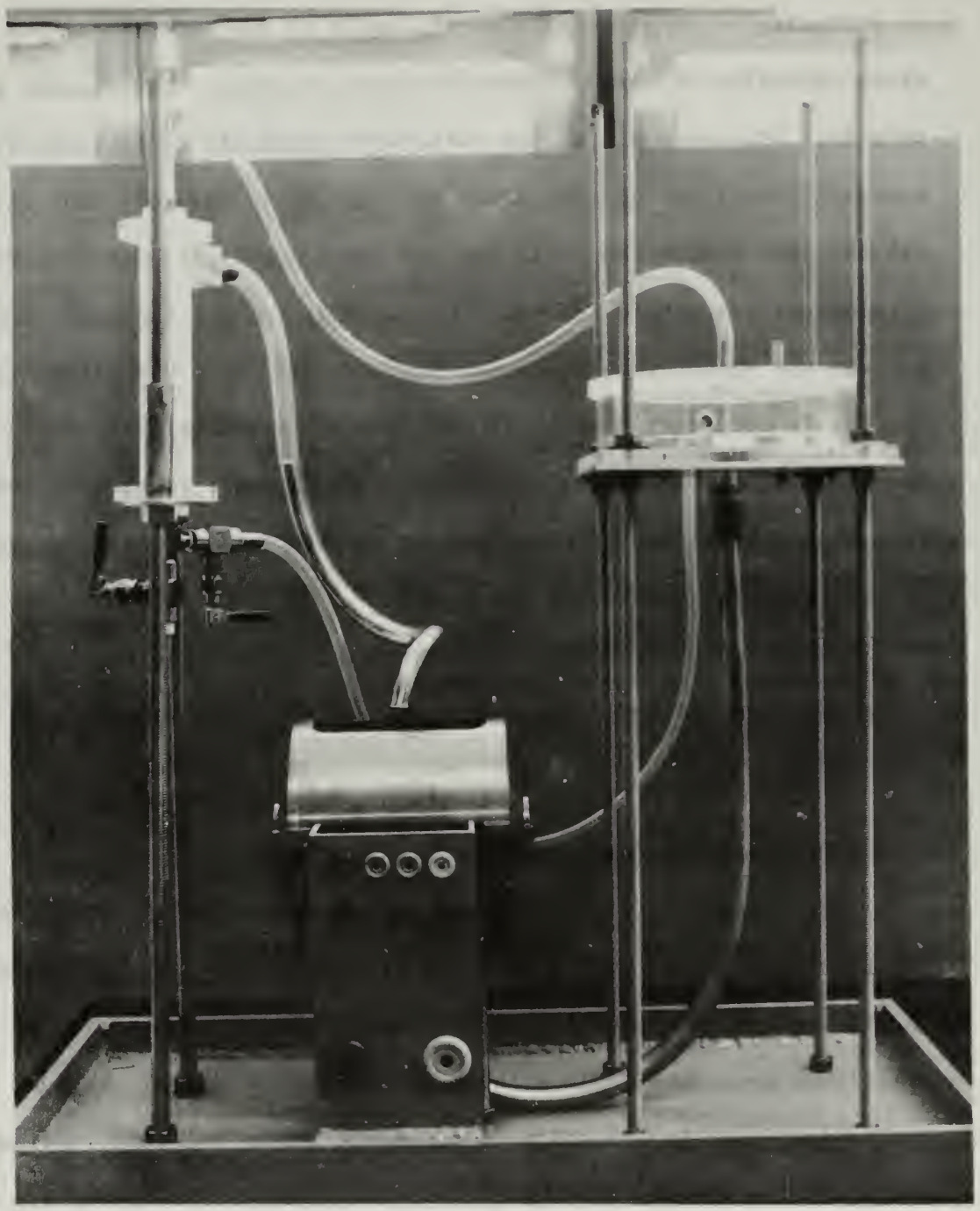

FIGURE 17a
SECOND SYSTEM

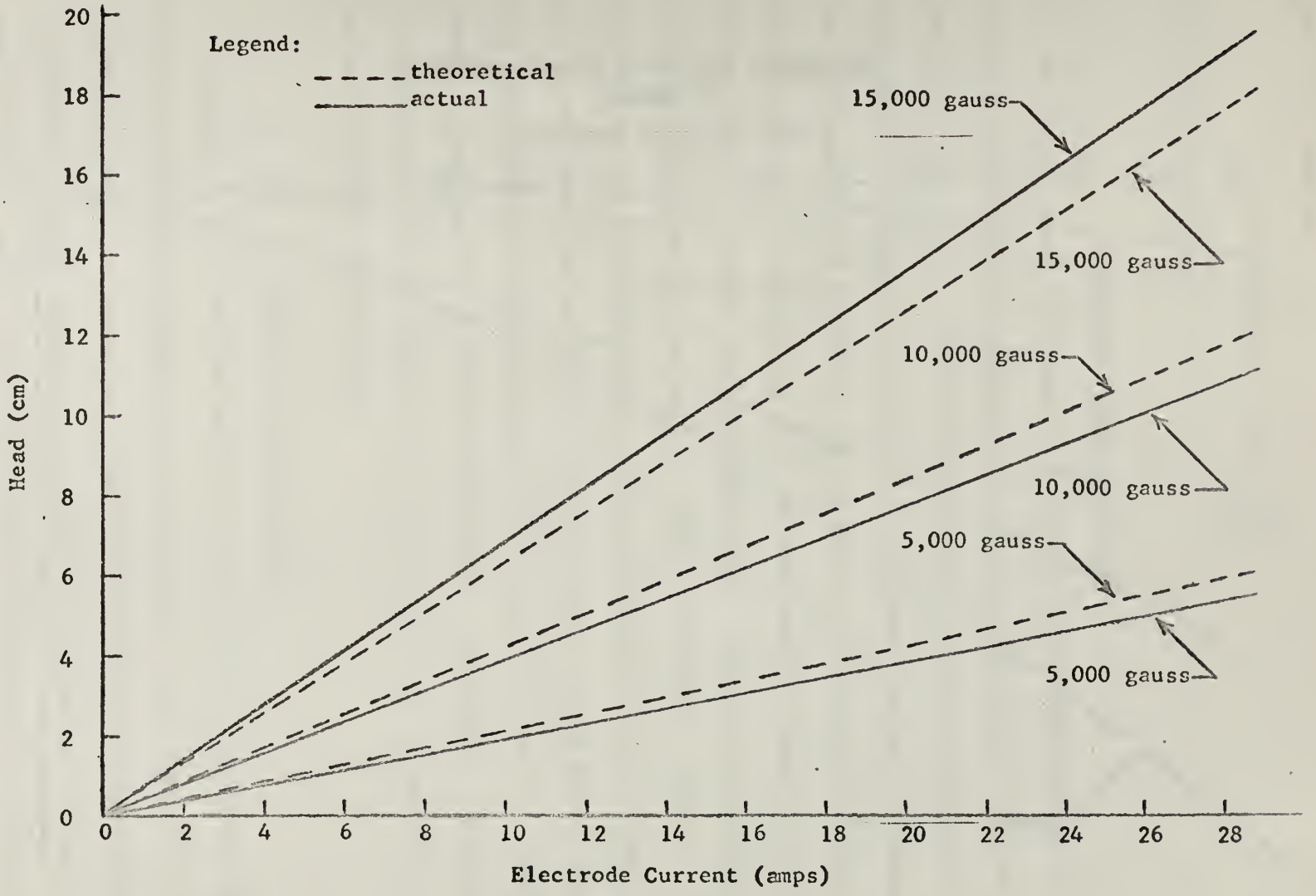

FIGURE 18
STATIC HEAD VS. ELECTRODE CURRENT

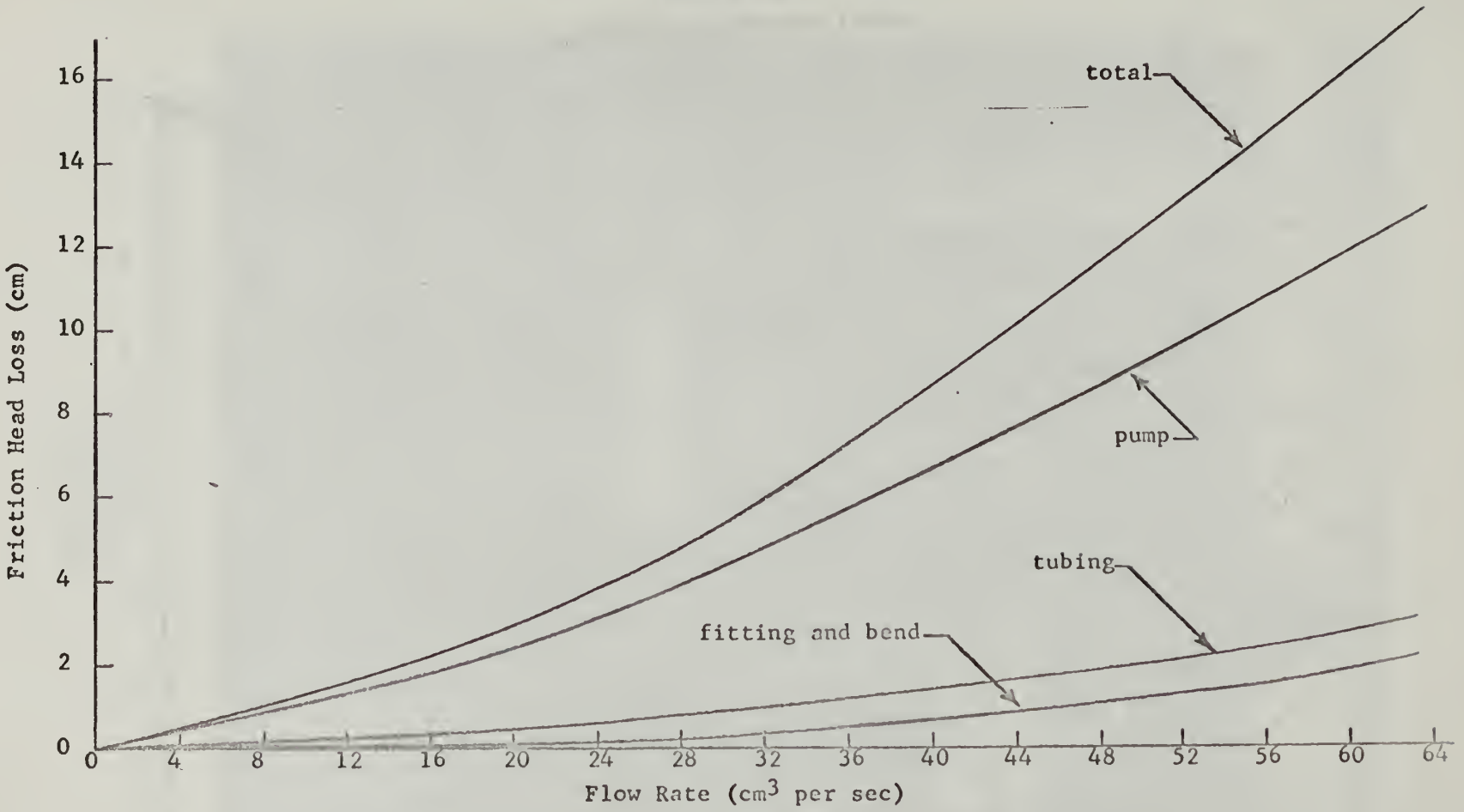

FIGURE 19
HYDRAULIC LOSSES OF SYSTEM NUMBER TWO

authors applied the use of theoretical Reynolds numbers and the basic fluid flow equation

$$\text{Friction head} = (4f)\ \frac{v^2 L}{2g_o D}$$

for various flow rates.

FLOW RATE DETERMINATIONS

Previously there was presented a quality factor modification in an attempt to force more realistic theoretical predictions. This modification is also applicable to determination of flow rate. Figures 20, 21 and 22, illustrate the results of this modification and present the experimental data obtained. As can be seen, the theoretical predictions are still lacking, but they are considerably closer than those used for pump #1. Again, the differences are a result of inaccuracies in the determination of flux-current fringe interactions. Such inaccuracies are more pronounced in flow measurements than in static head measurements because flow of the fluid causes a back EMF in the pole region and therefore the current distribution between the electrodes changes. Consequently, the quality factor will change as a function of fluid velocity and this would have to be accounted for in any truly accurate flow rate predictions.

EFFICIENCY DETERMINATION

In Section 3 the authors modified accepted theory to include the effects of contact resistance on pump efficiency. Using equation (21a) the theoretical efficiencies are compared with the actual efficiencies in Figure 22. Actual values are determined on a power out divided by power in basis. Again the power consumed by the magnet is not considered.

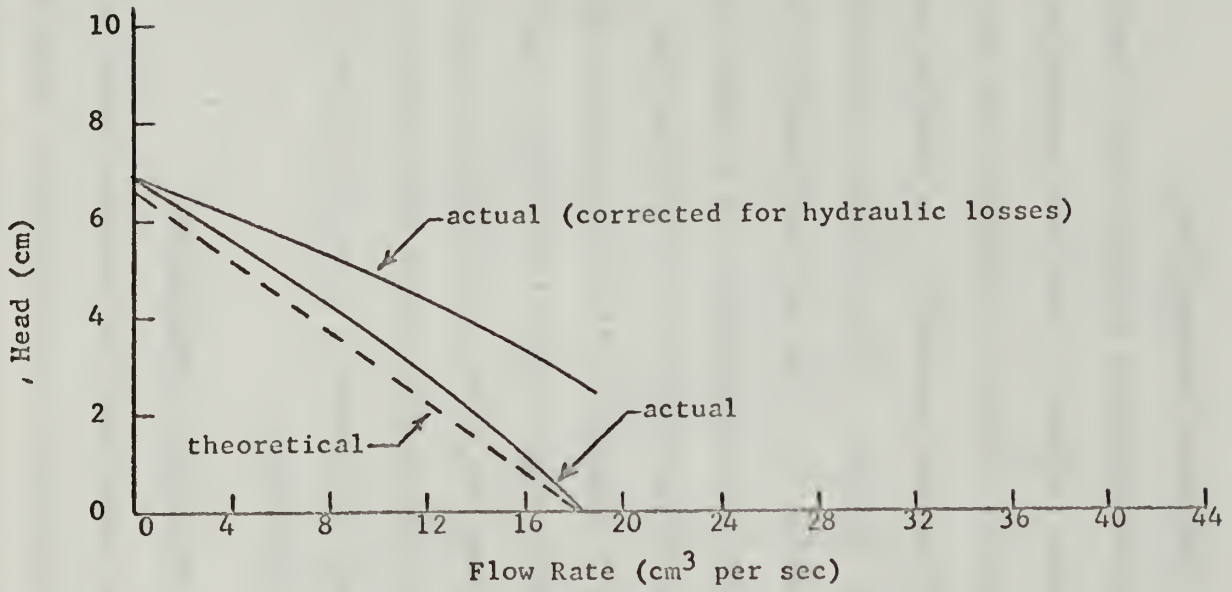

FIGURE 20
FLOW RATE VS. HEAD AT I = 10.4 AMPS.

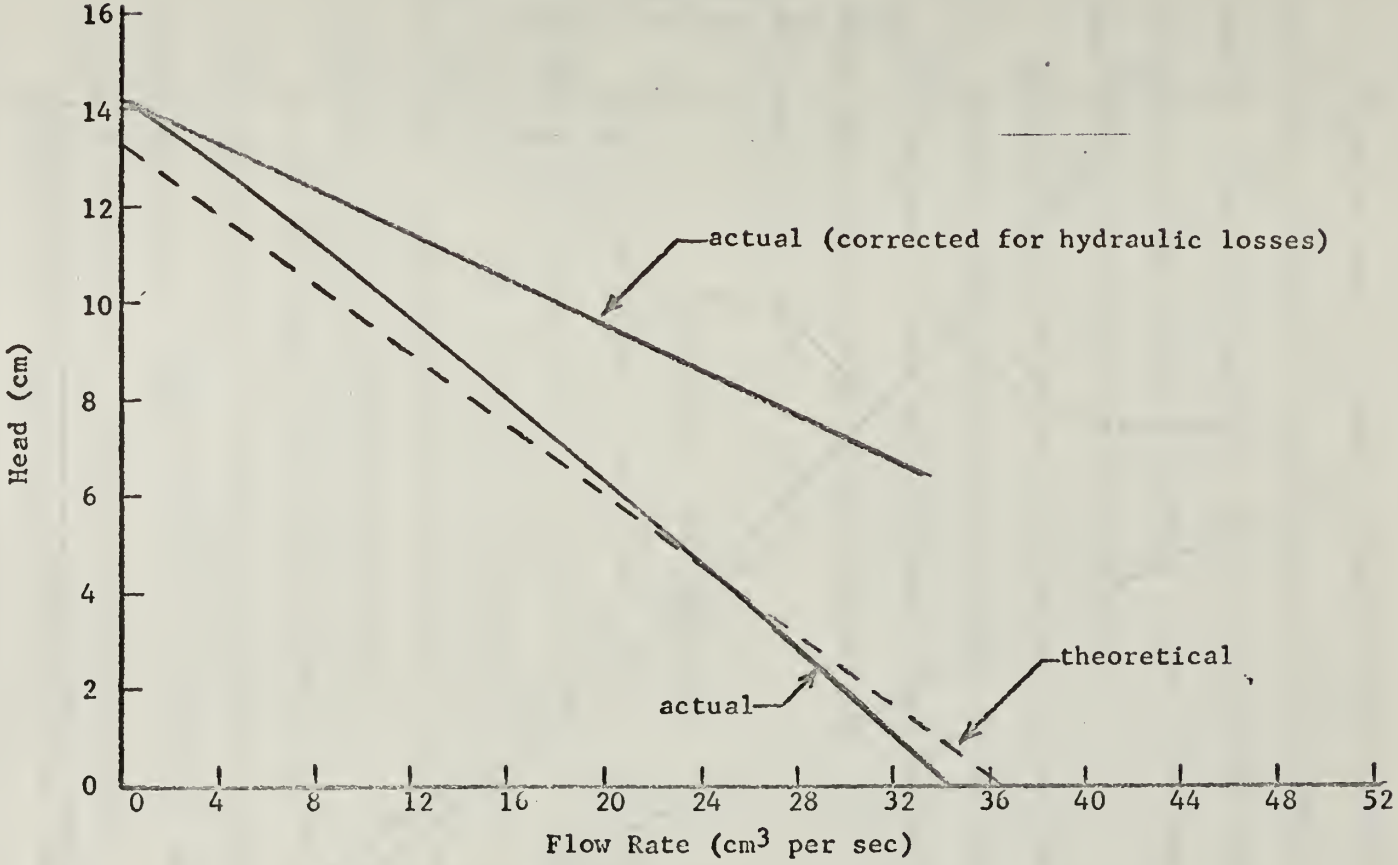

FIGURE 21
FLOW RATE VS. HEAD AT I = 19.7 AMPS.

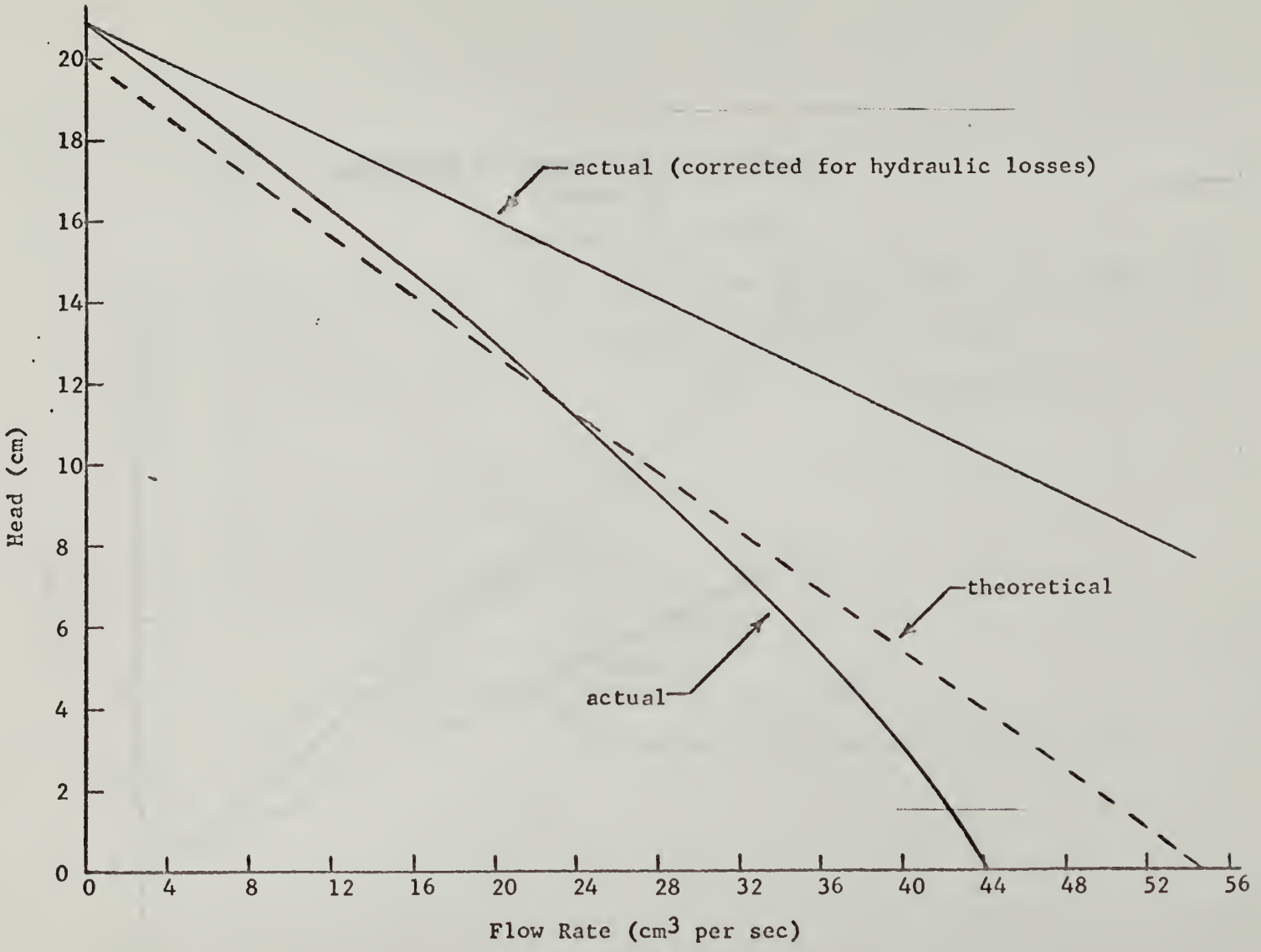

FIGURE 22
FLOW RATE VS. HEAD AT I = 30.4 AMPS.

Figure 23 shows much better correlation between actual and theoretical values than did the data of the first pump. This is due to the inclusion of contact resistance in the theoretical calculations and to the improved actual efficiency of the second pump.

As can be seen by comparing Figure 23 with Figure 14 actual efficiency is almost six times greater with this pump than it was with pump #1. The major reason for this is the greatly reduced contact resistance of the rhodium electrodes of the second pump over the tungsten ones of the first pump (see Appendix IV).

The fact that all actual efficiencies are very low is characteristic of a channel of thin width such as employed in this pump. One could easily increase its over-all efficiency merely by increasing the channel width (air gap) and either accept somewhat lower flux densities or change the characteristics of the magnet.

DISCUSSION AND CONCLUSIONS

From the preceding it can be seen that as hypothesized in Section 3, theoretical predictions of flow rate and static head were improved by including fringe flux-current interactions. Also, theoretical predictions of pump efficiencies were improved when contact resistance was included in the theoretical development.

It was also observed that friction was decreased significantly in the system when 1/2 inch tubing and larger transition inlets were used. This had the effect of increasing flow rates and decreasing the tendency of the pump to cavitate at high flow rates.

Further it was noted that pump efficiency was increased sixfold with the utilization of rhodium electrodes combined with reduced system friction.

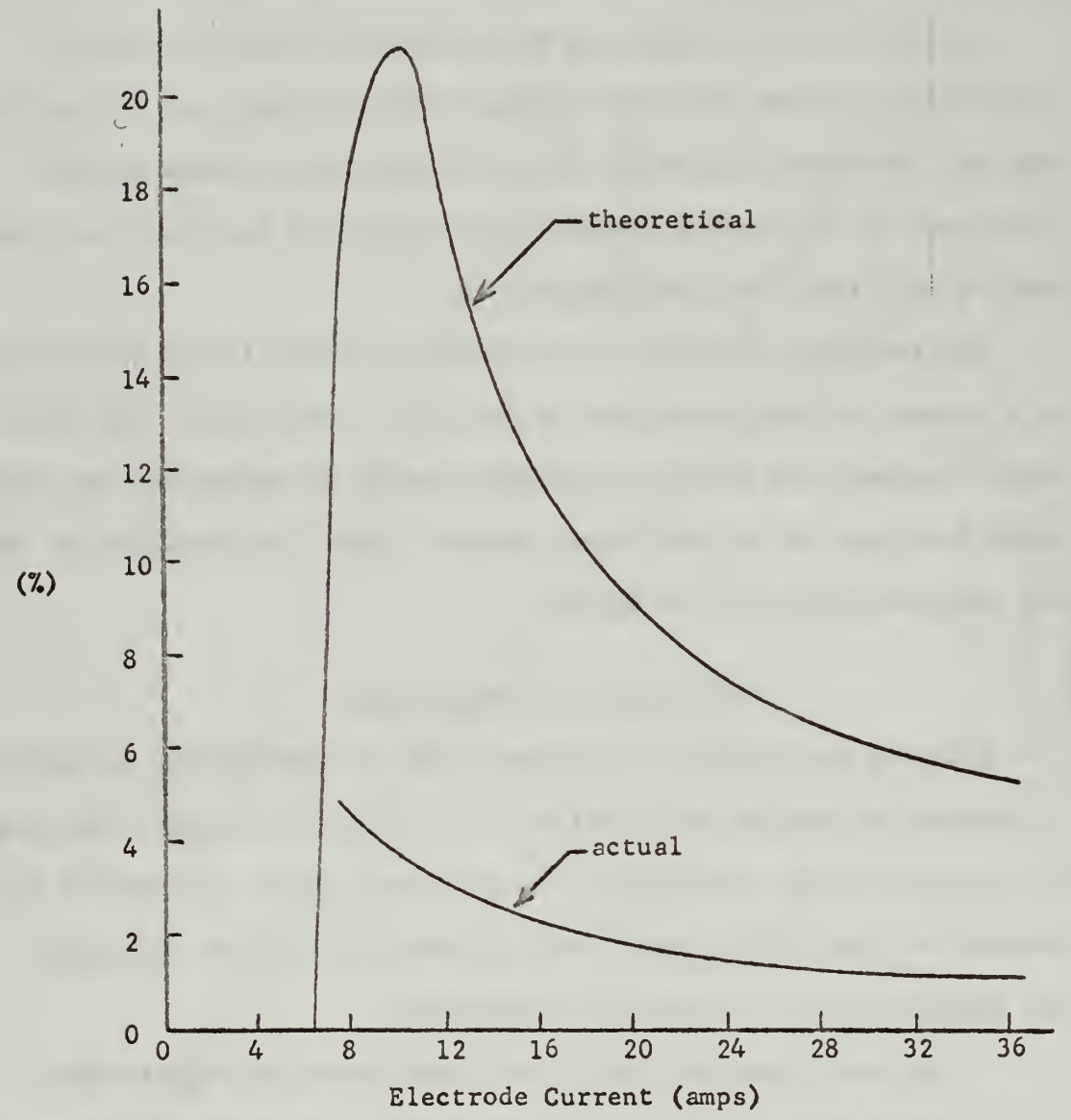

FIGURE 23
PUMP EFFICIENCY VS. ELECTRODE CURRENT

It is worth noting that even a theoretical quality factor of 85% is apparently lower than actual. It is the unique geometrical configuration of the channel of thin width and rectangular inlets immediately preceding and following the poles which enables attainment of such a high quality factor. A still higher quality factor could be obtained if the distance between the electrodes was lessened, or if the shape of the pole faces was changed to more closely coincide with the current distribution.

5. SUMMARY

CONCLUSIONS

By building and successfully testing two small D C. conduction pumps the authors have shown the feasibility of using small currents to obtain reasonable mercury flow rates. Further, the feasibility and usefulness of acrylic as a construction material for the pump has been demonstrated.

The authors have shown the desirability of including the effects of contact resistance and of flux-current fringe interactions in the theoretical calculations to more accurately describe actual pump performance. A feasible method of including these effects has been demonstrated.

Finding a definite lack of concrete information concerning metal-mercury contact resistance, the authors conducted some basic research into this problem. It was found that both rhodium and nickel were wet by mercury at room temperature, while tungsten was not. Rhodium however, had the smallest contact resistance and seemed insensitive to mercury while nickel showed signs of mercuric interaction with time.

RECOMMENDATIONS

ELECTRODE RESEARCH

The topic of suitable electrode materials usable with mercury could well be the object of a Master's Degree thesis. The chemical properties of several likely materials should be thoroughly investigated particularly under the influence of high current densities. Efforts

should be made to understand the phenomenon of wetting, the procedures required to wet various types of materials, and the effect of wetting on rate of corrosion.

FINGE EFFECTS

Much work is yet to be done in the field of flux-current fringe interactions in electromagnetic pumps. Such an investigation could include the effects of flow rates on interaction patterns; the effects of various magnet pole shapes on interaction patterns under both flow and static conditions; and the effects of channel and electrode configurations on these patterns.

PLASTICS

While acrylic worked admirably under the conditions used by the authors, beneficial research could be conducted into the capabilities of several plastics to perform under various conditions of pressure, stress and heat. Because of the inherent advantage of using non-conducting walls, a thorough investigation into this area could be very valuable.

MAGNET DESIGN

Accurate magnet design relies heavily upon flux plotting techniques. As such, three dimensional plotting by hand is virtually impossible if accuracy is desired due to the presence of three mediums -- iron, current and air. Therefore, a good thesis topic could well be the building of an iterative computer program to construct three dimensional flux plots. Such a program would be of definite value in a field where, apparently, practical design is based on a "cut and try" method.

ACKNOWLEDGEMENTS

In the course of arriving at a successful conclusion to this thesis, several people materially assisted the authors. Foremost among these were Frank Abbe and Gordon Gulbranson who were of invaluable assistance in the construction of the hardware and Professors R. Panholzer and M. L. Wilcox who contributed significantly to the theoretical and technical accuracy of this paper.

BIBLIOGRAPHY

1. Agte, C. and Vacek, J. Tungsten and Molybdenum. A Technical Translation by National Aeronautics and Space Administration. F-135, Washington, D. C., 1963.

2. Attwood, Stephen S. Electric and Magnetic Fields. John Wiley and Sons, Inc., New York, 1958.

3. Barnes, A. H. Direct Current Electromagnetic Pump. Nucleonics Vol. 11, No. 1, pp. 16-21, January 1953.

4. Bewley, L. V. Two-Dimensional Fields in Electrical Engineering. The MacMillan Company, New York, 1948.

5. Bitter, Francis. Introduction to Ferromagnetism. McGraw-Hill Book Company, Inc., New York, 1937.

6. Bitter, F., and Reed, F. A New Type of Electromagnet. The Review of Scientific Instruments. Vol. 22, No. 3, March 1951.

7. Corcorran, G. F. Basic Electrical Engineering. John Wiley and Sons, Inc., New York, 1949.

8. Dwight, H. B., and Abt, C. F. The Shape of Core for Laboratory Electromagnets. Review of Scientific Instruments, Vol. 7, 1936.

9. Evans, U. R. The Corrosion and Oxidation of Metals. St. Martin's Press, Inc., New York, 1960.

10. Gauster, W. F. Some Basic Concepts for Magnet Coil Design. American Institute of Electrical Engineers, Vol. 79, Part 1, 1960.

11. Gutierrez, A. U. and Heckathorn, C. E. Electromagnetic Pumps for Liquid Metals. U. S. Naval Postgraduate School, Monterey, California, 1965.

12. Hansen, Max. Constitution of Binary Alloys. McGraw-Hill Book Company, Inc., New York, 1958.

13. Hartman, Jul. Hg-Dynamics I. Levin and Munks Gaard. Copenhagen, 1937.

14. Head, M. A. A Comparison of Two D.C. Electromagnetic Pumps. General Engineering Laboratory R53GL 183. General Electric Company, September, 1953.

15. Hilditch, J. A. S. The Electromagnetic Pumping of Liquid Metals. Atomics and Nuclear Energy, April 1958.

16. Hoag, J. Barton. Nuclear Reactor Experiments. D. Van Nostrand Company, Inc., New York, 1958.

17. Holm, Ragnar. Electric Contacts Handbook. Springer-Verlag OHG., Berlin, Germany, 1958.

18. Kolm, H.;Lax, B.; Bitter, F. and Mills, R. High Magnetic Fields. Proceedings of the International Conference on High Magnetic Fields. The M.I.T. Press and John Wiley and Sons, Inc., New York, 1961.

19. LaQue, F. L. and Copson. H. R. Corrosion Resistance of Metals and Alloys. (2nd Edition) Reinhold Publishing Corp., New York, 1963.

20. Lyon, Richard N. Liquid Metals Handbook. Atomic Energy Commission, Department of the Navy, Washington, D. C., June 1952.

21. McKinney, C. W. Comparison of Electromagnetic Pumps with and without Conducting Walls. AEDC-TDR-64-174, 1964.

22. Moore, A. D. Fundamentals of Electrical Design. McGraw-Hill Book Company, Inc., New York, 1927.

23. Parke, Harry G., and Parke, Ursula T. Minimum Resistance Coil Design. Electrical Engineering, November 1961.

24. Phillips, W. L., Jr. Oxidation of the Platinum Metals in Air. American Society of Metals, Vol. 57, 1964.

25. Rossow, Vernon J.; Jones, Wm. Prichard; Huerta, Robert H. Technical Note D-347. On the Induced Flow of an Electrically Conducting Liquid in a Rectangular Duct by Electric and Magnetic Fields of Finite Extent. Ames Research Center, Moffett Field, California, National Aeronautics and Space Administration, Washington, D. C., January 1961.

26. Roters, Herbert C. Electromagnetic Devices. John Wiley and Sons, Inc., New York, 1961.

27. Steiner, Julius, and John, Hans. Uber electromagnetische Pumpen ohne bewegte Teile zur Förderung flüssiger Metalle. Chemie-Ing. Techn. Jahrg., 1956.

28. Stevenson, A. R., Jr., and Park, R. H. Graphical Determination of Magnetic Fields. Theoretical Considerations. AIEE, February 1927.

29. Strachan, J. F., and Harris, N. L. The Attack of Unstressed Metals by Liquid Mercury. Journal of the Institute of Metals, Vol. 85, 1956-1957.

30. Sucksmith, W., and Anderson, S. P. A General Purpose Electromagnet. Journal of Scientific Instruments, Vol. 33, June 1956.

31. Underhill, Charles Reginald. Coils and Magnet Wire. McGraw-Hill Book Company, Inc., 1925.

32. Vitola, J. Electromagnetic Coil Design Charts. Electrical Manufacturing, Vol. 65, No. 3, March 1960.

33. Watt, D.A. The Design of Electromagnetic Pumps for Liquid Metals. Institution of Electrical Engineers. Paper No. 2763U, December 1958.

34. Weber, Ernst. Electromagnetic Fields, Vol. I - Mapping of Fields. John Wiley and Sons, Inc., New York, 1950.

35. Windred, G. Electrical Contacts. MacMillan and Company, Limited, London, England, 1940.

36. Wollen, W. B. Electromagnetic Pumping of Liquid Metals. Fluid Handling, March 1955.

APPENDIX I

PUMP DESIGN

PRIMARY FEATURES

Design point: 15,000 gauss, 30 amperes main current

Electrode current density = 480 amperes per square inch

l_m = 0.0625 inches

l_h = 1.000 inches

l_e = 1.000 inches

R_{tot} = 0.258 milliohms

R_e = 0.369 milliohms

R_b = 0.860 millohms

R_c = 0.520 milliohms

Electrodes: 0.0625 inches by 1.000 inch rhodium plated copper, epoxied to pump

Pump body: Laminated clear acrylic plastic bonded by fusion

Transition pieces: Die formed clear acrylic plastic. Make transition from 0.0625 inch by 1.000 inch rectangular cross section to 0.500 inch diameter circular cross section.

Window thickness in way of pole pieces = 0.025 inch

Window diameter = 1.25 inch

Maximum static head = 14.93 centimeters mercury

Maximum flow at zero head = 37.7 cubic centimeters per second

Fluid to be pumped: Mercury

End Fittings: Stainless steel

Length of rectangular portion of channel = 2.5 inches

Electrode length = 2 inches overall

Electrode end fittings: Standard allen screw lugs, silver soldered to electrodes

Pump potential at 30 amperes and zero field = 0.023 volts

Power loss at 30 amperes and zero field = 0.700 watts

DISCUSSION OF DESIGN

GENERAL FEATURES

This pump was one of the smaller capacity pumps that has been built. The primary restriction on size was the available DC power supply. It was known from the outset that pumps of small capacity have inherently very low efficiency. Furthermore, the Faraday pump has an inherently low head capability. The primary task was to build a pump which could be used as a laboratory demonstration model. It was desired to be able to demonstrate the high volume capabilities of the Faraday pump and build in a reasonable head capability. Non-conducting walls were used to take full advantage of the small DC current supply. Acrylic plastic was chosen because it was easy to form or machine and was readily available. To obtain a relatively large head capability the channel dimension in the direction of magnetic flux had to be small, but not so small that large friction losses would be sustained. Since main current supply was low, high magnetic flux density was required to obtain reasonable performance. A small air gap was required in order to get a strong magnetic field with low weight. Therefore, the pump was designed with a thin "window" in way of the magnet pole pieces. The pole pieces were accurately fitted to the window to provide support to the plastic against the hydraulic pressure. The rectangular section of the channel was kept as short as

possible to keep friction losses to a minimum. The choice of rhodium plated copper electrodes was based on experiment. See Appendix IV, "Contact Resistance."

TRANSITION PIECES

In order to obtain a satisfactory transition from the rectangular channel to the more efficient circular cross-section a special male die was made. The transitions were formed in two halves over the die, after the acrylic material was heated to 400°F. To obtain strength at connections with external tubing, stainless steel spuds were threaded to the transition pieces. The threads were sealed with 0.005 inch "Teflon" tape.

SHAPE OF MAGNETIC FIELD

Another design feature worthy of mention was the use of circular cross-section pole pieces. This was primarily for ease of construction. However, the manner in which the circular shape was employed served to decrease the force on the fluid at the sides of the channel and increase the force at the center of the channel. This is not presented as the most efficient pole piece shaping by any means. However, this shaping definitely has a beneficial effect on the fluid velocity profile. The pronounced detrimental effect of square shaped pole pieces has been clearly demonstrated by Doctor Vernon J. Rossow [25].

FRINGING EFFECTS

Experience with the prototype pump demonstrated that the simple equivalent circuit theory developed by A. H. Barnes [3] produced only a "ball park" estimate of performance, even with rectangular pole pieces, due to the magnetic field fringing effects. Now the air gap was small in

comparison with the radial dimensions of the pole tip. However, the use of tapered pole pieces resulted in very significant fringing, as determined by flux plotting and verified by measurement (see Figures 24 and 25).

ELECTRICAL RESISTANCE DISCUSSION

The values of electrical resistance used in the theory must be estimated from flux plots to be of any value in design. Even when this is done, only the static (no flow) condition can be accounted for and the resistances R_e and R_b can only be assumed to be constant throughout the operating range. This assumption is known to be incorrect. Consequently the resulting linear relation between head and flow rate cannot be relied upon to give a close prediction of performance. However, since the inaccuracies are on the conservative side, it was safe to design the pump with this theory. See Sections 3 and 4 for a more complete discussion of the theory.

ELECTRICAL RESISTANCE DETERMINATION

Refer to the flux plot of Figure 25. Note that the 15,000 gauss line applies from the pole piece outer diameter to the center of the plot. The Barnes' theory assumes that all magnetic flux is contained within the region bounded by the pole piece diameter. On this basis $I_e=(0.70)(I_{tot})$. Now the resistance of every full flux tube is the same. Therefore the resistance of only one tube need be computed from the plot. Then, the resistance of any number of tubes in parallel can be easily calculated. The first tube off the center line was used as a basis for these computations.

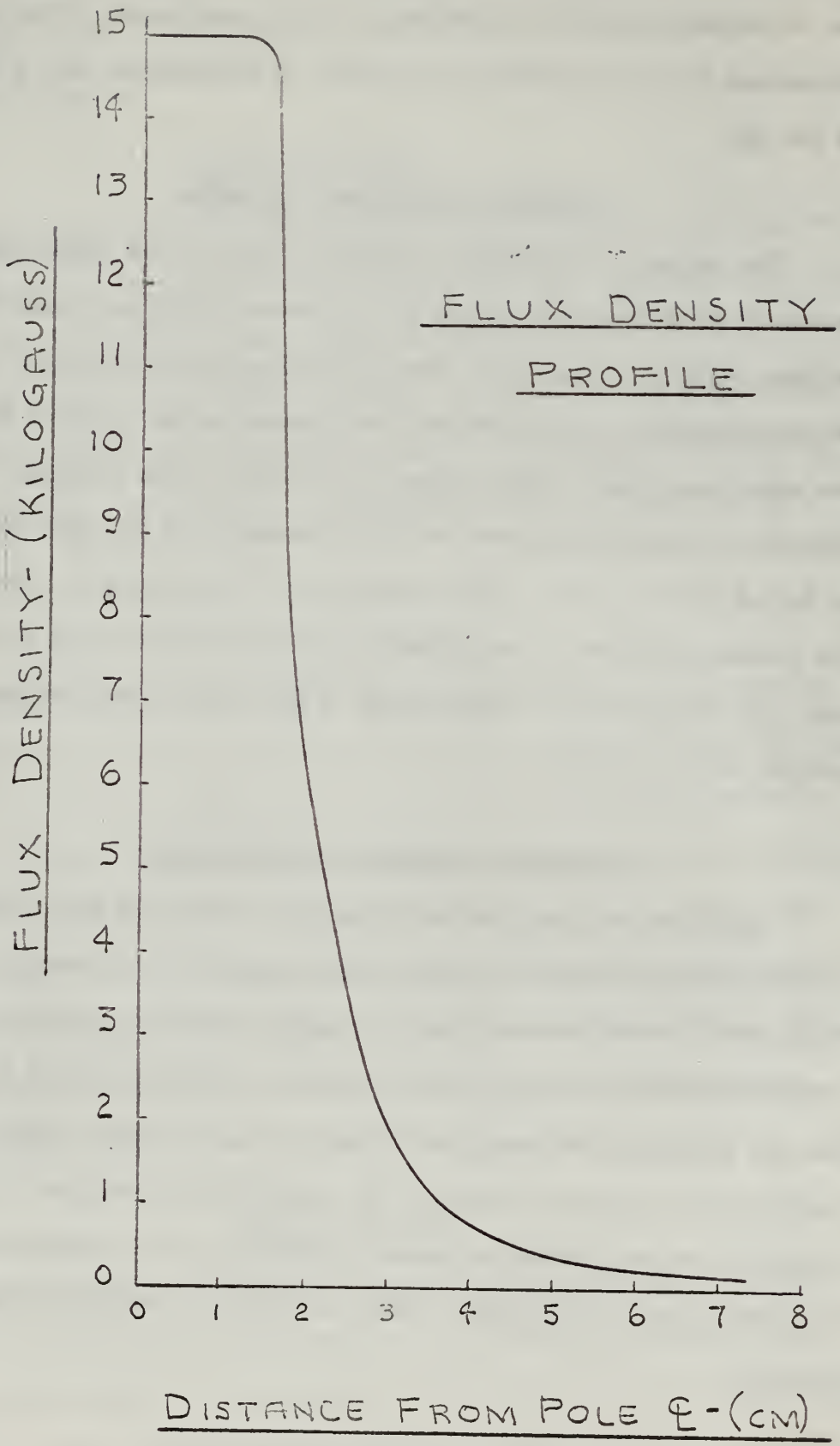

FIGURE 24
MAGNETIC FLUX DENSITY PROFILE

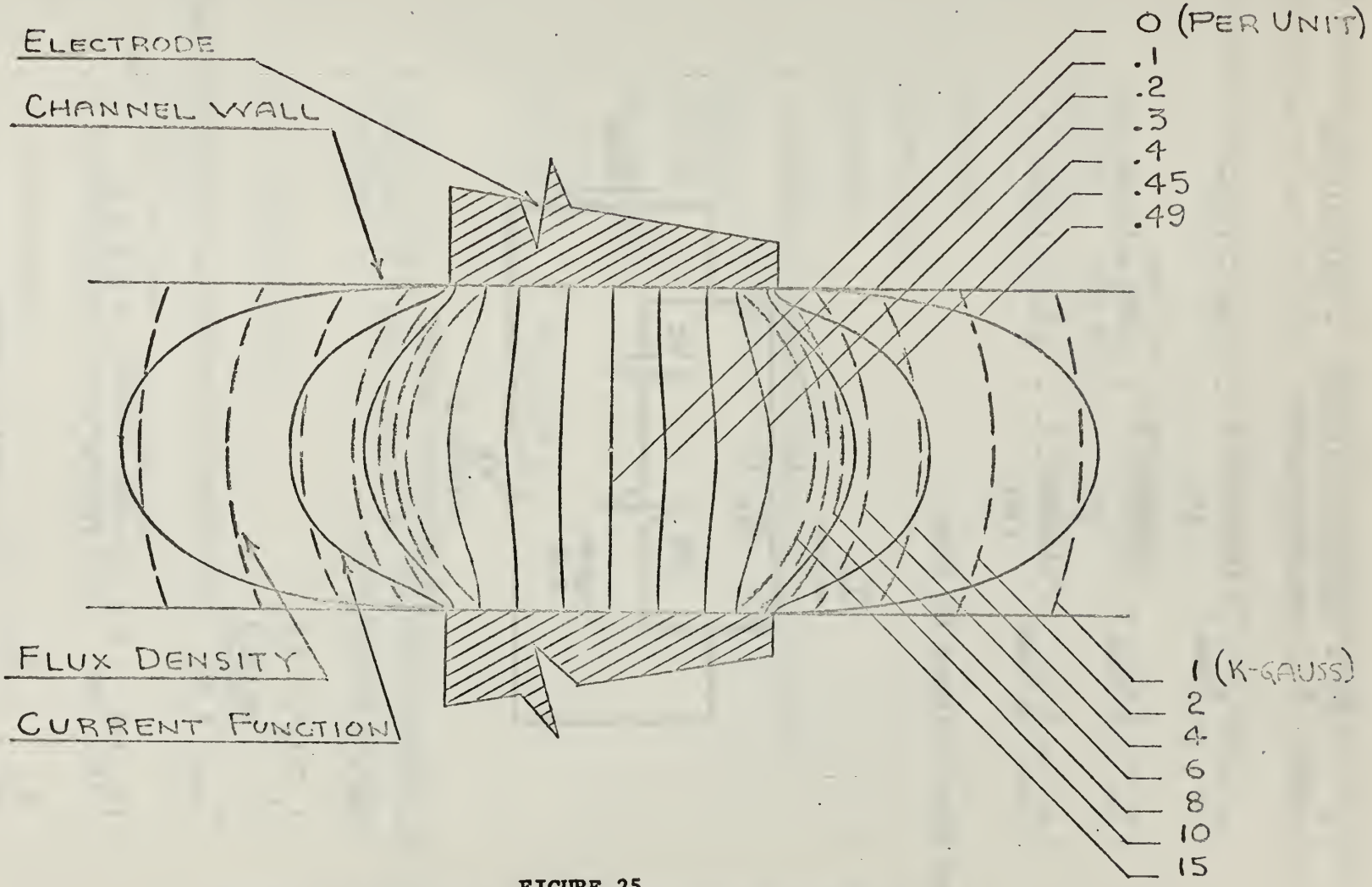

FIGURE 25
MAGNETIC FLUX DENSITY AND CURRENT FUNCTION CONTOURS

$$R_{tube} = \frac{\rho l}{A} = \frac{(96.28)(10^{-6})(2.54)}{(0.1588)(0.596)} = 2.58 \text{ milliohm}$$

$$R_e = \frac{1}{7} R_{tube} = \frac{(2.58)(10^{-3})}{(7)} = 0.369 \text{ milliohm}$$

$$R_b = \frac{1}{3} R_{tube} = \frac{(2.58)(10^{-3})}{(3)} = 0.860 \text{ milliohm}$$

$$R_{tot} = \frac{1}{10} R_{tube} = \frac{(2.58)(10^{-3})}{(10)} = 0.258 \text{ milliohm}$$

Now refer to Figure 26, below

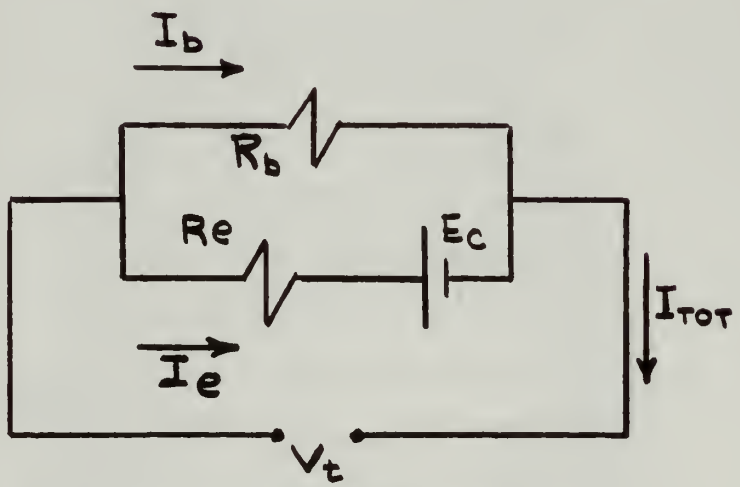

FIGURE 26
PUMP EQUIVALENT CIRCUIT

For $Q = V = 0$, $E_c = 0$.

$$V_t = I_b R_b = I_e R_e$$

$$R_{tot} = \frac{(R_b)(R_e)}{R_b + R_e}$$

$$(I_{tot})(R_{tot}) = V_t = \frac{(I_{tot})(R_b)(R_e)}{(R_b + R_e)} = (I_e)(R_e)$$

$$\frac{I_e}{I_{tot}} = \frac{R_b}{R_b + R_e} = 0.7 = \text{quality factor}$$

This compares with the quality factor of 0.6 for the square pole piece configuration of the prototype. Therefore, the static head capability of the final pump will be 7/6 the capability of the prototype.

OTHER PUMP COMPUTATIONS

$$P_s = \frac{KBI(R_b)}{l_m(R_e+R_b)} = \frac{KBI\ (0.7)}{l_m}$$

$K = (10.2)10^{-8}$

$B = 15{,}000$ gauss

$I = 30$ amperes

$$P_s = \frac{(15{,}000)(30)(10.2)(10^{-8})(0.7)}{(0.1588)} = 0.2023 \text{ kg/cm}^2$$

$$H_s = \frac{(P)(10^3)}{(13.55)}$$

$$H_s = \frac{(0.2023)(10^3)}{(13.55)} = 14.93 \text{ cm}$$

$$Q = \frac{l_m(10^8)}{B}\left[IR_b - \frac{P(l_m)(R_b+R_e)}{KB}\right]$$

$$= \frac{(0.1588)(10^8)}{(15{,}000)}\left[(30)(0.860)(10^{-3}) - \frac{P(0.1588)(1.229)(10^{-3})}{(10.2)(10^{-8})(15{,}000)}\right]$$

$$Q = 27.3 - P(134.7) \text{ cm}^3/\text{sec}$$

Voltage across pump at 30 amperes and zero field

$R_{tot} = 0.258$ milliohms

$R_c = 0.520$ milliohms (From Appendix IV)

$R = 0.778$ milliohms

$V_t = IR = (30)(0.778)(10^{-3}) = 0.0233$ volts

Power loss at 30 amperes and zero field

$$P = I^2R = (900)(0.778)(10^{-3}) = 0.700 \text{ watts}$$

$$\text{Electrode current density} = \frac{30}{(1)(0.0625)} = 480 \text{ amp/in}^2$$

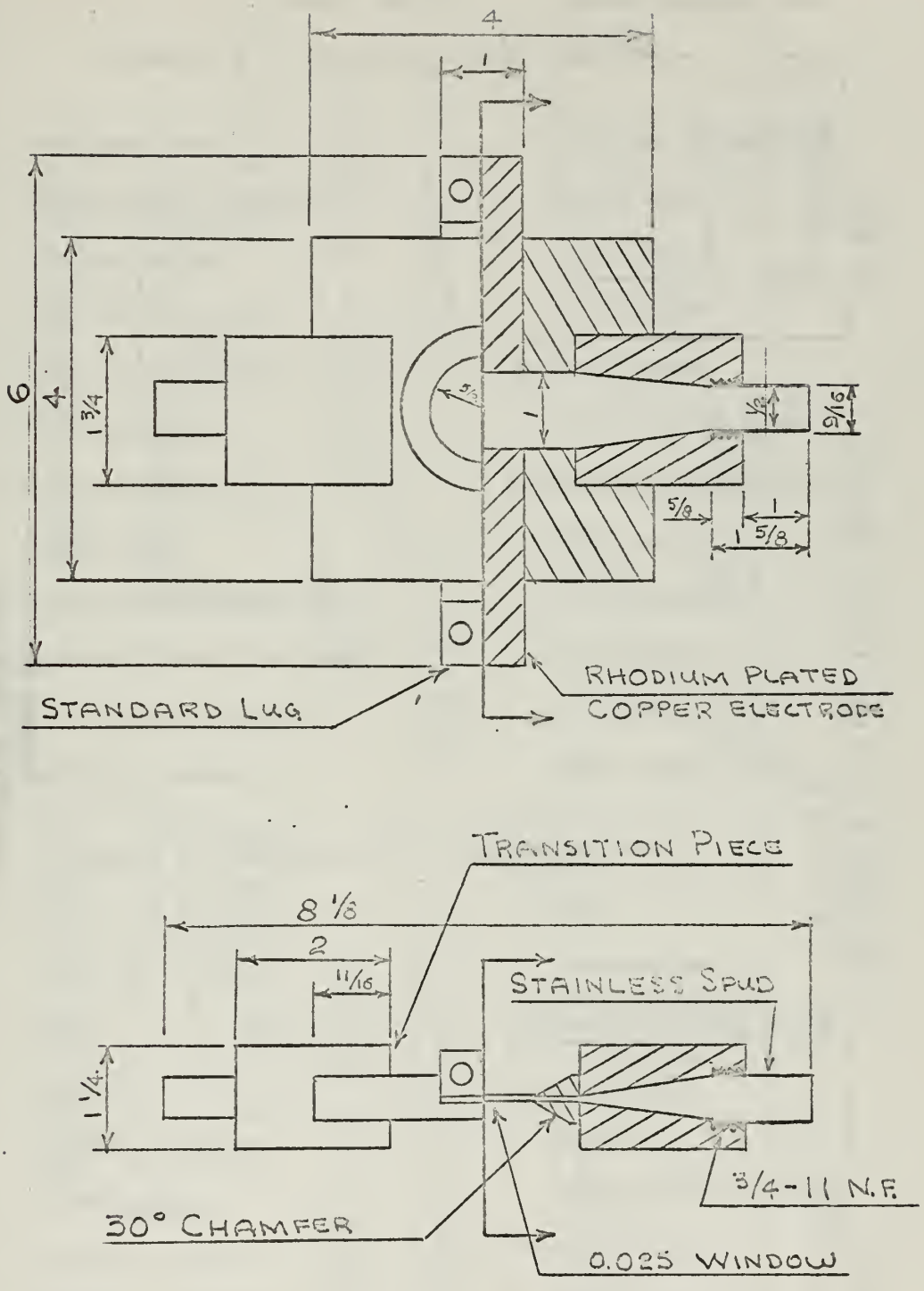

FIGURE 27
PUMP ELEVATION AND PLAN VIEWS

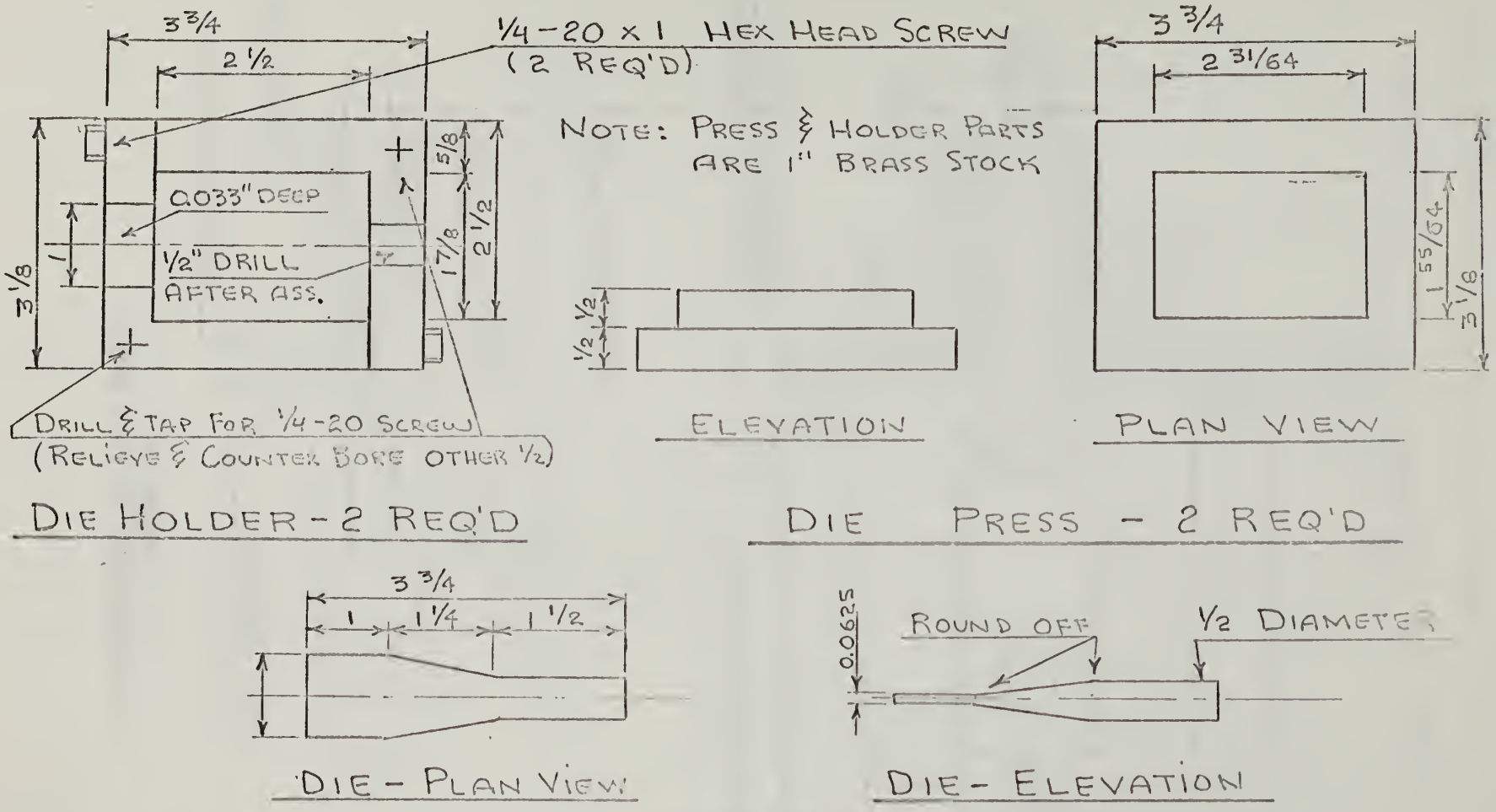

FIGURE 28
TRANSITION PIECE JIG

APPENDIX II

MAGNET DESIGN

SUMMARY OF IRON CIRCUIT DESIGN FEATURES

Configuration	Modified cylindrical
Air gap flux density	15,000 gauss
Air gap length	0.120 inches
Pole tip diameter	1.25 inches
Pole piece diameter	2.00 inches
Frame material	Surplus mild steel
Pole material	Surplus mild steel
Frame length	8.00 inches
Frame outside diameter	7.875 inches
Maximum frame flux density	8,000 gauss
Iron circuit weight	45 pounds
MMF requirements	4200 ampere turns

SUMMARY OF MAGNETIZING COIL DESIGN FEATURES

Number of coils	Two
Location of coils	Pole pieces
Type	Copper bobbin wound
Wire size	20 gauge
Insulation type	Formvar
Wire weight	8.88 pounds per coil
Turns per layer	53
Number of layers	53
Turns per coil	2809

Ampere turns per coil	2100
Current	0.748 ampere
Power loss per coil	19.3 watts

BASIC CONSIDERATIONS

A number of factors had a considerable influence on the magnet configuration. The most important of these are briefly discussed in the following text.

PUMP REQUIREMENTS

The load bank utilized to supply the main pump current had a capacity in the neighborhood of 50 amperes. Furthermore, experience with the prototype indicated that vaporization of mercury might occur at currents considerably less than 50 amperes if the pump were allowed to cavitate, or allowed to pump for too long a time against a static head. These conditions were brought about by friction in the pump loop and contact resistance at the electrodes, respectively. While considerable effort was made to minimize these effects (see Appendices III and IV), the fact remained that even at best the pump would be a relatively low current device. In order to obtain a reasonable head capability under these conditions, a relatively high magnetic field strength was called for. After studying the magnetic characteristics of the materials involved it was decided to design for a maximum air gap flux density of 15,000 gauss.

WEIGHT REQUIREMENTS

It was desired to keep the magnet weight below 100 pounds so that the entire pump and loop assembly (of which the magnet was responsible

for the bulk of the weight) would be portable.

POWER SUPPLY

It was desired to operate the magnet from the 120 volt DC laboratory supply. Control was to be by a slide wire rheostat readily available in the laboratory. This latter consideration limited the maximum current to be carried in the coils. This, in turn, necessitated the use of one of the smaller wire gauge sizes.

COST CONSIDERATIONS

In order to keep expenses to a minimum, it was decided to utilize material already on hand, or procurable at nominal cost. This resulted in the use of government surplus steel for the iron circuit and enamelled magnet wire for the coils. The effect was to produce a magnet of somewhat greater bulk and weight than if more sophisticated materials had been used.

DISCUSSION OF DESIGN PROCESS

The design process was one of iteration, guided by the performance of the prototype magnet. The major problems were to determine the size and shape of pole pieces required and the amount of flux to be carried by the yoke. Once these items were established, the magnet configuration was determined and reluctance drops calculated. Finally the coils were designed to furnish the required magneto-motive force.

The design process was initiated by attempting to predict the performance of the prototype magnet with the aid of a pole piece flux plot. This attempt proved to be reasonably successful. Furthermore, this flux plot (not shown here) together with a preliminary magneto-motive force estimate and coil design, furnished a first estimate of pole piece dimensions.

Consideration was now given to the yoke configuration. After some deliberation the modified cylindrical yoke was chosen because it resulted in the smallest configuration. This type of yoke had an added distinct advantage in that its components could be machined on the lathe in a manner that would eliminate alignment problems during final assembly.

Having decided on an approximate configuration, a final pole piece flux plot was made. Then the final pole piece dimensions and approximate coil dimensions were established. Frame leakage was estimated and approximate frame dimensions determined. Then the final coil dimensions were determined, and frame dimensions modified to suit. This at last established the final magnet dimensions.

IRON CIRCUIT DESIGN

POLE PIECE FLUX PLOT THEORY

This flux plot was an attempt to describe the pole flux without regard for the other iron in the circuit or the presence of the current carrying conductors. Prior to making this plot, an attempt was made to plot the entire configuration, taking into account the yoke iron, current carrying conductors, and the pole pieces. This proved to be extremely time consuming and had to be abandoned in order to complete the project.

The flux plot used represented a three-dimensional field. As a result the geometric relationship between flux lines and equipotentials was not established by curvilinear squares. The relationships establishing the geometry are described below.

In Figure 29, lines a, b, c, d represent equally spaced equipotentials. Lines x and y define a flux tube. In three-dimensional space the tube has a kind of annular shape. For lines x and y to define a flux tube, the

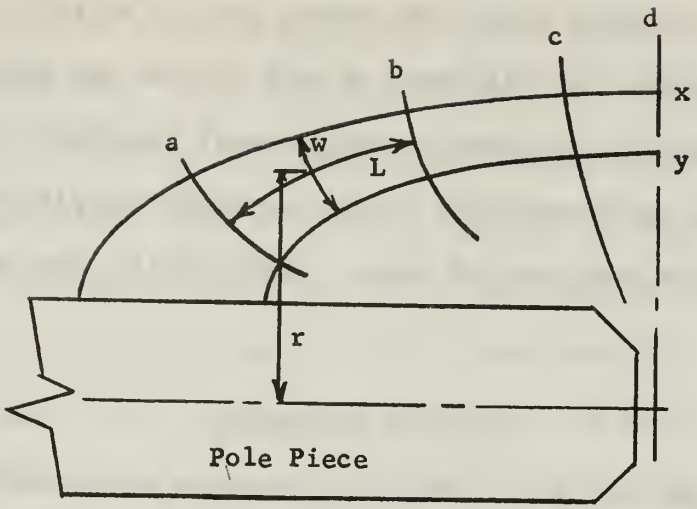

FIGURE 29
FLUX PLOT NOMENCLATURE

flux in all parts of the tube must be the same. Now, the equipotentials a, b, c, d divide the tube into sections of equal MMF. Since $R = MMF/\phi$, it follows that each section of the tube must have the same reluctance. Now if the sections are taken small enough, the reluctance of each section is given by

$$R = \frac{L}{2\pi rw} \text{ (oersteds)}$$

Where

L = mean length of section (cm)

r = mean radius of section (cm)

w = mean width of section (cm)

Now, in the two-dimensional field the method of plotting is purely a graphical process. The final result is a plot embodying tubes of equal flux. The correctness of the plot is established by eye. Computation is particularly simple and quick after the plot is established. In the three-dimensional field, however, correctness of the plot must be

established by computation. Furthermore, no practical method exists to plot tubes of equal flux. The method used is to arbitrarily sketch in a tube, compute the reluctance of each section and guess at which parameters require adjustment to obtain equal reluctance volumes between equally spaced equipotentials. After adjusting the plot the process is repeated for the next several tubes. Occasionally, the entire plot must be adjusted.

FLUX PLOT DISCUSSION

The reader may gain a small appreciation of the difficulties in attempting to plot the entire magnet configuration by considering the following brief discussion. There are three media involved instead of the one medium considered in the flux plot actually used. These media are the air, the iron, and the region encompassed by the current carrying conductors. The reluctance relationships differ for each region and the number of iterations increases manifold over the single medium plot. The principal source of difficulty lies with the current carrying region, which takes up the bulk of the space within the magnet. It is well known that there are no equipotentials in this region, but there are instead "lines of no work" along which the magneto-motive force continuously changes according to the amount of current enclosed. Furthermore, all lines of no work must meet at a common point within the region known as the kernel. The position of the kernel is influenced by the geometry of the iron and the geometry of the conducting region. Reluctance relationships are not difficult to establish mathematically. For example see [28]. However, the iterative process required to establish the location of the kernel, and simultaneously meet the reluctance relationships required in the iron, copper and air are extremely tedious and time consuming.

However, very powerful magnets are being constructed today, wherein it is desired to incorporate the highest possible degree of refinement. Therefore, it is felt that it would be very desirable to be able to obtain accurate flux plots of the entire iron, air, and current configuration. Some of the most advanced of these magnets incorporate a cylindrical shape and have a considerable amount of symmetry. It is felt that a computer program might be developed for a general cylindrical shape without too much difficulty. This would permit the determination of a more or less optimum configuration for a required air gap flux.

FINAL POLE PIECE FLUX PLOT

The final flux plot used in the design is presented here, together with associated computations. See Figure 30.

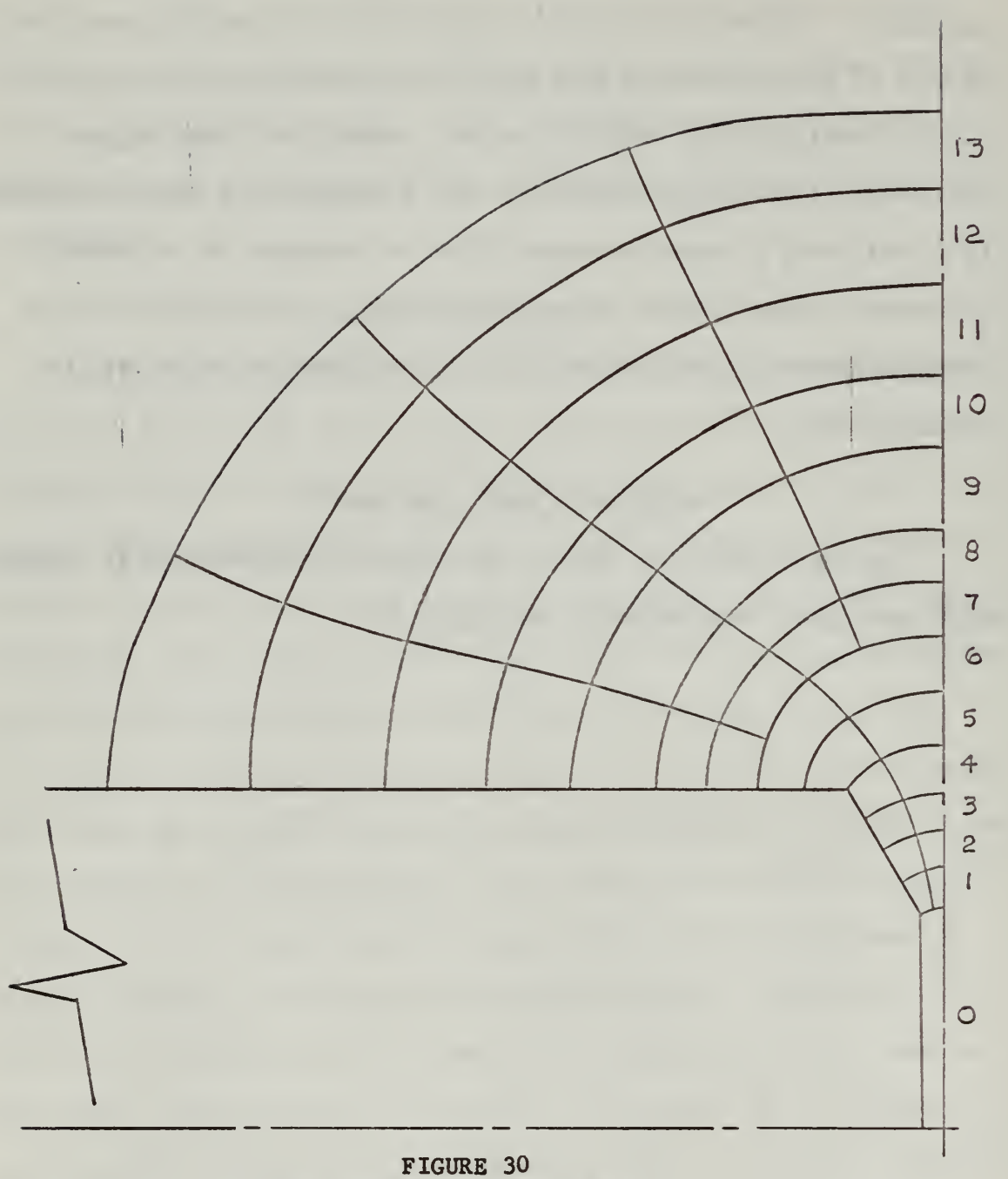

FIGURE 30
FINAL POLE PIECE FLUX PLOT

POLE PIECE FLUX PLOT SUMMARY

Tube No.	R (Oer.)	MMF (Gil.)	ϕ_{leak} (Lines)	ϕ_{iron} (Lines)	B_{iron} (Gauss)	L_{iron} (Cm)	ΔL_{iron} (Cm)
0	0.0192	2280	119,000	119,000	15,000	0.152	0.152
1	0.0892	2284	25,600	144,600	15,810	0.30	0.148
2	0.1096	2287.4	20,850	165,450	13,900	0.435	0.136
3	0.1380	2288.8	15,850	181,300	10,810	0.6065	0.1715
4	0.1224	2289.3	18,700	200,000	9,860	0.710	0.1035
5	0.1680	2290.7	13,620	213,620	10,540	1.025	0.315
6	0.2420	2292.5	9,450	223,070	10,970	1.40	0.375
7	0.2860	2294.5	8,010	231,080	11,370	1.78	0.380
8	0.3290	2296.7	7,000	238,080	11,730	2.16	0.380
9	0.2460	2300.6	9,340	247,420	12,170	2.805	0.645
10	0.2880	2304.9	8,000	255,420	12,560	3.45	0.645
11	0.2670	2310.5	8,630	264,050	13,000	4.20	0.750
12	0.2700	2319.1	8,560	272,610	13,450	5.22	1.020
13	0.3530	2328.7	6,580	279,190	13,750	6.30	1.080

SAMPLE COMPUTATION

Tube 1:

$$\phi_{leak} = \frac{2280}{0.0892} = 25{,}600 \text{ lines}$$

$$\phi_{iron} = 119{,}000 + 25{,}600 = 144{,}600 \text{ lines}$$

$$A_{iron} = \frac{\Pi}{4} (3.41)^2 = 9.14 \text{ cm}^2$$

$$B_{iron} = \frac{144{,}600}{9.14} = 15{,}810 \text{ gauss}$$

$$H_0 = 15 \text{ oersted}$$

$$H_1 = 38$$

$$H_{ave} = 27$$

$$MMF_1 = 2280 \div (27)(0.148) = 2284 \text{ gilberts}$$

At this point, if the calculated MMF was appreciably larger than 2280 the computation would have been repeated utilizing the calculated value of MMF. The iteration would be continued until good agreement was obtained between assumed initial MMF and final calculated MMF. In this manner, the approximate MMF requirement of the pole piece is determined even though the flux plot assumed the iron an equipotential surface.

POLE PIECE DESIGN

The 30 degree pole tip chamfer was arbitrarily selected as near optimum (see [18]). Now the flux plot was made for a 2.5 inch long pole; space considerations actually dictated a 2.75 inch long pole.

Pole flux = 279,190 + 4,000 = 283,191 lines

Pole MMF = (2328.7 - 2280) + 3.5 = 52 gilberts

Additional MMF along pole inside frame = 35 gilberts

FRAME DESIGN

Maximum frame leakage was assumed to be 40% of the pole flux. This was an arbitrary figure arrived at from experience with the flux plots. This type of estimation is tolerable in this magnet since the frame reluctance drop is a small percent of the total drop. Therefore, a relatively large error in frame MMF will result in only a small error in total MMF requirements.

Maximum frame flux = (1.40)(285,000) = 396,000, say 400,000 lines.

The frame was designed to carry 400,000 lines at any point, operating at a flux density of about 8,000 gauss. This was done in an effort to obtain a slightly conservative design.

IRON CIRCUIT MMF REQUIREMENT

ITEMS	AMPERE TURNS
Main air gap	3,632
Air gaps due to construction	292
Frame	190
Pole tip	78
Total magnet	4,192

COIL DESIGN

POWER CONTROL

The coils were designed to be operated in series. The method of control was by slide wire rheostat used as a voltage divider.

Appropriate slide wires	110 ohm, 2 ampere
	54 ohm, 5 ampere
	890 ohm, 1 ampere
	110 ohm, 2.3 ampere

SUMMARY OF DESIGN FEATURES

Ampere turns	2100
Wire gauge	20
Insulation type	Formvar
Wire diameter	33.8 mils
Turns per layer	53
Layers	53
Total turns	2809
Turns per inch	29.5
Current	0.748 ampere
Vertical embedding factor	0.95
Coil length	1.790 inches
Inside diameter	2.00 inches
Outside diameter	5.53 inches
Coil bobbins	Copper
Thermal contact	"Good"
Effective surface area	73.1 square inches
Mean diameter	3.77 inches
Mean turn length	1.020 feet
Total length of wire	0.985 feet
Resistance at 20°C	29.2 ohm
Weight of wire	5.88 pounds
Impregnating compound	Epoxy
Maximum temperature	105°C
Ambient temperature	25°C
Average coil temperature	63.5°C (equilibrium)
Resistance at 63.5°C	34.4 ohm

Power loss	19.3 watts
Coil volume	37.2 cubic inches
Watts/cubic inch	0.518
Watts/square inch	0.272
Heat dissipation coefficient	0.0068 watts/in^2°C avg. temp. diff.
Heat dissipation capacity	0.504 watts/°C avg. temp. diff.
Thermal capacity	
Copper	1600 watt-sec/°C
Pole piece (55% effective)	198 watt-sec/°C
Insulation	329 watt-sec/°C
Total	2127 watt-sec/°C
Thermal time constant	70.5 minutes

DISCUSSION OF THERMAL CHARACTERISTICS

Coil computations were based on theory developed by Herbert C. Roters [26]. The assumption of good thermal contact was felt justified in view of the facts that the copper bobbins were to be butted up against the cylindrical frame ends, and made a tight sliding fit over the pole pieces. However, computations were also made assuming poor thermal contact. These computations indicated that it would be safe to operate the magnet continuously for two hours at designed maximum current, i.e., 0.748 ampere, even under conditions of poor thermal contact. It is evident that the coil has considerable reserve capacity, in view of the fact that pump test runs are ordinarily of very short duration.

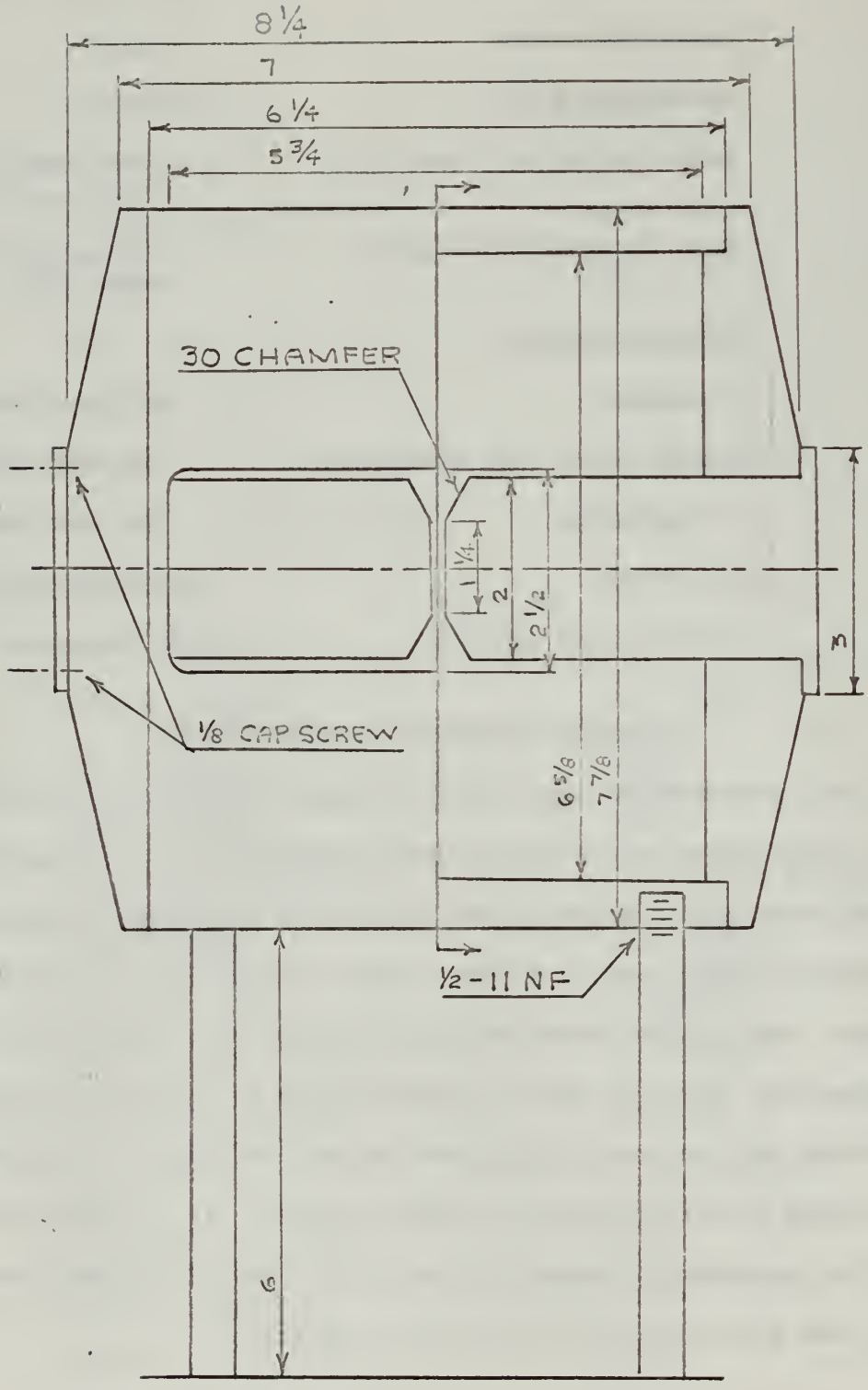

FIGURE 31
PROFILE OF MAGNET FRAME AND POLES

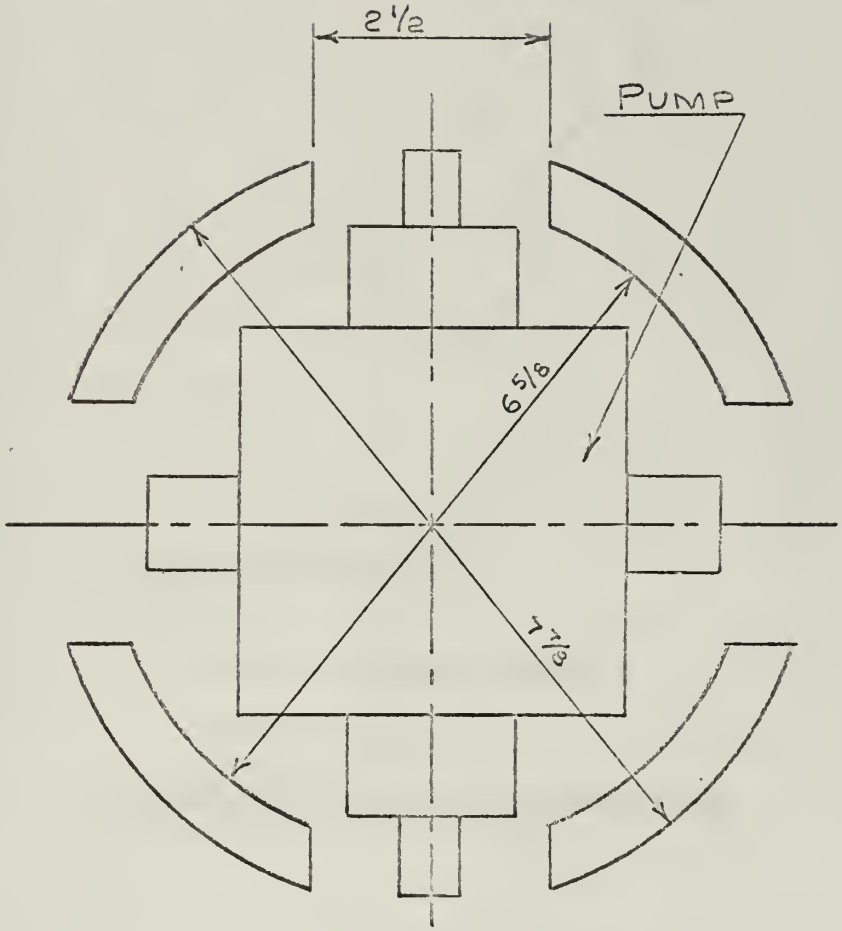

FIGURE 32
SECTION THROUGH CENTER OF MAGNET

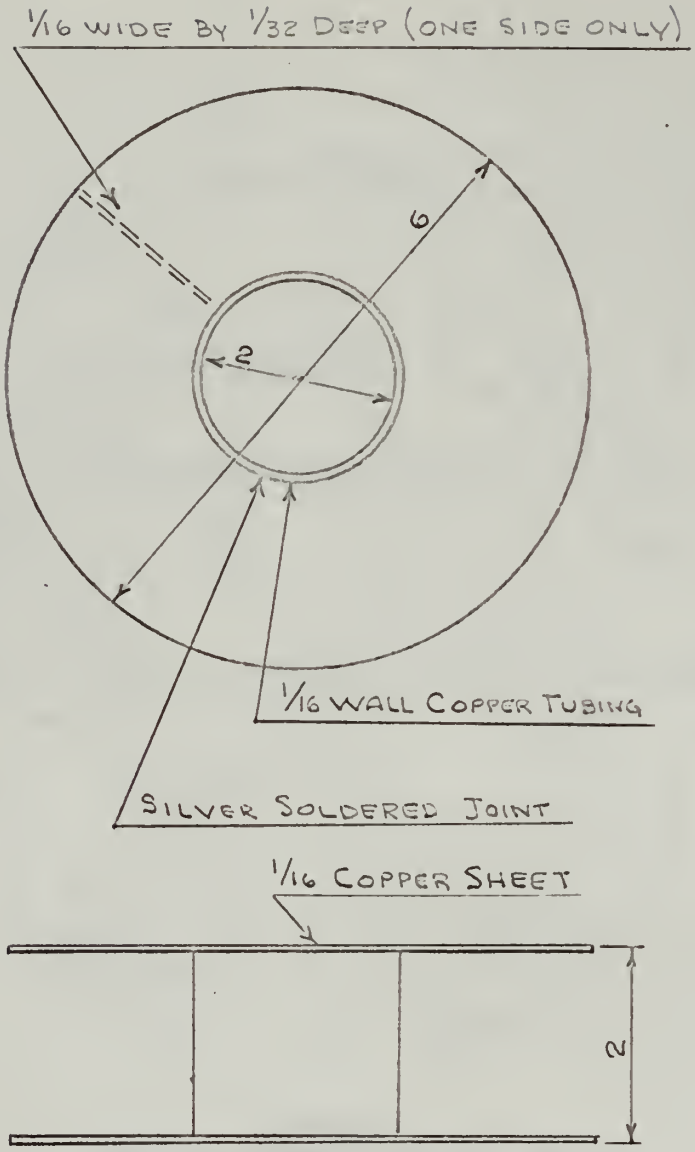

FIGURE 33
COIL BOBBIN

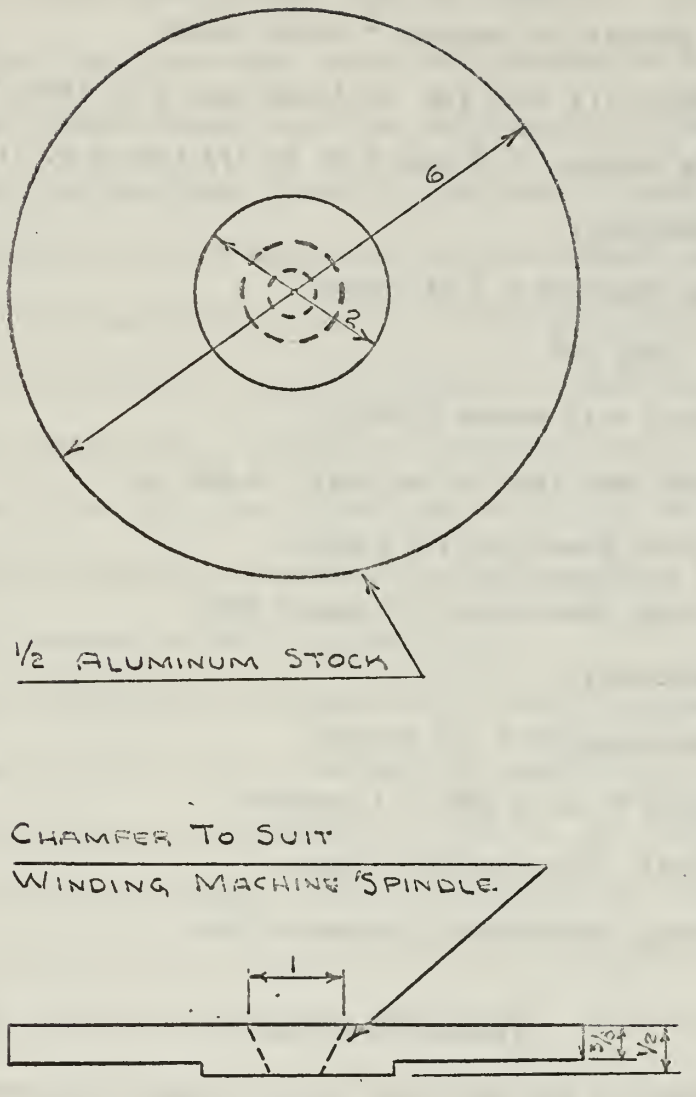

FIGURE 34
COIL BOBBIN SUPPORT

APPENDIX III

PUMP TEST LOOP DESIGN

SUMMARY OF DESIGN FEATURES

Minimum quantity of mercury = 14.24 pounds

Main tubing: 1/2 inch I.D. by 13/16 inch O.D. clear "Tygon"

Auxiliary tubing: 3/8 inch I.D. by 1/2 inch O.D. clear "Tygon"

Lower reservoir:

- Inside diameter = 7.75 inches
- Area = 304 cm^2
- Capacity = 23 pounds mercury
- Suction head drop during test = 0.452 cm
- Material: Clear acrylic plastic
- Mounting: Continuously threaded rods

Upper Reservoir:

- Inside diameter = 1.5 inches
- Capacity = 137.3 cm^3 (4.1 pounds)
- Material: Clear acrylic plastic
- Mounting: Continuously threaded rods

DISCUSSION OF DESIGN

The purpose of the test loop was to determine the mechanical quantities required to analyze pump performance. At the same time it was desired to operate the pump over as wide a range of loading as possible. To obtain a high load (i.e., high head) performance was no problem. To obtain a low low load performance it was necessary to design a test loop with relatively small hydraulic losses.

It was desired to keep the test loop as simple as possible, and be able to see the mercury in all parts of the loop. Other than electrical quantities, it was only required to be able to measure flow rates at various heads in order to determine pump performance. Using the two reservoir system, pump flow rates could be determined at various potential heads. System friction losses could be determined by allowing the fluid to flow between the reservoirs under the influence of gravity and applying Bernoulli's equation to the system. In the same manner, losses could be obtained for the piping system alone (i.e., with the pump removed from the system). By subtraction, then the hydraulic losses for the pump itself could be determined. Knowing the system hydraulic losses and the electrical quantities, the pump performance could then be analyzed. A meter stick and an electric timer were the only measuring devices required to obtain all necessary mechanical quantities.

An internal baffle was installed in the upper reservoir to provide a smooth mercury surface on the side used for measurement. Both reservoirs were designed to operate at atmospheric pressure. The upper heads of both reservoirs were made removable to facilitate cleaning. All threaded joints were sealed with 0.005 inch "Teflon" tape. For strength, stainless steel spuds were used throughout at tubing connections. Upper and lower reservoir vents were interconnected to provide overflow safety. Stainless steel valves were provided to drain from the upper to the lower reservoir, and to drain the system itself. The pump and test reservoirs were mounted on a painted aluminum stand with raised sides to provide containment in event of mercury spillage. The stand also provided for electrical connections to the pump and magnet. The pump was mounted six inches off the stand to allow for a large radius bend in the suction tubing.

The suction and discharge tubing were deliberately chosen with large inside diameter and heavy wall thickness to keep friction losses low. This was accomplished by providing a large cross-sectional area for flow and preventing kinking at the bends. The inside diameter of the tubing connections was made the same as that of the tubing to keep fitting loss low. Furthermore, since the tubing was stretched over the fittings, absolutely tight joints were maintained, and hose clamps were not required. Sufficient mercury was placed in the system to prevent dry suction in event of overflow.

COMPUTATIONS

Upper Reservoir

$$\text{Capacity} = \left[\frac{(\Pi)}{(4)} (1.5)^2 - (1.5)(0.0625) \right] (5)(2.54)^3 = 137.3 \text{ cm}^3$$

$$\text{Time to fill at } 50 \text{ cm}^3/\text{sec} = \frac{137.3}{50} = 2.74 \text{ seconds}$$

Lower Reservoir

$$\text{Cross-section area} = \frac{(\Pi)}{(4)} (7.75)^2 (2.54)^2 = 304 \text{ cm}^2$$

$$\text{Total capacity} = (2.54)(304) = 772 \text{ cm}^3$$

$$\text{Bottom head capacity} = \frac{1}{3} (304)(0.375)(2.54) = 98.4 \text{ cm}^3$$

$$\text{Suction head capacity} = \frac{137.3}{304} = 0.452 \text{ cm (maximum)}$$

Tubing

$$\text{Suction line capacity} = (80) \frac{(\Pi)(0.5)^2}{4} (2.54)^2 = 101.4 \text{ cm}^3$$

$$\text{Discharge line capacity} = (60) \frac{(\Pi)(0.5)^2}{4} (2.54)^2 = 76.1 \text{ cm}^3$$

$$\text{Overflow line capacity} = (90) \frac{(\Pi)(0.375)^2}{4} (2.54)^2 = 64 \text{ cm}^3$$

Mercury Required

Volume = 101.4 + 76.1 + 64.0 + 137.3 + 98.4 = 477.2 cm^3

Weight = $\frac{(477.2)(13.55)}{1000}$ (2.205) = 14.24 pounds (minimum)

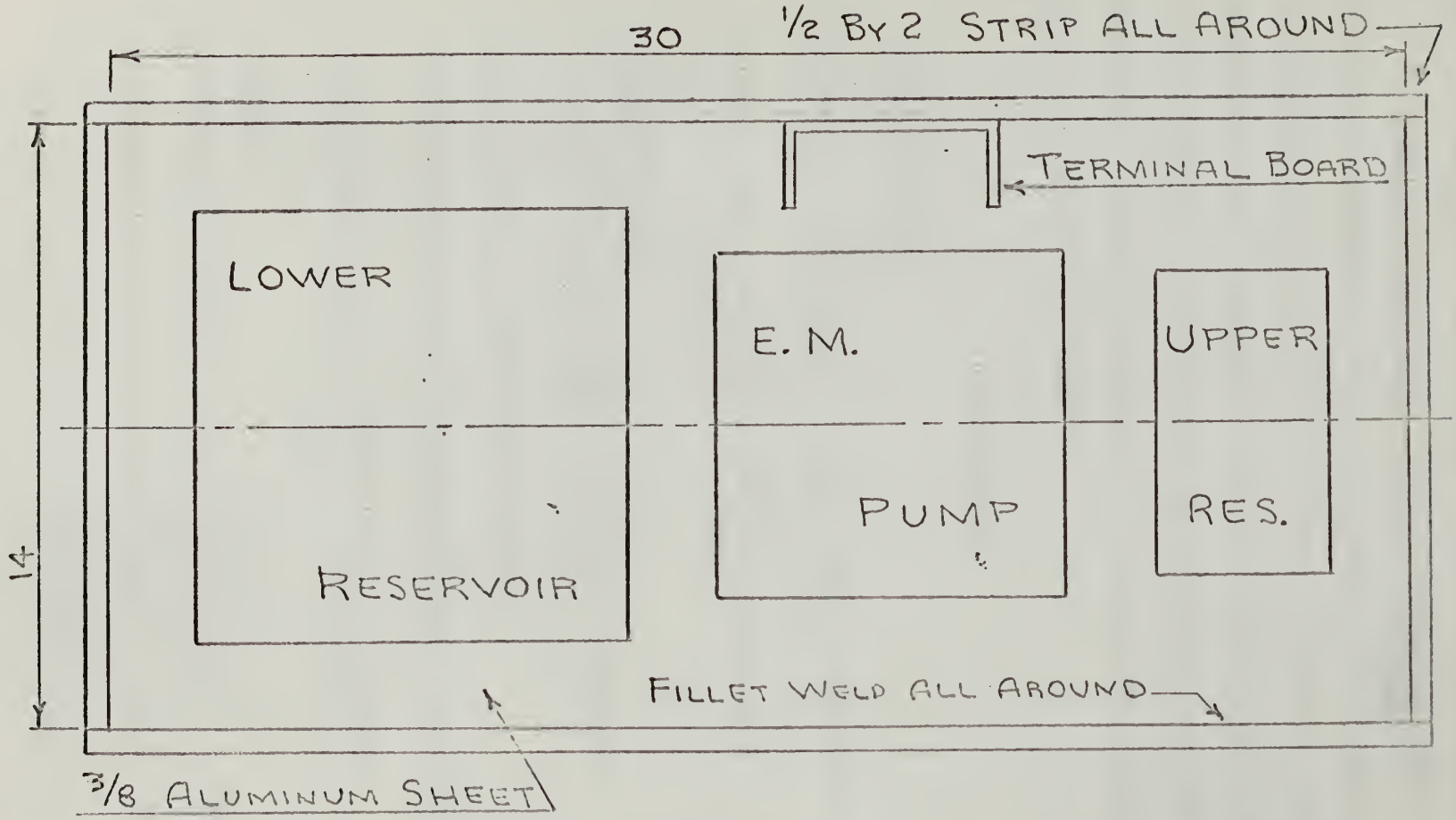

FIGURE 35
PUMP TABLE LAYOUT

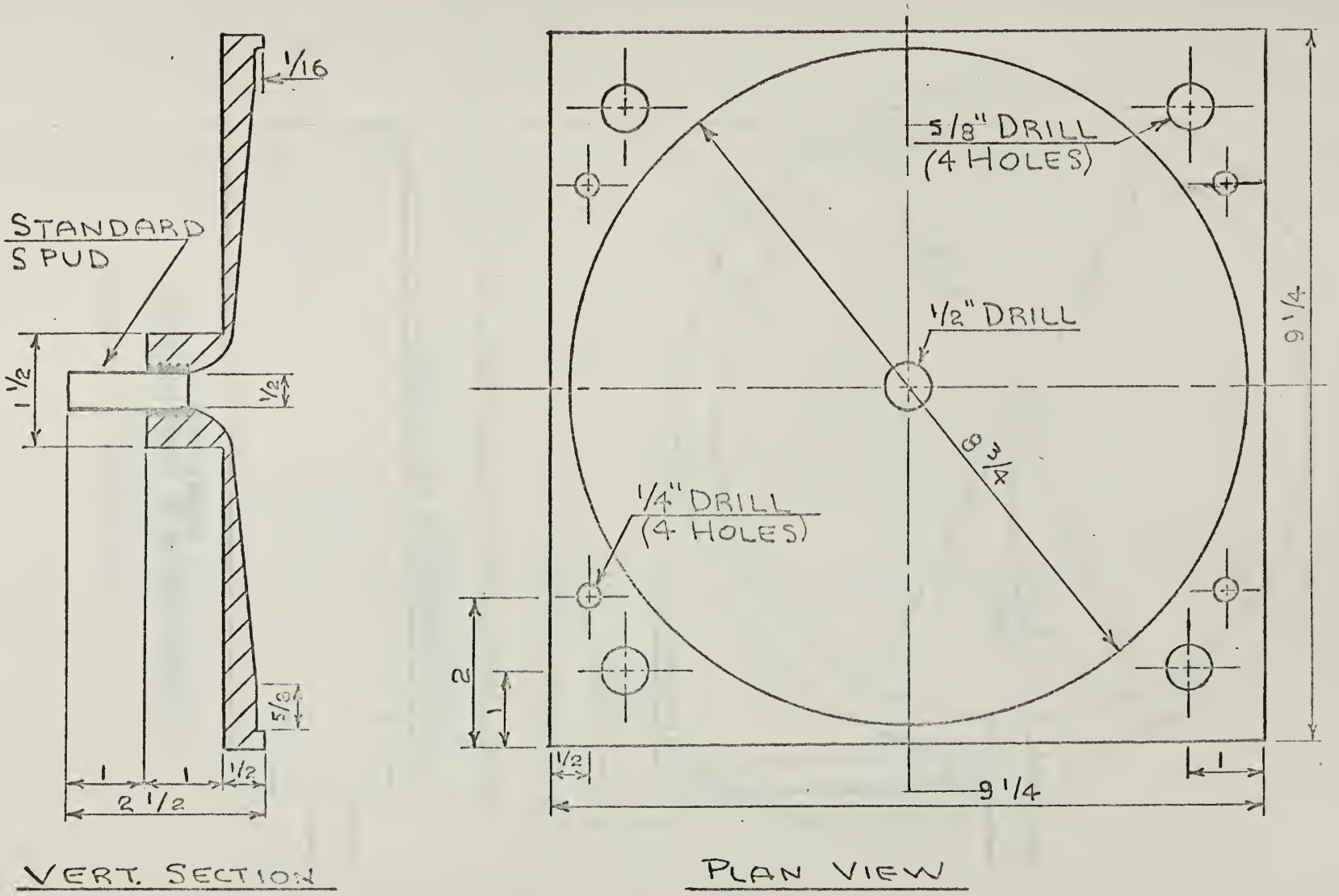

FIGURE 36
BOTTOM HEAD OF LOWER RESERVOIR

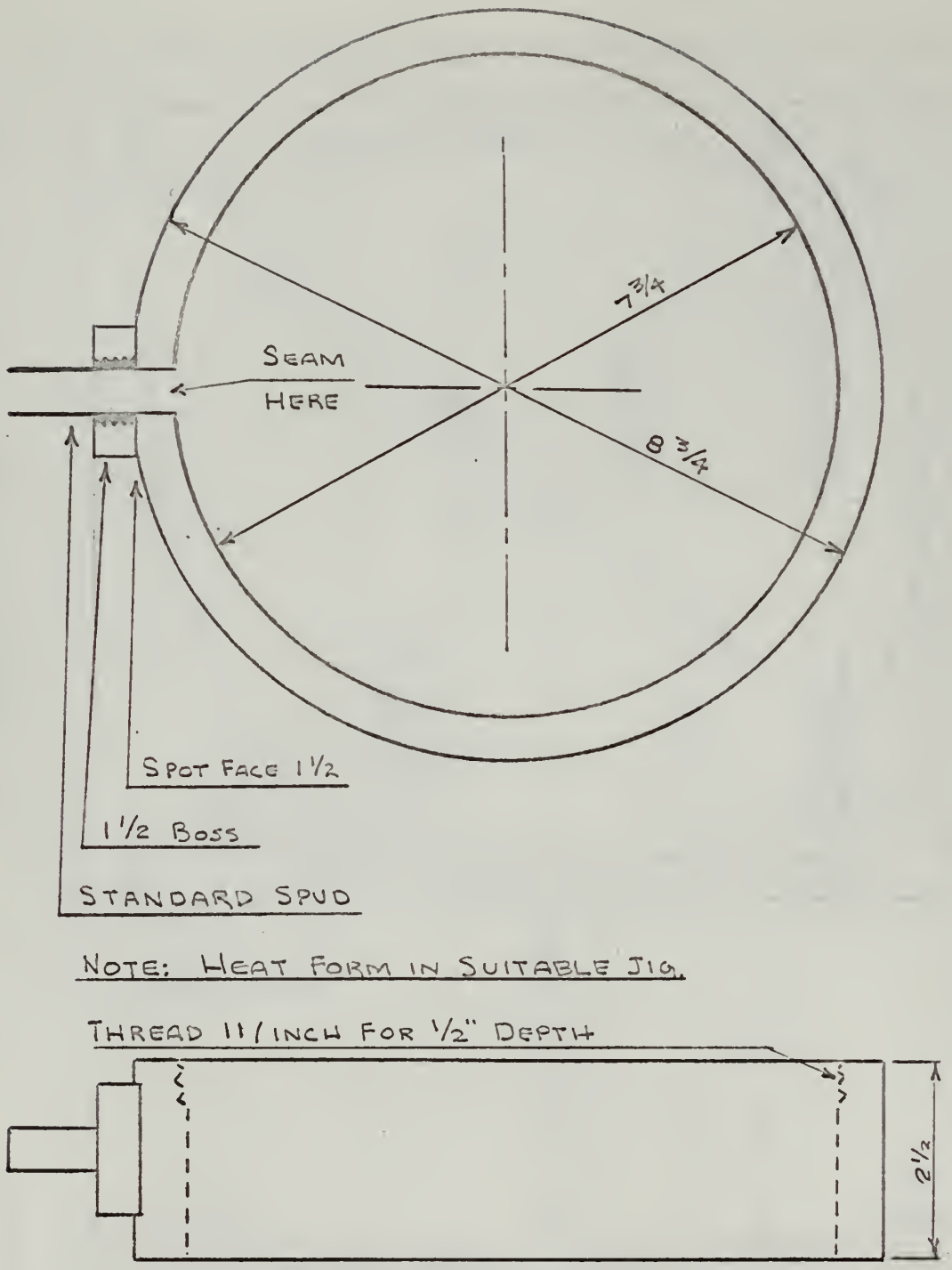

FIGURE 37
CYLINDER PORTION OF LOWER RESERVOIR

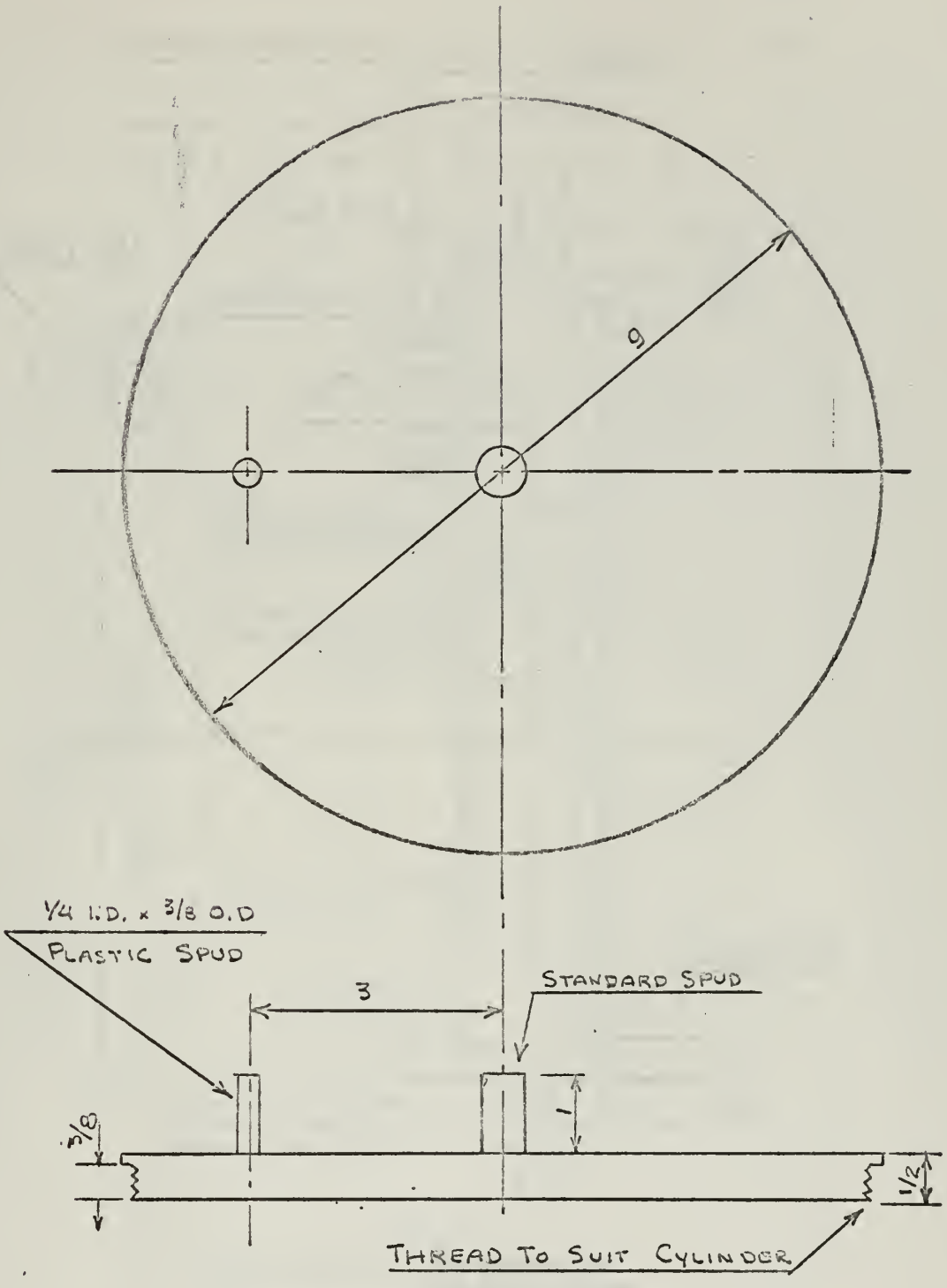

FIGURE 38
TOP HEAD OF LOWER RESERVOIR

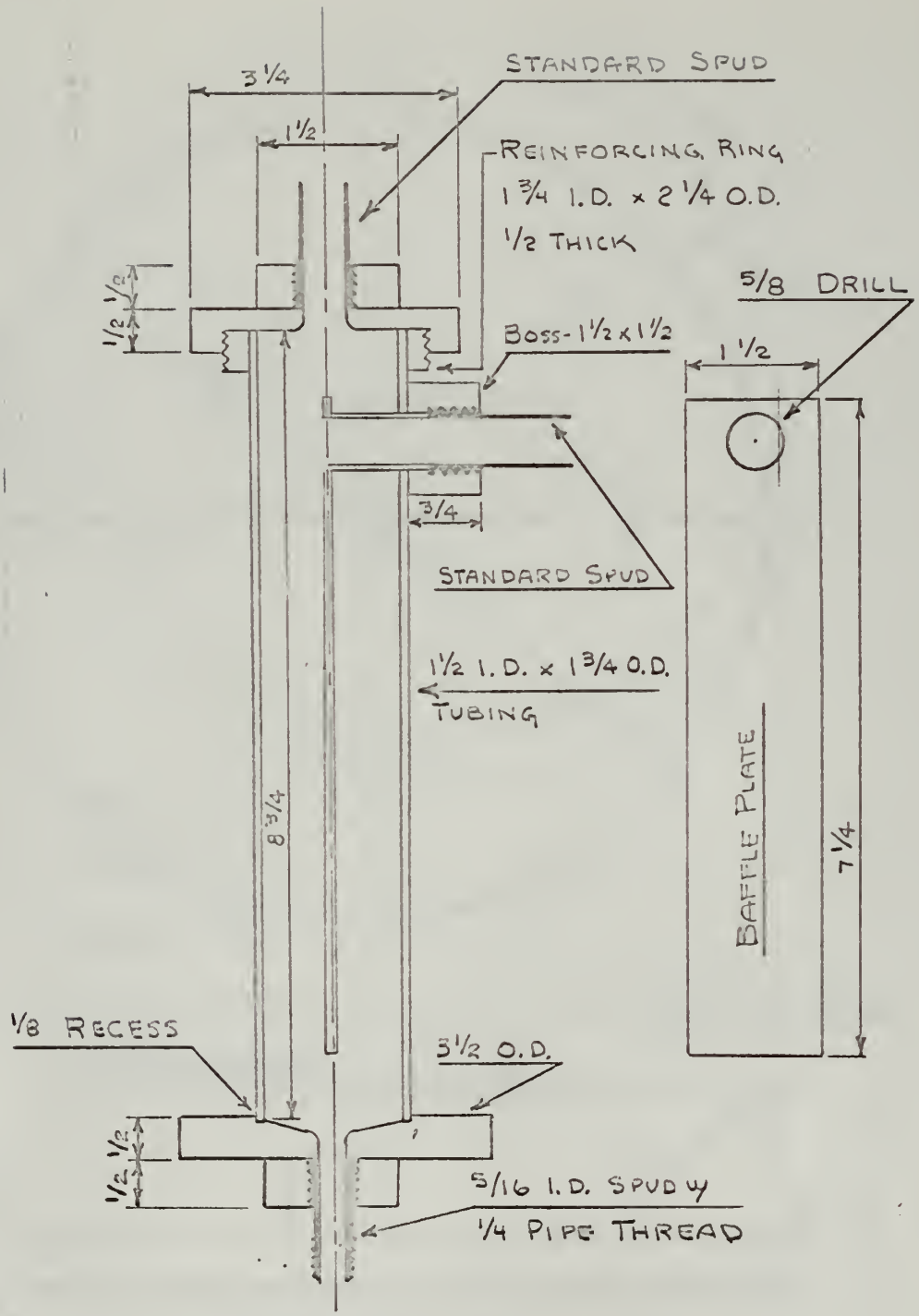

FIGURE 39
UPPER RESERVOIR

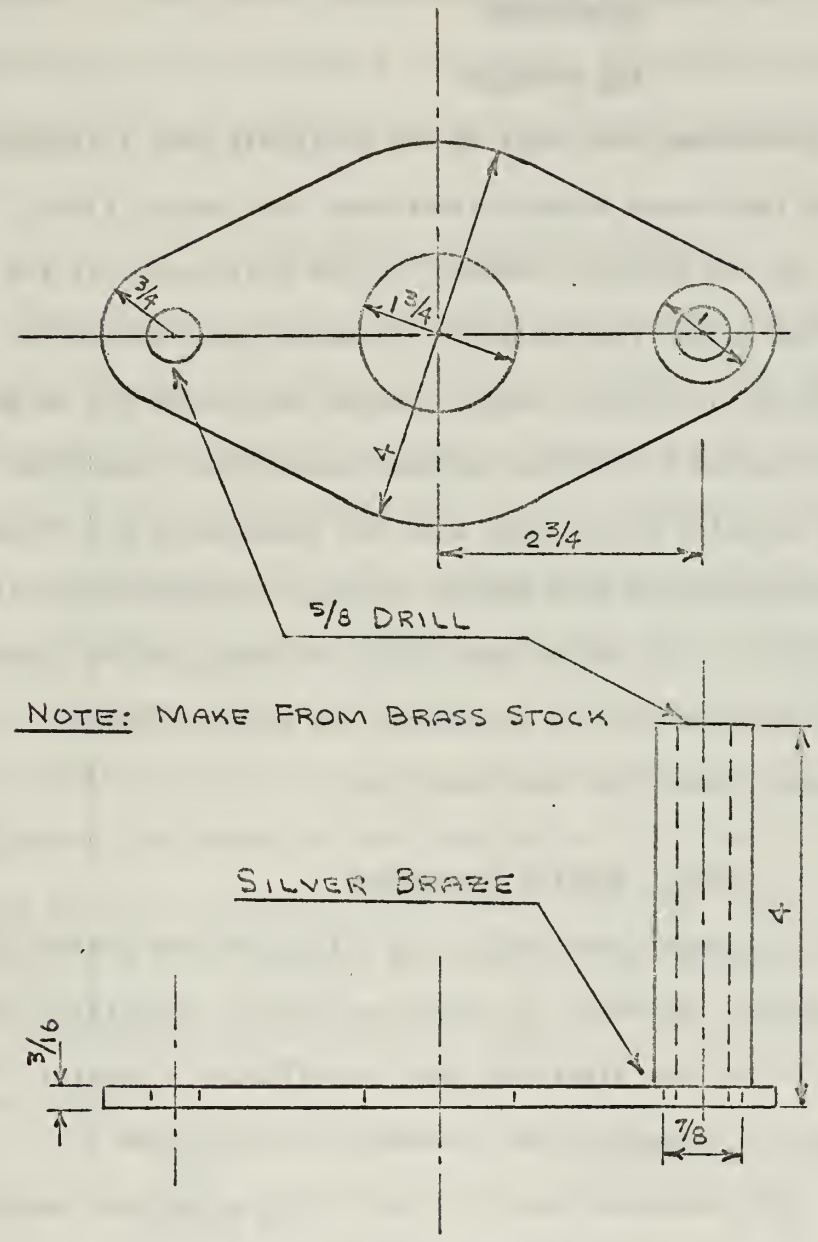

FIGURE 40
UPPER RESERVOIR SUPPORT PLATE

APPENDIX IV

CONTACT RESISTANCE

BACKGROUND

THE PROBLEM

Infrequent references were made in the available pump literature regarding contact resistance between electrodes and pumping fluid. When mention was made of the subject, however, it was indicated that the phenomenon could be quite troublesome, particularly when attempting to pump mercury. As was discovered later, contact resistance may be many times that of the pumped fluid under adverse conditions. According to [36], holes have actually been burned thru the channels of A.C. conduction pumps due to this phenomenon when pumping against a static head. It would appear then, that the utmost care should be exercised to insure that the pump is operated with an acceptably low value of contact resistance to insure proper and safe operation.

SPECIAL WETTING PROCEDURES

A number of the pumps described in the literature had austenitic stainless steel walls. In order to insure low contact resistance the mercury was made to wet the electrode area by utilizing a special wetting procedure. A rather typical procedure was described by D. A. Watt [33]. The procedure was to raise a lithium-mercury amalgam slowly into the channel. A small quantity of water was introduced. The resulting nascent hydrogen cleaned the surface, which was immediately contacted and wetted by the mercury. Care was taken to exclude air from the rig after the wetting to prevent oxidation of the steel surface.

This, it was asserted, resulted in practically unmeasurably small contact resistance. To wet electrodes in this manner would have required a considerably different and more complex type of test loop than the one desired. It was hoped that an electrode material would be found for our application that exhibited a consistent, relatively low value of contact resistance and which would not require special wetting procedures.

ELECTRODES IN PROTOTYPE PUMP

Construction of the prototype was done early in the project in order to gain experience with the problems involved. Very little was known of contact resistance at the time. However, it was known that at least one pump had been constructed utilizing molybdenum electrodes. Molybdenum was not immediately available, but quantities of tungsten were on hand at the school. A little research revealed that the properties of the two metals were very similar [1]. With respect to tendency to oxidize and solubility in mercury, tungsten was evidently superior to molybdenum. Therefore, the prototype was constructed with tungsten electrodes. Data taken with the electrodes installed in the pump indicated a wide variation in contact resistance from time to time depending, it was assumed, on the condition of the electrode surface. Some representative data are shown below.

DATE	CONTACT RESISTANCE (MILLIOHMS)
January 12	1.04
February 3	55.1
February 10	7.2

The January 12 data was taken shortly after the pump was constructed, and represents by far the lowest reading ever obtained on the prototype

electrodes. The data of February 3 was taken the day the pump was installed in its test loop, the electrodes having been exposed to the air for the previous two weeks or so. On the same date considerable dynamic and static testing of the pump was done. Mercury flashing occurred twice. One occurrence was under static (no flow) conditions and at about 45 amperes. This occurrence was directly attributed to the extremely high contact resistance. The other occurrence was at 30 amperes under flow conditions with cavitation. Due to the extreme conditions imposed by cavitation, the flashing may well have taken place with lower contact resistance. However, the high value of contact resistance certainly contributed to the phenomenon. The February 10 measurement was taken after the electrodes had been immersed in the mercury about a week. Due to the erratic nature of the prototype contact resistance and generally high values involved, it was decided to conduct an experiment to determine if a more suitable electrode material could be found.

POSSIBLE MATERIALS

The use of nickel or rhodium was briefly mentioned in several papers as possible choices for electrode materials. Rhodium plated copper brush rings were included in the design of a large homopolar generator [33]. In these discussions it was stated or implied that the use of these materials would result in low contact resistance. However, none of these discussions gave any quantitative data, nor justified the use of these materials.

DESIRABLE PROPERTIES

Some study into the problem revealed at least the following to be desirable properties of electrode materials for this application:

1. Minimum tendency to form oxide or tarnish films at room temperature, under normal atmospheric conditions. Mercury wets almost any metallic surface, if it can be made absolutely clean, according to [20]. Even fresh broken iron surfaces will wet if the specimen is broken under mercury.

2. Minimum tendency to dissolve in, or otherwise be corroded by mercury at the temperatures involved. This property is required to prevent the destruction of the electrodes and contamination of the mercury.

SELECTION OF MATERIAL TO BE TESTED

Further study showed that while tungsten and molybdenum are relatively impervious to mercury, they both rapidly form an oxide film in ordinary atmospheric air. This property would make it difficult to wet these substances under the conditions involved in this pump. Nickel was found to have relatively good oxidation and corrosion resistance properties in ordinary atmospheric air. Furthermore, it was found to be relatively immune to attack by mercury at room temperature. Rhodium was found to have outstandingly good oxide and corrosion resistance, but no data could immediately be found regarding its resistance to mercury attack. Despite the lack of any mercury corrosion data on rhodium, it was decided to test the contact resistance properties of both rhodium and nickel electrodes. Test electrodes were prepared by electroplating on pure annealed copper. The rhodium electrodes were first nickel plated. Sets of tungsten and uncoated copper electrodes were also prepared. Tungsten was included because it was utilized in the prototype. Copper was chosen because it could be easily wet, and in this condition should exhibit a very low contact resistance, thereby serving as the basis for

comparison of the other electrodes.

CONTACT RESISTANCE JIG

A special jig was designed and constructed to determine the contact resistance to mercury of the electrodes in question. The jig consisted of a fifteen inch long by 0.060 square inch cross section mercury channel with suitable fixtures at the ends to hold the electrodes. With a knowledge of the channel and electrode dimensions and the resitivities of the materials involved, the resistance of the electrodes and mercury channel could be computed. The total resistance could then be measured by passing a current thru the electrodes and mercury. By subtraction then, the total contact resistance could be determined. The primary features of the jig are listed below:

Length of mercury channel = 15.060 inches or 38.2 cm

Channel depth = 0.060 inches

Channel width = 1.000 inches

Channel area = 0.060 in^2 or 0.387 cm^2

Resistance of channel at 20°C = 0.00945 ohm

Electrode area = 0.060 in^2 or 0.387 cm^2

Electrode length = 2.5 inches or 6.35 cm

MEASURING EQUIPMENT

The voltmeter-ammeter method was used to determine the resistances involved (A Kelvin double bridge was available, but its use was not felt necessary). A precision laboratory ammeter was used to measure current. A digital voltmeter (checked against a Hewlett Packard No. 425-A micro volt-ammeter) was used to measure potential. At, say, five amperes, the potentials involved would be of the order of 100 millivolts. The input

impedance of the volt-meter was 10^6 ohms. Therefore the current drawn by the instrument would be of the order of 10^{-7} amperes. If, say the instrument lead and contact resistance were of the order 100 ohms, then the error in voltage measurements would be 10^{-5} volts, a negligible quantity in this application.

CONTACT RESISTANCE TESTS

Tests were applied to the electrodes under three different conditions, namely:

1. Electrodes cleaned, but not wetted by mercury.
2. After immersion in mercury for ten days.
3. After immersion in mercury for 50 days.

TEST RESULTS, DRY ELECTRODES

MATERIAL	CONTACT RESISTANCE (MILLIOHMS)
Copper	0.56
Tungsten	1.95 - 10.60
Nickel plated copper	2.18 - 2.83
Rhodium plated copper	1.25 - 2.39

The copper electrodes were sanded bright and cleaned with alcohol. Only one reading was taken because of the rapid formation of amalgam on the electrode surfaces. Several readings were taken on the tungsten electrodes. Contact resistance was extremely sensitive to the surface condition, depending on whether they were sanded down, how much sanding was done, and how carefully they were cleaned. The tungsten was included purely for comparison, as its performance was already known to be poor from experience with the prototype.

TEST RESULTS, RHODIUM AND NICKEL ELECTRODES IMMERSED IN MERCURY FOR TEN DAYS

MATERIAL	CONTACT RESISTANCE (MILLIOHMS)
Wetted copper	0.49
Rhodium plated copper	0.52
Nickel plated copper	0.62

Both the nickel and rhodium electrodes were wetted by the mercury to some extent. The rhodium wetting was not as good as that of the copper, nor was the nickel wetting as good as that of the rhodium. The appearance of both sets of electrodes was good, and there appeared to be no adverse interaction between electrode surface and mercury. A slight darkening appeared at the rhodium surface that had been in contact with the mercury. This phenomenon was unexplained.

CHOOSING ELECTRODES FOR THE PUMP

Due to time limitations, the pump had to be constructed on the basis of the tests in the previous paragraph. The data indicated that either the rhodium or nickel electrodes would be superior to the tungsten electrodes of the prototype from a contact resistance standpoint. The contact resistance of the two materials was about the same. However, the wetting action of the rhodium was evidently better. Since the rhodium had better all around corrosion and oxidation resistance it was chosen to be utilized in the pump.

TEST RESULTS, RHODIUM AND MERCURY ELECTRODES AFTER PROLONGED IMMERSION IN MERCURY (50 DAYS)

MATERIAL	CONTACT RESISTANCE (MILLIOHMS)
Rhodium plated copper	0.51
Nickel plated copper	0.59

The values of contact resistance did not change appreciably from those of the previous test. However, some interesting effects were noted. Both sets of electrodes showed considerably more wetting than before, with the rhodium plated electrodes being considerably wetter than the nickel plated ones. After testing, the electrodes were wiped off with a soft cloth and inspected. The rhodium appeared unchanged, but the nickel electrodes were damaged. Spots (quite visible to the naked eye) had appeared at the area where current had passed from the nickel to mercury. These spots appeared to be an amalgam formed on the electrodes. It is possible that the electroplating was faulty and that a copper-mercury amalgam had been formed. However, it is also quite possible that a nickel-mercury amalgam was formed. No conclusive explanation was found.

CORROSION BY MERCURY

Further literature search was made in an attempt to secure conclusive information on mercury-nickel and mercury-rhodium complexes. No information was immediately available that applied specifically to the problem at hand. However, a considerable amount of solubility data was available on nickel-mercury under static conditions. Information on rhodium-mercury was very difficult to find. One report was found [29], that compared the saturated solubility of the various metals in mercury at room temperature. Some of the results are tabulated herewith.

MATERIAL	SOLUBILITY - wt%
Tungsten	< 0.001
Molybdenum	< 0.001
Nickel	0.002
Rhodium	0.160
Copper	0.007

Now, according to the Liquid Metals Handbook, static data cannot be relied upon to determine corrosion under dynamic conditions, since these effects may be greatly accelerated, depending on the materials involved. Furthermore, static corrosion data from the various sources showed wide variations on the materials that could be compared. Therefore, one cannot safely rely upon one set of data. However, based on the static data above, it would appear that the rhodium is a poor material to be utilized in contact with mercury. However, the use of rhodium in the large homopolar generator mentioned before is evidence that at least one engineering group feels that rhodium is adequate to the task. This enigmatic situation can only be resolved by further study.

CONCLUSIONS

This study into the subject of electrodes was conducted over too short a period of time to be truly conclusive. There were neither sufficient man-hours nor calendar days available to conduct a thorough study of the subject. Nickel plated electrodes may possibly have merit, but the matter of the damaged surfaces would have to be investigated. There are indications that the rhodium plated electrodes show promise as electrode materials. Rhodium's good properties with respect to oxidation and corrosion suggest that consistently low contact resistances may be maintained with this material. Both materials will be wet with mercury if sufficient time is allowed for the mercury to break up any superficial surface films. Materials that oxidize or corrode easily are not satisfactory except for use in a system in which the atmosphere is excluded. Low values of contact resistance cannot be maintained unless wetting is accomplished.

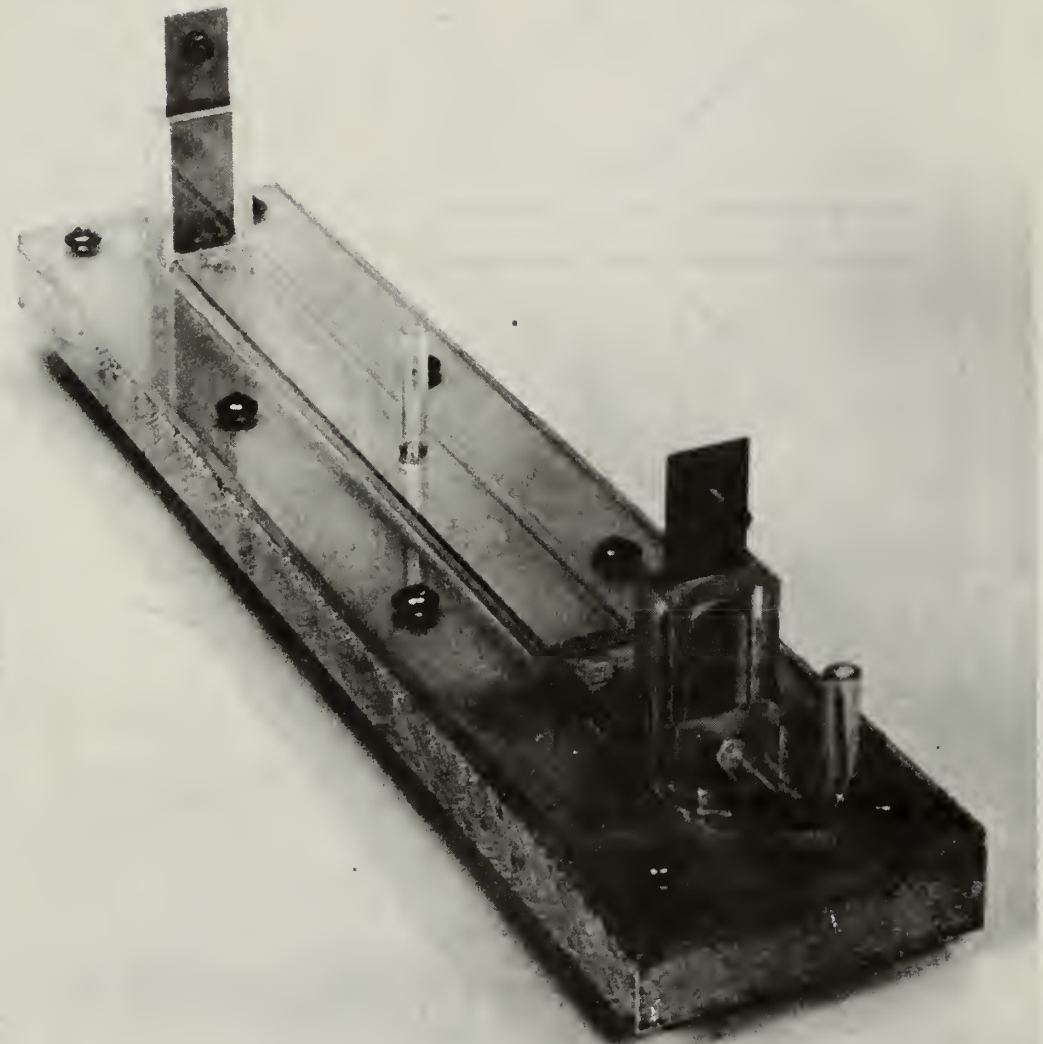

FIGURE 41
CONTACT RESISTANCE JIG

NOTE: DETAILS ON FOLLOWING DRAWINGS

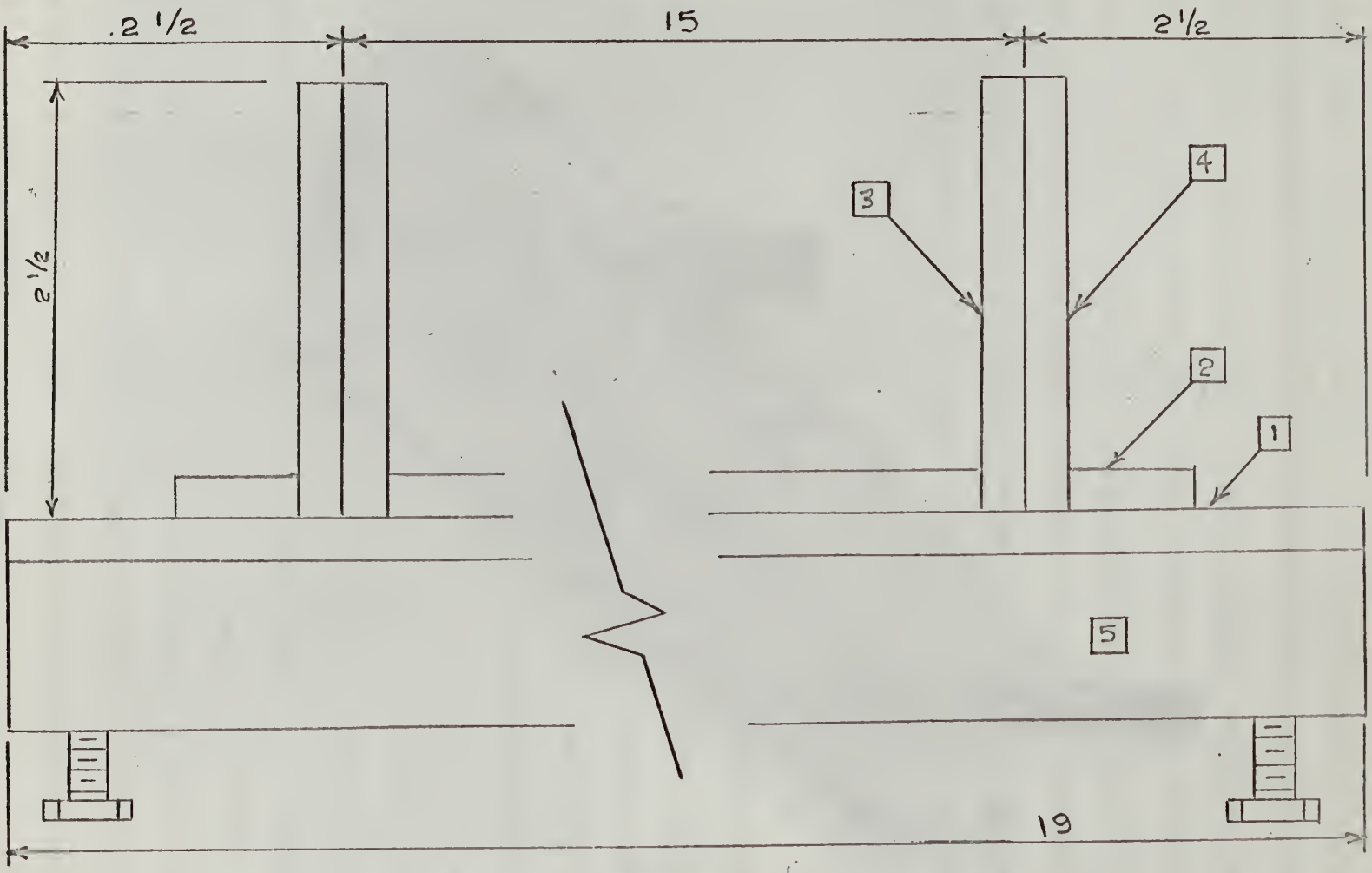

FIGURE 42
CONTACT RESISTANCE JIG PROFILE

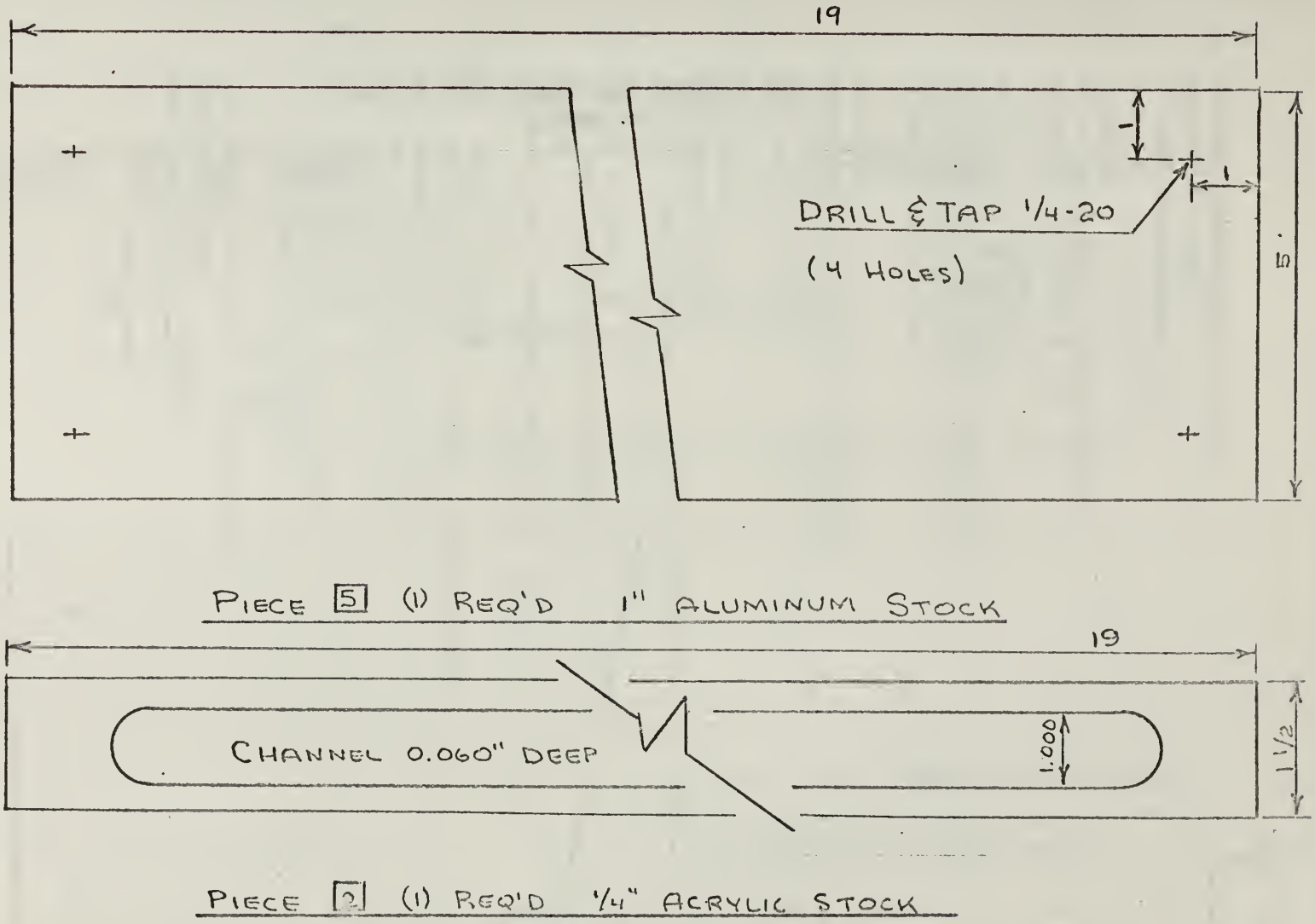

FIGURE 43
CONTACT RESISTANCE JIG DETAILS (1)

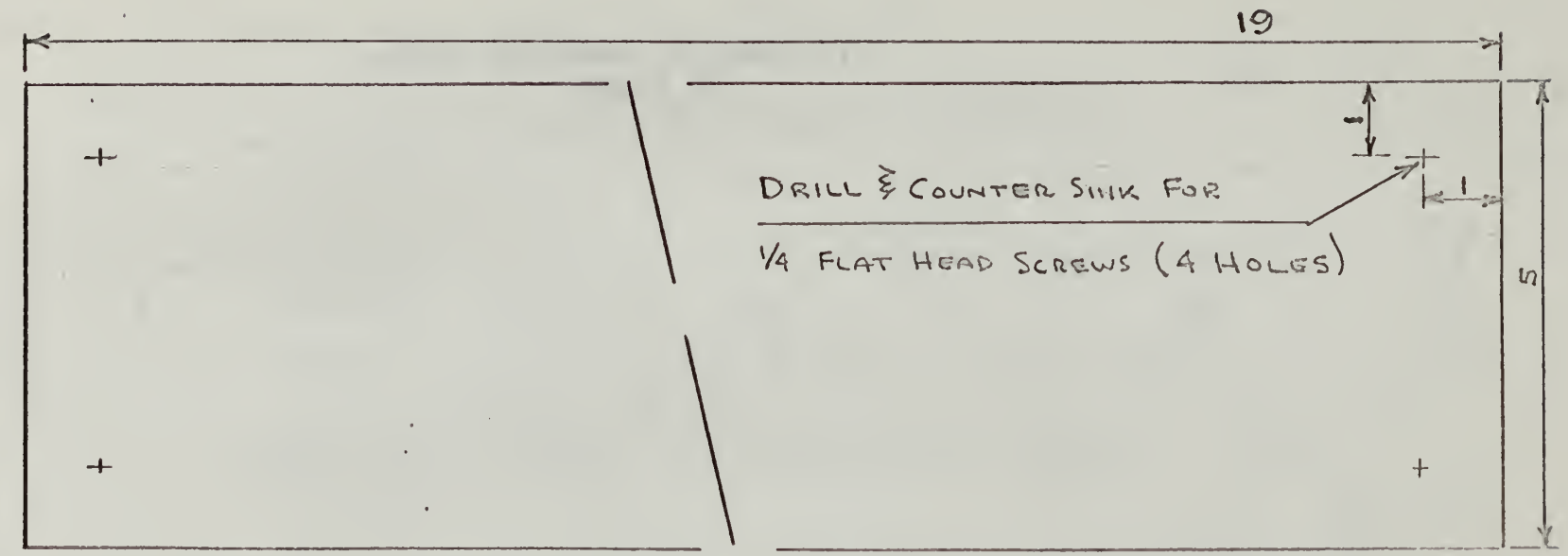

PIECE [1] (1) REQUIRED - 1/4" ACRYLIC STOCK

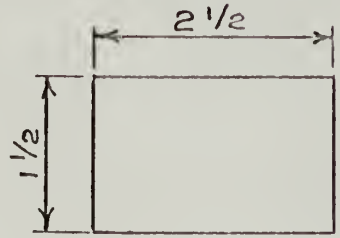

PIECE [3] (2) REQ'D

NOTE: PIECES 3 & 4 ARE 1/4" ACRYLIC

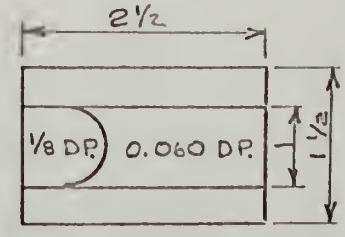

PIECE [4] (2) REQ'D

FIGURE 44
CONTACT RESISTANCE JIG DETAILS (2)

INITIAL DISTRIBUTION LIST

		No. Copies
1.	Defense Documentation Center Cameron Station Alexandria, Virginia 22314	20
2.	Library U. S. Naval Postgraduate School Monterey, California	2
3.	Professor R. Panholzer Department of Electrical Engineering U. S. Naval Postgraduate School Monterey, California	2
4.	Professor M. L. Wilcox Department of Electrical Engineering U. S. Naval Postgraduate School Monterey, California	1
5.	LCDR Robert L. Ediin USS Markab (AR-23) c/o FPO, San Francisco, California 96601	2
6.	LT Jay W. Lamb U. S. Naval Ship Repair Facility Box 34 c/o FPO, San Francisco, California 96601	2
7.	Dr. Vernon J. Rossow National Aeronautics and Space Administration Ames Research Center Moffett Field, California 94035	1
8.	Mr. Joseph G. Lamb U. S. Naval Electronics Laboratory San Diego, California 92152	1
9.	Commander, Naval Ship Systems Command Navy Department Washington, D. C. 20360	1

DOCUMENT CONTROL DATA - R&D

(Security classification of title, body of abstract and indexing annotation must be entered when the overall report is classified)

1. ORIGINATING ACTIVITY (Corporate author) UNITED STATES NAVAL POSTGRADUATE SCHOOL MONTEREY, CALIFORNIA	2a. REPORT SECURITY CLASSIFICATION UNCLASSIFIED 2b. GROUP ---

3. REPORT TITLE

INVESTIGATION OF SMALL D.C. ELECTROMAGNETIC PUMPS

4. DESCRIPTIVE NOTES (Type of report and inclusive dates)

Master's Thesis

5. AUTHOR(S) (Last name, first name, initial)

Ediin, Robert L. and Lamb, Jay W.

6. REPORT DATE	7a. TOTAL NO. OF PAGES	7b. NO. OF REFS
May 1966	105	36

8a. CONTRACT OR GRANT NO. b. PROJECT NO. c. d. Unlimited distribution	9a. ORIGINATOR'S REPORT NUMBER(S) 9b. OTHER REPORT NO(S) (Any other numbers that may be assigned this report)

10. AVAILABILITY/LIMITATION NOTICES

Qualified requesters may obtain copies of this report from DDC;

11. SUPPLEMENTARY NOTES	12. SPONSORING MILITARY ACTIVITY
	U. S. Naval Postgraduate School Monterey, California

13. ABSTRACT

A small, direct current electromagnetic conduction pump was designed according to the equivalent circuit theory of A. H. Barnes. Design was aided by data from a prototype also constructed by the authors. Distinguishing features of the pump are its small size, the use of non-conducting pump walls, and the use of mercury as the working fluid. Performance was compared with theory. Deviations were attributed to electrode contact resistance and to the interaction between magnetic leakage flux and fringe current. Contact resistance to mercury of rhodium and nickel electrodes was determined with the aid of a jig designed for the purpose. A magnet design using flux plotting techniques is presented. Distinguishing feature of the magnet is its cylindrically shaped yoke.

14. KEY WORDS	LINK A		LINK B		LINK C	
	ROLE	WT	ROLE	WT	ROLE	WT
Electromagnetic Pumps						
Liquid Metal Pumps						
Conduction Pumps						
Contact Resistance						
Electromagnets						

INSTRUCTIONS

1. ORIGINATING ACTIVITY: Enter the name and address of the contractor, subcontractor, grantee, Department of Defense activity or other organization *(corporate author)* issuing the report.

2*a*. REPORT SECURITY CLASSIFICATION: Enter the overall security classification of the report. Indicate whether "Restricted Data" is included. Marking is to be in accordance with appropriate security regulations.

2*b*. GROUP: Automatic downgrading is specified in DoD Directive 5200.10 and Armed Forces Industrial Manual. Enter the group number. Also, when applicable, show that optional markings have been used for Group 3 and Group 4 as authorized.

3. REPORT TITLE: Enter the complete report title in all capital letters. Titles in all cases should be unclassified. If a meaningful title cannot be selected without classification, show title classification in all capitals in parenthesis immediately following the title.

4. DESCRIPTIVE NOTES: If appropriate, enter the type of report, e.g., interim, progress, summary, annual, or final. Give the inclusive dates when a specific reporting period is covered.

5. AUTHOR(S): Enter the name(s) of author(s) as shown on or in the report. Enter last name, first name, middle initial. If military, show rank and branch of service. The name of the principal author is an absolute minimum requirement.

6. REPORT DATE: Enter the date of the report as day, month, year; or month, year. If more than one date appears on the report, use date of publication.

7*a*. TOTAL NUMBER OF PAGES: The total page count should follow normal pagination procedures, i.e., enter the number of pages containing information.

7*b*. NUMBER OF REFERENCES: Enter the total number of references cited in the report.

8*a*. CONTRACT OR GRANT NUMBER: If appropriate, enter the applicable number of the contract or grant under which the report was written.

8*b*, 8*c*, & 8*d*. PROJECT NUMBER: Enter the appropriate military department identification, such as project number, subproject number, system numbers, task number, etc.

9*a*. ORIGINATOR'S REPORT NUMBER(S): Enter the official report number by which the document will be identified and controlled by the originating activity. This number must be unique to this report.

9*b*. OTHER REPORT NUMBER(S): If the report has been assigned any other report numbers *(either by the originator or by the sponsor)*, also enter this number(s).

10. AVAILABILITY/LIMITATION NOTICES: Enter any limitations on further dissemination of the report, other than those imposed by security classification, using standard statements such as:

(1) "Qualified requesters may obtain copies of this report from DDC."

(2) "Foreign announcement and dissemination of this report by DDC is not authorized."

(3) "U. S. Government agencies may obtain copies of this report directly from DDC. Other qualified DDC users shall request through _____."

(4) "U. S. military agencies may obtain copies of this report directly from DDC. Other qualified users shall request through _____."

(5) "All distribution of this report is controlled. Qualified DDC users shall request through _____."

If the report has been furnished to the Office of Technical Services, Department of Commerce, for sale to the public, indicate this fact and enter the price, if known.

11. SUPPLEMENTARY NOTES: Use for additional explanatory notes.

12. SPONSORING MILITARY ACTIVITY: Enter the name of the departmental project office or laboratory sponsoring *(paying for)* the research and development. Include address.

13. ABSTRACT: Enter an abstract giving a brief and factual summary of the document indicative of the report, even though it may also appear elsewhere in the body of the technical report. If additional space is required, a continuation sheet shall be attached.

It is highly desirable that the abstract of classified reports be unclassified. Each paragraph of the abstract shall end with an indication of the military security classification of the information in the paragraph, represented as *(TS)*, *(S)*, *(C)*, or *(U)*.

There is no limitation on the length of the abstract. However, the suggested length is from 150 to 225 words.

14. KEY WORDS: Key words are technically meaningful terms or short phrases that characterize a report and may be used as index entries for cataloging the report. Key words must be selected so that no security classification is required. Identifiers, such as equipment model designation, trade name, military project code name, geographic location, may be used as key words but will be followed by an indication of technical context. The assignment of links, roles, and weights is optional.